To the Graduate Council:

I am submitting herewith a dissertation written by Ioannis Anastasiou entitled "Model Validation and Control Systems Analysis for Pressurized Water Reactor Components." I recommend that it be accepted in partial fulfillment of the requirements for the degree of Doctor of Philosophy, with a major in Nuclear Engineering.

T. W. Kerlin

T. W. Kerlin, Major Professor

We have read this dissertation and recommend its acceptance:

P F Pasqua

E. M. Katz

J M Googe

J C Robinson

Accepted for the Council:

L Evans Roth

Vice Chancellor
Graduate Studies and Research

MODEL VALIDATION AND CONTROL SYSTEMS ANALYSIS FOR PRESSURIZED WATER REACTOR COMPONENTS

A Dissertation

Presented for the

Doctor of Philosophy

Degree

The University of Tennessee, Knoxville

Ioannis Anastasiou

August 1979

DEDICATION

To my parents.

ACKNOWLEDGEMENTS

The author would like to thank Dr. T. W. Kerlin, the major professor, for his guidance and valuable suggestions during the development of this dissertation.

He wishes to express his gratitude to Dr. G. Zwingelstein of Centre d' Etudes Atomiques in Saclay, France for making the undertaking of this work possible and for his great help and encouragement in each step of this study.

The help of Dr. P. F. Pasqua, Head of the Nuclear Engineering Department, in obtaining a Research Assistantship during the graduate studies at The University of Tennessee is greatly appreciated.

Special thanks for their valuable help and friendship during this work is forwarded to all of the members of the Signal and System Analysis Laboratory in CEA-Saclay, namely Miss. Nicolas, Messrs. Deat, Grillon, Guillier, Janot, Maury, Poujol, Thabet, and Thonnet.

The Doctoral Committee members are thanked for their suggestions and corrections on the dissertation.

Helpful discussions with Dr. B. Upadhyaya are deeply appreciated. The author is indebted to Miss. Jacki Googin for her great help and encouragement during the last and most difficult months of this work.

Mr. H. Hashemian's help and friendship are warmly acknowledged.

ABSTRACT

A study of the water level control in a U-tube recirculation type steam generator of a 900 MWe pressurized water reactor was undertaken for operation at full power and at 30% power level. The need to simulate the complete power plants and controls for load following transients required the use of low-order physical models for the core and the steam generator and simulation of the control system components presently in use.

The validation of the models, necessary for any control study, was accomplished at both power levels by performing model parameter identification and using experimental transients from 100-90% and 30-20% power demand step perturbations. The large, complex, industrial processes modeled required the design of a multi-input, multi-output time domain identification scheme, using the model-adjustment method with a least-squares estimator and the simplex optimization scheme for its minimization. The results of the model validation work have demonstrated that the physical models used represent the dynamic behavior of the main components of the pressurized water reactor satisfactorily and realize a very good trade off between accuracy and complexity.

The importance of high quality experimental data in model validation work, and the existence of various problems associated with the electronics of the data transmition, acquisition and recording required careful treatment.

The implementation of the overall system simulation in real time on a minicomputer was achieved. Special care was taken for a detailed

simulation of the control rod nonlinear movement. It was shown that the presently used control system is sufficient in controlling the water level after load following transients at the power levels studied. The use of a medium size minicomputer in this work showed that safety and functional analyses of a large process can be achieved with economy and flexibility as well as accuracy. The use of the Linear-Quadratic-Gaussian theory was attempted as a modern control theory application for an industrial process, but numerical problems were encountered and the approach was found to be impractical.

TABLE OF CONTENTS

LIST OF FIGURES

CHAPTER 1

INTRODUCTION

1.1 Statement of the Problem

Even though the technology that has been developed for nuclear power plants has reached a very high level of sophistication for some time now, the control loops of certain subsystems deserve additional attention. Start-up and operation at low power levels are carried out with manual control and there is a major problem in controlling the water level in the steam generators of PWR plants.

Large variations in water level can affect system power and hydrodynamic stability, and in severe cases result in reactor shutdowns. With a low water level in the steam generators, insufficient cooling is provided to the primary coolant loop and thus the nuclear fuel may be endangered. When there is a high water level condition, the steam turbine may be jeopardized by the high degree of moisture carried over into the steam line. In order to minimize these adverse effects, it is desirable to maintain the water level as close to the predetermined set-point as possible during all operating conditions.

The above task is especially difficult during operation at low power levels. During that time there is a low feedwater rate and low temperature that result in a much stronger demonstration, than in higher power levels, of the "shrink" and "swell" phenomena, and because of that, manual control at lower power levels could lead to wrong commands.

This is why the traditionally used schemes of control, which are based on manual control at power levels below 15%, have to be modified so that they can allow automatic control of the steam generators from 0% to 100% of full power. The statistics of PWR's operating experience in the United States (10) show the strong contribution of operator errors in shutdowns due to failure of the main feedwater system at low power level. Thus, by using a control design to eliminate the need for manual control of the feedwater system during low power operations, the possibility of a related plant shutdown can be greatly reduced and the availability of the power plant can be significantly increased.

The main problems associated with the design of a new control system or the evaluation and improvement of the existing control system are:

(a) To simulate the physical processes involved in open loop; in our case, the core and the steam generator models.

(b) To validate these models in open loop, using test data.

(c) To close the loop by adding the control system.

A primary concern, when attacking each one of the problems above, is minimization of the computer cost. The possibility of using a minicomputer in this study helps considerably to this effect, but also adds the problem of adapting the various computer codes for the minicomputer.

With the problem of model validation, real tests have to be performed in a nuclear power plant. In this research program, data were taken during the start-up of a 900 MWe PWR plant with three U-tube steam generators. The tests consist primarily in step changes of various amplitudes (between 5 and 13%) in the power demand level, while the reactor was between 20 and 100% of nominal power.

For safety reasons it is not possible to have direct access to the sensor outputs. Consequently, the only way to obtain the signals is after one or several isolation amplifiers and in some cases after special purpose low-pass filters placed at the output of some of the sensors. There may be also other problems associated with the transmission, acquisition and recording of the signals. Thus, the signals obtained in practice through the data acquisition system, do not represent exactly the true variations of the physical quantities monitored. In order to achieve the model validation using real input and output signals, all the problems that might exist with the transmission, acquisition and recording of the signals have to be resolved. Only then is the system identification procedure undertaken, using a suitable optimization method.

1.2 Objectives of this Study

The main concern that originated this study was steam generator water level control, as it was discussed in the previous section. An inexpensive simulation capability for predicting accurately the dynamic response of the water level, using the currently-used control system, was desirable. This could allow not only a fast and easy evaluation of the control system in use, but also evaluation of possible modifications and improvements of it in the future, with very little additional effort.

It could also serve as a reference control system performance for comparison with the performance of control systems that could be developed with completely new methods, such as using modern optimal control theory methods.

Since this work involves the complete effort from the plant test to parameter identification of the models used and study of modern control theory methods, there were many other objectives along this study that had to be reached, and thus they were of primary importance.

The parameter identification of the reactor core and especially the steam generator model is one of these objectives. The compromise for a low order but accurate model requires good knowledge of certain nonmeasurable parameters, so that confidence in the model predictions is gained. To have a routine and fast way of accomplishing that is very important, not only for control purposes but also in open-loop simulations for better understanding of the system.

Another objective is to attack in a systematic way possible problems associated with the acquisition of the plant test signals, as was discussed in the previous section. Since good quality plant test data is of capital importance to a meaningful system identification work, every effort must be taken to assure that the signals recorded represent accurately the true variations of the physical quantities monitored.

The reduction of the computer cost, by making maximum use of the minicomputer available in the various steps and subtasks of this study, is another objective of this work. Since its memory size of only 32k and its low speed are serious limitations for its use, special care must be taken to modify and optimize the various computer codes used.

Finally, the study of a new control method was undertaken and its applicability to our specific problem with the existing formulation was examined. It is based on Modern Linear Control Theory, and in particular on the Linear-Quadratic-Gaussian (LQG) Theory. In contrast to the deterministic classical transfer function approach used at present, it takes into account the random uncertainties associated with the plant, the actuators and the sensors. A stochastic control system designed by such a method, could exhibit a superior performance, if all the problems associated with its implementation could be resolved. The objective was to study and examine the theory in the light of its potential application to the control of industrial processes, and to document the steps and difficulties in implementing it for the control of the core-steam generator system under study.

1.3 General Review

In a parameter identification work for industrial processes there are many methods that can be followed, depending on the nature of the physical process, the type of test data used, the model, and the objective in mind. Concentrating on linear models, one can have time-domain or frequency-domain identification with either deterministic or stochastic data (1)-(6).

However, in our case of multi-input, multi-output processes for the core and the steam generator model, and the large magnitude of the perturbation with very good signal to noise ratio, a time-domain, deterministic parameter identification in the least-squares sense was the natural choice.

Classical control theory has played a very important role in the solution of most feedback control problems, and it has been readily implemented through analog circuitry and servomechanisms. Up to the present, the water level control designs for the boilers of almost all nuclear and fossil power plants, are still based on classical control, and use analog and hybrid modelling approaches.

Nahavandi and Batenburg (7), using a hybrid model for the steam generator, designed a water level control system consisting of standard proportional and reset controls on water level deviation from a desired set point and the difference between the steam and the feedwater mass flow rates.

Hennebicq (8) examined the performance of the water level control system that exists in the French PWR's, by using simplified physical models. He gives only selected results but describes the control system in sufficient detail, so that it was possible for it to be adopted in this study as our reference control system.

Hocepied (9) presents the results of a multi-part effort to achieve an automatic water level control from 0 to 100% of power. The classical three-element controller was re-evaluated and additional functions were considered: These include control circuit for the feed-water valve, compensation for the "shrink" and "swell" phenomena due to steam flow variations, and an automatic system for the adaptation of the water level regulator parameters.

Chungpeng Fan (10) presents results of a comprehensive effort by Combustion Engineering to extend the automatic control of the water level to low power levels. Using detailed models for the core and the steam generator, an extensive stability analysis was undertaken of the steam generator dynamic characteristics at low power that resulted in an optimal choice of controller setpoints. The automatic system, so designed, demonstrated a very satisfactory performance at low power levels.

In the last 25 years, there has been a very rapid development in control theory. Dynamic-programming and the maximum principle, that were outgrowths of various approaches to variational problems, were key elements in this development. At the same time, continuous advances in computer technology, provided the engineer with the appropriate tools to apply this theory. However, application of modern control theory to industrial processes has not quite followed the same pace with all these developments. The conversion to Direct Digital Control (DDC) is going quite slowly, especially in the case of nuclear power plants, where issues of safety and standardization introduce a conservatism in adopting new technology. The following paragraphs present some of the activity in the domain of modern control theory applications to nuclear power plants.

Lipinski (11) has done an extensive review, up to the year 1968, of the literature on the use of modern control theory in nuclear engineering, including references to the general control literature. A more recent survey is given by Cummins and Butterfield (12). Hagen and Kerlin (13) made a review of three symposiums in Europe on the subject of DDC. Lunde (14) made a review of current trends in applications of process control computers to nuclear power plants.

Bjorlo et al. (15) presented an on-line plant control, based on Dynamic Programming and Estimation Theory, that was developed for the vessel pressure loop of the Halden HBWR plant in Norway. They conclude that the digital control is faster and more effective than the analog control, and promising to be extended to a multi-loop arrangement.

Josefsson et al. (16) succeeded to achieve an improvement in the load-following capability of a Swedish BWR, using digital on-line techniques and results from optimum linear control theory.

Using simplified models for an entire prototype heavy water PWR in W. Germany, Atary and Shah (17) applied modern control theory for the design of an optimal control system for the complete plant. The results demonstrated the feasibility of this approach to control systems design for large scale multivariable industrial processes.

Frogner (18) used linear estimation and optimal control for the feedback control of a simulated BWR plant. The algorithm presented was considered feasible for DDC implementation. It was found that the assumptions inherent in the LQG approach used do not pose a severe limitation by using a simplified model for the simulated plant.

De Keyser and Van Cauwenberghe (19) investigated the possibility of applying self-tuning controller's to an industrial process like a PWR power plant. The control design is based on a rather simple mathematical low-order model with unknown time-varying parameters which are identified in real time. A self-tuning controller was used to control the primary coolant temperature with very encouraging results.

1.4 Organization of the Text

In Chapter 2, a description of the physical system under study is given. It consists of the reactor core, the steam generator, and the reactivity and feedwater control systems.

In Chapter 3, a description of the models used to represent the dynamic behavior of the system components is provided. The nodal representation of the core and the steam generator models is also given. Derivation of the model equations and the data used are presented in Appendix I for the reactor core and in Appendix II for the steam generator model.

In Chapter 4, the plant test signals for two load step perturbations, at full power and at low power, are presented along with the effort to solve problems associated with the acquisition of these signals.

In Chapter 5, a sensitivity analysis of the steam generator model dynamic behavior to small changes in some nonmeasurable parameters is presented, to serve in the evaluation of the model validation work. Also, the effect of the feedwater temperature is given to evaluate the importance of omitting its feedback effect in the overall system simulation later.

In Chapter 6, the whole procedure for the parameter identification work is discussed for the reactor core and the steam generator models, at full power and at low power. The agreement between model prediction and experiment is presented using the initial a-priori parameter estimates, and the optimal values. The simplex optimization method used is outlined in Appendix III.

In Chapter 7, the simulated dynamic response of the overall core-steam generator-control systems closed loop to step perturbations in power demand is presented. The integration method used that allows the real-time simulation of the overall system in the minicomputer is presented and a description of the computing facilities available is given. The performance of the control systems using the optimal values found for its components is discussed.

In Chapter 8, an introduction to modern linear control theory is given. The formulation and the solution of the theoretical problems associated with the Linear-Quadratic-Gaussian (LQG) Theory is provided along with the procedure for implementing it. The effort taken to apply the LQG Theory for the control of the core-steam generator system is outlined.

Finally, conclusions about the various steps of this work along with recommendations for future study are given in Chapter 9.

CHAPTER 2

DESCRIPTION OF THE SYSTEM

2.1 Introduction

The Pressurized Water Reactors (PWRs) are the most widely used nuclear power plants in the world. There are about 100 of them operating today and another 200 under construction or in the planning stage. The power output of the first PWRs built was between 300 and 700 MWe. However, most of the ones built today are of 900 to 1300 MWe capacity.

The PWR of our study is a 900 MWe reactor with three coolant loops having vertical, U-tube, recirculation type steam generators (UTSG). A schematic of the three primary loops is given in Figure 2.1. The pressurizer is not simulated in our study and a schematic of a primary and a secondary loop without the pressurizer is shown in Figure 2.2.

A brief description of the reactor core and the steam generator and of their function is given below. A description of the associated reactivity control and feedwater flow control systems is also included.

2.2 The Reactor Core

The reactor is contained in the reactor vessel, which is a vertical cylinder of about 4m inside diameter and 10m height, closed on both ends by hemispherical heads. It consists primarily of the fuel in the form of 157 fuel assemblies, special equipment for the support of the core and the channeling of the water flow, and guide-tubes containing the core instrumentation. The height of the core is about 3.7m.

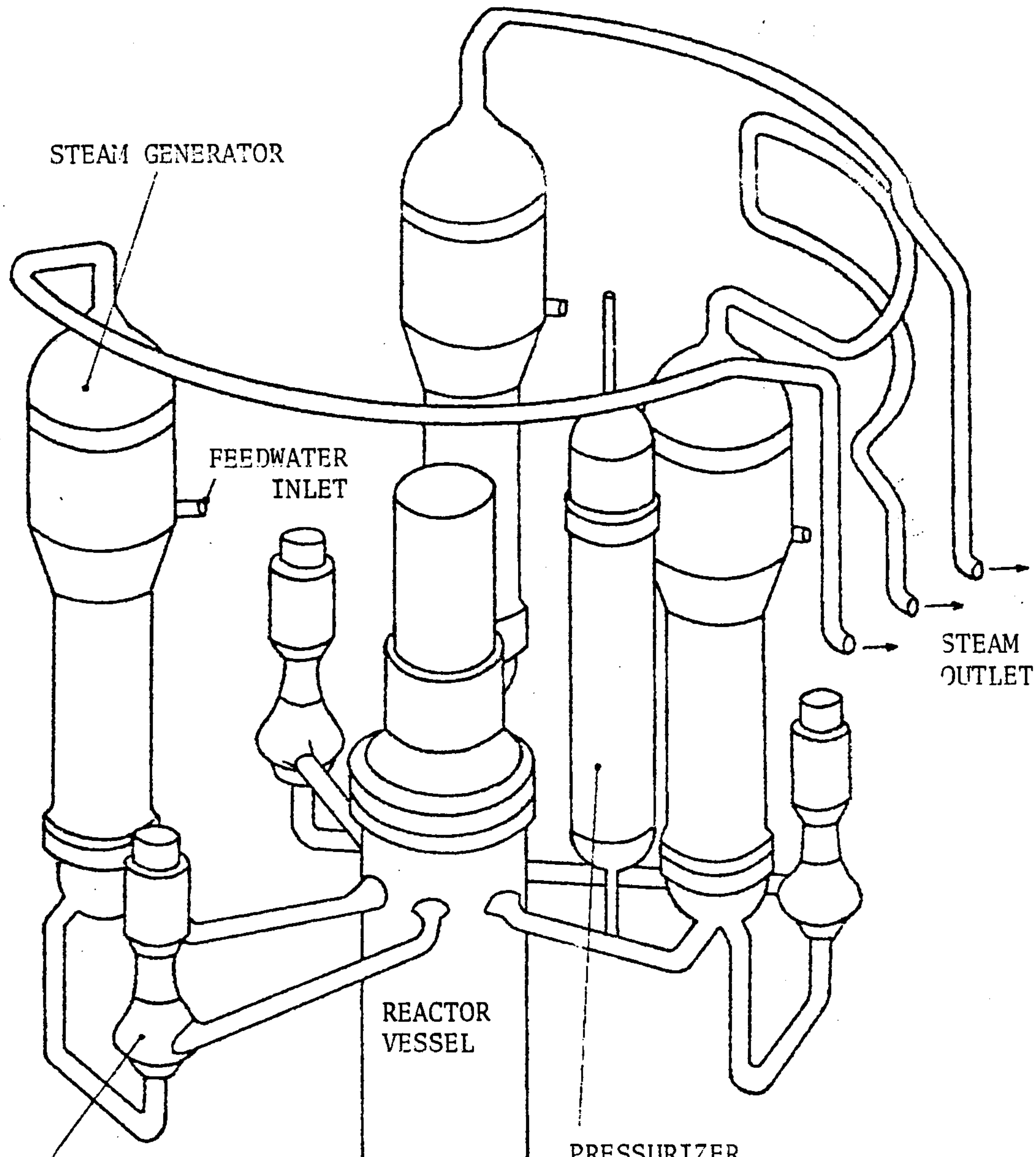

Figure 2.1 Schematic Outlay of the Reactor Vessel of a PWR with its Three Coolant Loops.

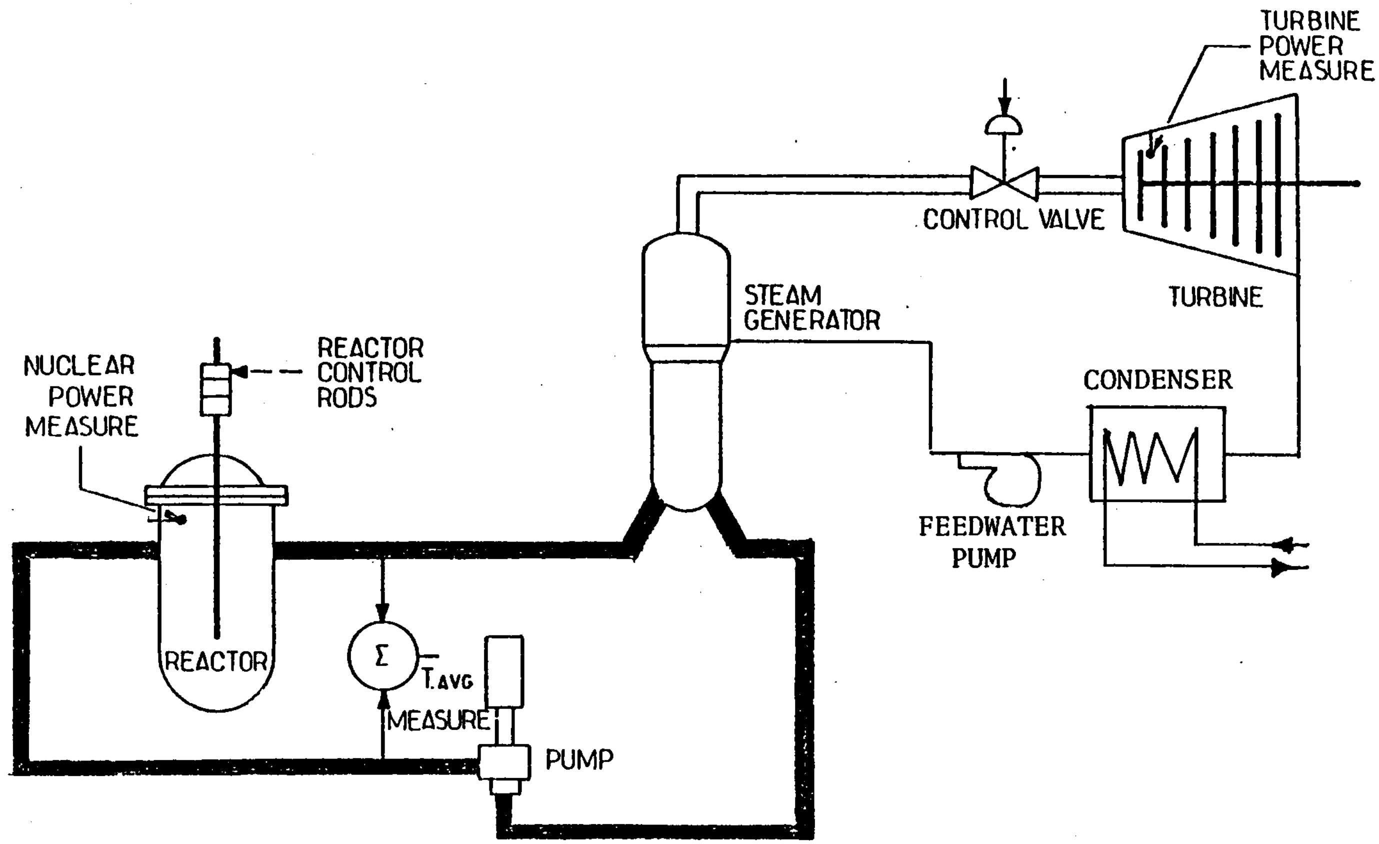

Figure 2.2 Schematic Outlay of the Primary and Secondary Loops in a PWR.

Each fuel assembly consists of 264 fuel rods placed in a square grid of 17 × 17 and containing slightly enriched uranium dioxide and 25 guide-tubes along which the components of control rods move. There are three regions of fuel assemblies with different degrees of enrichment. The assemblies with the lowest fuel enrichment are at the center of the core to help flatten the neutron flux distribution.

The reactor coolant-moderator flows upwards through the core and its input-output temperature difference is about 20°C. The reactor vessel is pressurized at about 155 bars to avoid water boiling, and this primary pressure is kept as constant as possible with the help of the pressurizer, which is connected to the hot leg of one of the three primary loops (Figure 2.1). The reactor vessel is the common point of the three primary loops, whose other ends are the steam generators (see Figure 2.1). An isometric section of a PWR reactor can be found in Figure 2.3.

2.3 The Steam Generator

The type of the steam generator used in most of the current PWRs is the vertical, U-tube, recirculation type steam generator. Details of such a steam generator are shown in Figure 2.4 and a schematic diagram is presented in Figure 2.5.

The hot primary coolant, carrying the heat generated in the core and flowing along the piping of the hot leg, enters at the bottom of the steam generator through the inlet nozzle to an inlet plenum, and flows through the U-tube bundle. The primary flow is parallel to the secondary flow in the inlet branch of the U-tubes and opposite to it in the exit

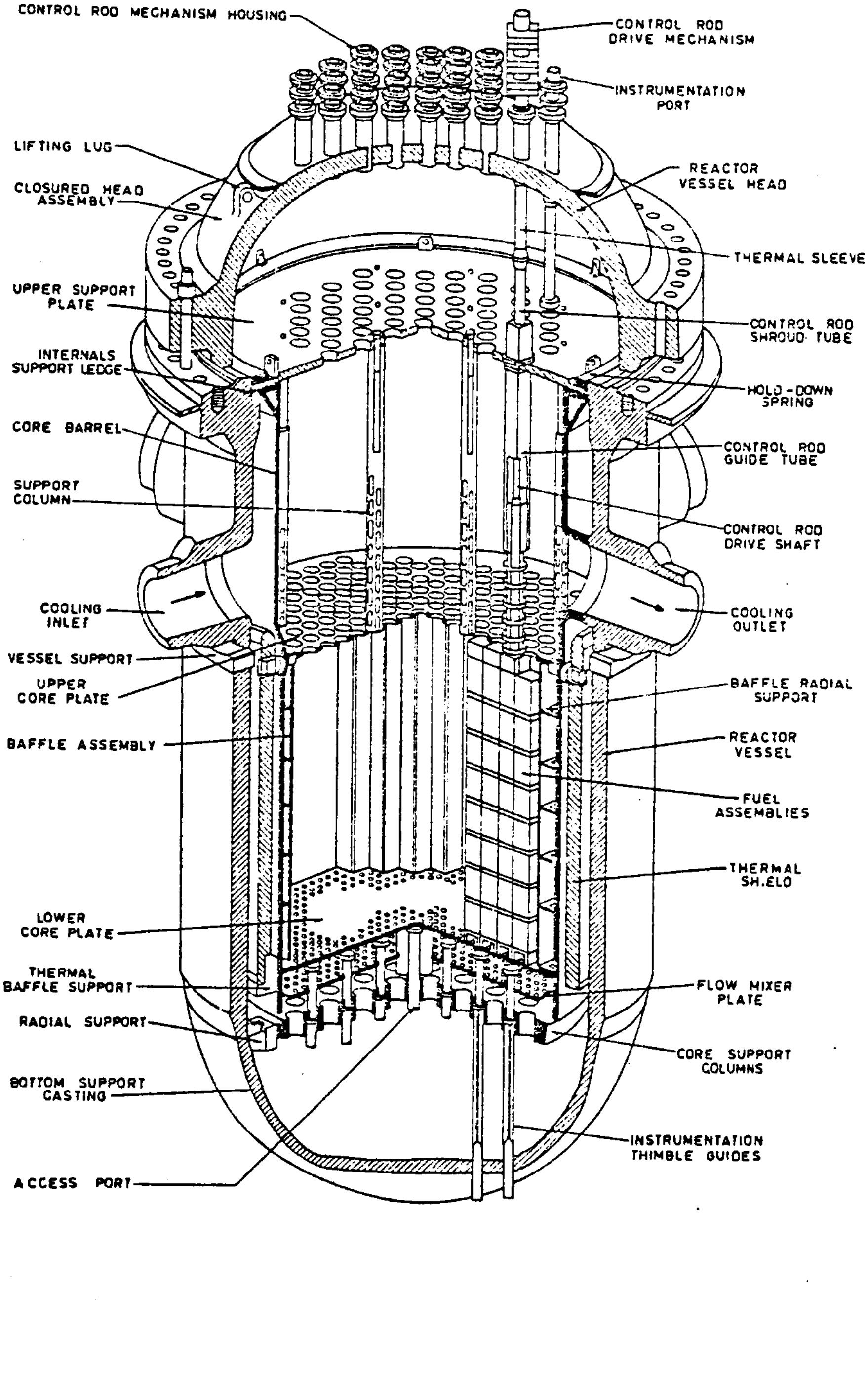

Figure 2.3 Isometric Section of a PWR Reactor Vessel.

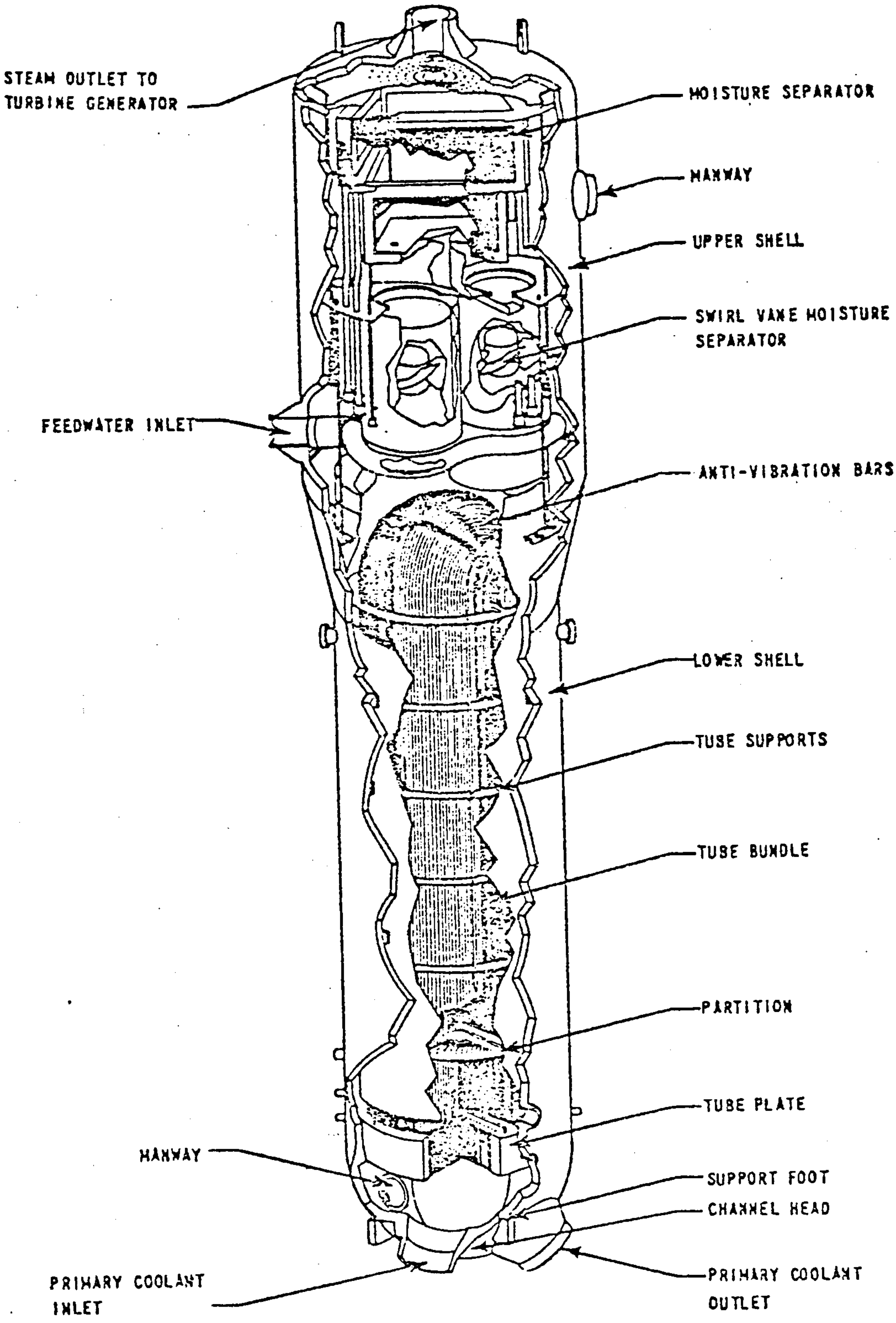

Figure 2.4 Details of a U-Tube Steam Generator.

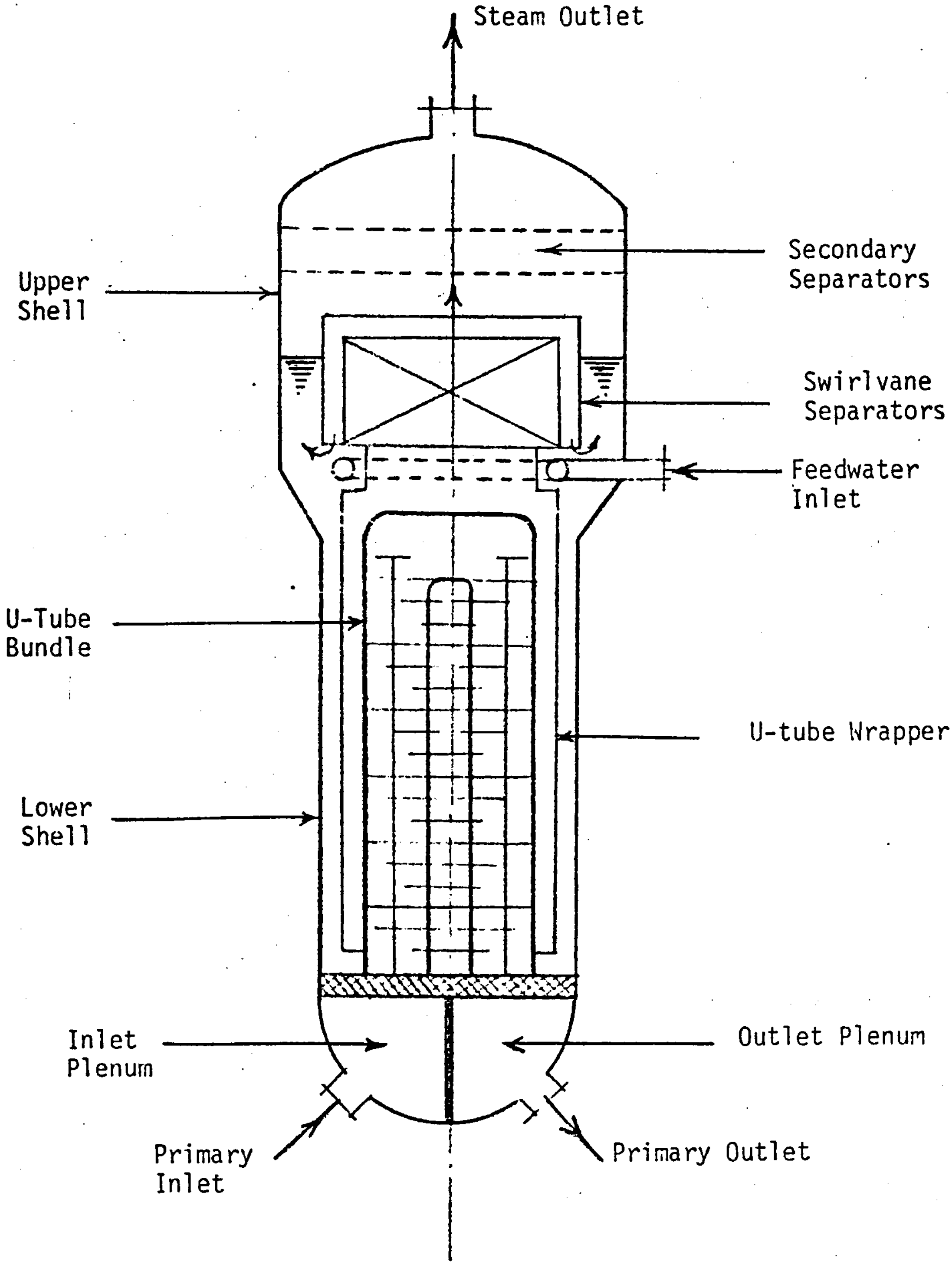

Figure 2.5 Schematic Diagram of a U-Tube Steam Generator.

branch. Thus, we have both parallel and counter flow with a common secondary fluid. The tube conductance together with the film heat transfer coefficients determine the effective heat transfer coefficients relating the bulk mean temperatures in the primary and secondary sides with the tube metal average temperature.

The feedwater enters through the feedwater ring into the annulus between the U-tube wrapper and the shell, referred to as the downcomer. Then it mixes with saturated water separated from the steam-water mixture in the steam separators and enters from the downcomer into the tube-bundle region. It flows upward around the U-tubes and its temperature is raised so that boiling occurs. A steam-water mixture is formed during the last part of the upward flow and it enters the steam separators where steam is separated and collected in the upper part of the steam generator shell. The steam exits at a rate determined by the turbine stop-valve opening, while separated water is mixed with feedwater and flows downward in the downcomer.

2.4 The Reactor Control System (20)

The control systems in a PWR are to adjust smoothly the thermal power furnished by the reactor core to the power absorbed by the turbine and condensers. They are designed to allow the plant to change load automatically in the range of 15% to 100% full power. The loading and and unloading rates of the plant are constrained. The plant is designed to accept ±10-15% step load changes and a ramp rate of loading of 5% per minute. A sudden large drop in demanded power can be absorbed by dumping the excess steam into the condenser. Below 15% the control is accomplished manually.

The reactor control system consists of three channels which are (a) the average reactor fluid temperature (Tavg), (b) the power mismatch and (c) the Tavg set point (Tref) channels (see Figure 2.6). The output from these three channels is used to drive the control rods via a rod program.

(a) A comparator selects the maximum mean temperature of the three primary loops and the signal is passed by a compensator of transfer function $(1 + \tau_1 s)/(1 + \tau_2 s)$ and a noise filter $1/(1 + \tau_3 s)$.

(b) The turbine first stage pressure signal, which is proportional to turbine load, is used as a direct measurement of turbine load. It passes by a filter of transfer function $(1/1 + \tau_6 s)$ and then it is used both in the Tref channel and in the power mismatch channel. The power mismatch channel serves two functions: to introduce an immediate control rod movement so that the reactor responds rapidly to load changes and does not overshoot excessively because of turbine load feedforward signal and to increase the control stability because of the flux feed-back signal. The filtered turbine load signal is compared to the nuclear power and the difference is applied to a circuit of transfer function $\tau_6 s/(1 + \tau_6 s)$ which prohibits action of this channel at steady-state when the power mismatch is not exactly zero. Then the signal passes through two nonlinear gain modifying circuits whose functions are shown in Figure 2.7. The first one has a low gain for weak signals and a high gain for strong signals while the second one has a constant gain until

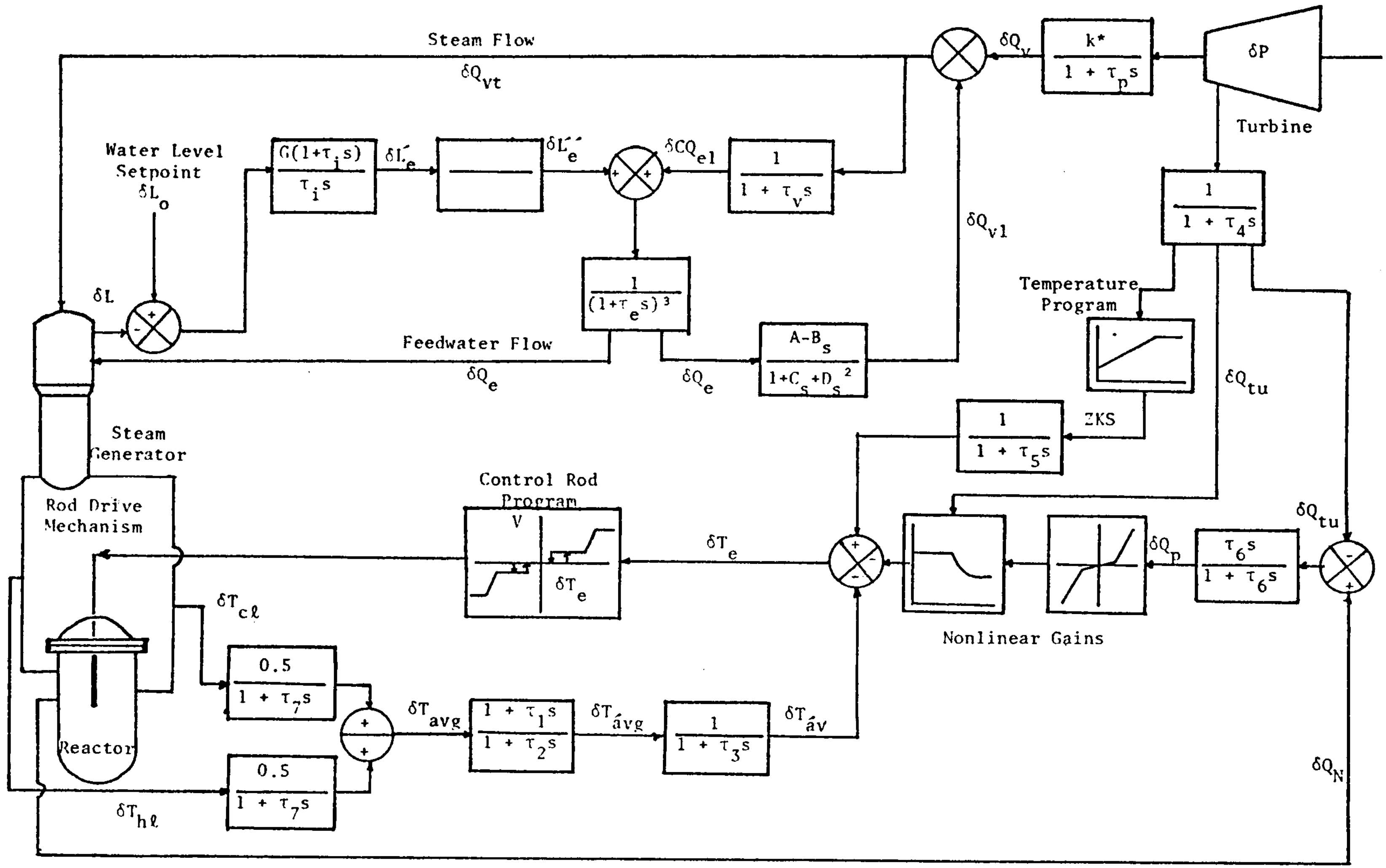

Figure 2.6 Schematic of the Reactor Control and the Feedwater Flow Control Systems.

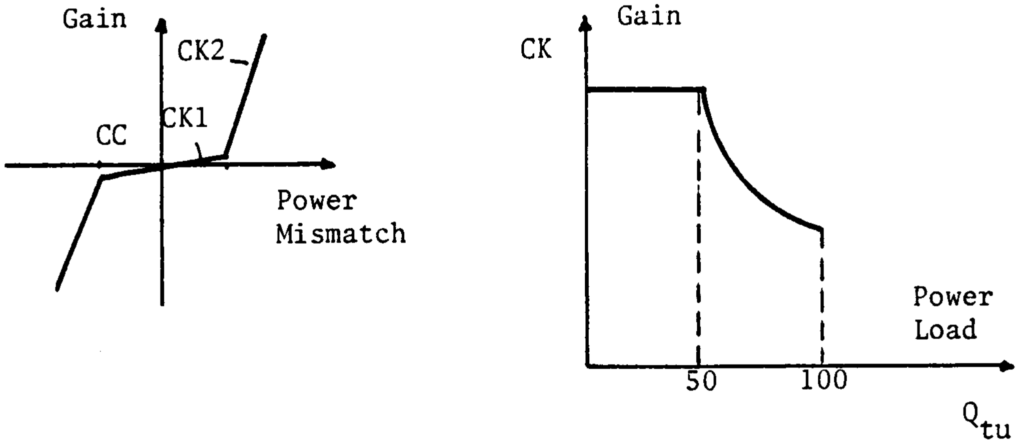

Figure 2.7 Nonlinear Gains Used in the Power Mismatch Channel of the Reactor Control System.

a certain power level and then it becomes inversely proportional to turbine load.

(c) The Tavg set point (Tref) channel is used to change the required Tavg temperature as a linear function of the turbine load signal (discussed in (b)], and according to the steady-state temperature program. The resulting set-point signal is passed by a low-pass filter of transfer function $1/(1 + \tau_5 s)$ and it is then compared to the average temperature.

The final result of the three control channels described above is an error temperature signal (Te) which drives the control rods. The program of their movement is shown in Figure 2.8. We can see that it consists of four distinct zones:

1. A zone of insensitivity containing a hysterysis.
2. A zone of rod movement at constant, low speed.
3. A zone of rod movement at a speed proportional to the error signal.

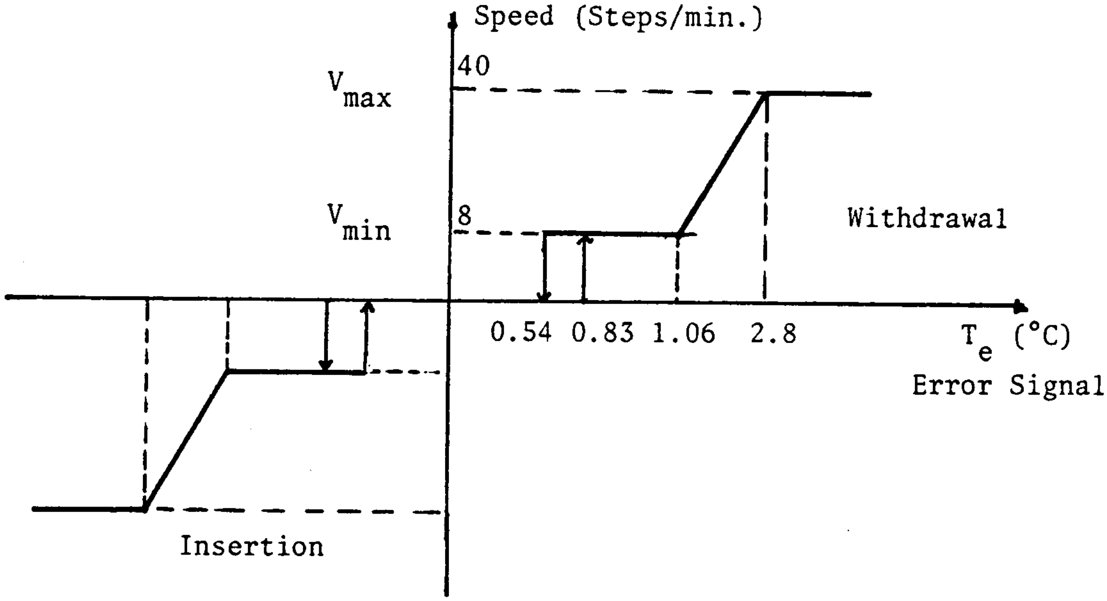

Figure 2.8 Control Rod Movement Program.

4. A zone of rod movement at a maximum, constant speed.

The system of differential equations simulating the reactor control system is presented in Chapter 3.

2.5 The Feedwater Control System (20)

The function of the feedwater control system is to insure that the feedwater flow is matched as closely as possible to steam flow and that water level in the steam generator is kept constant. During a load change transient, the shrink or swell phenomena (discussed in Chapter 1) occur, and the water level does change, but this level is restored quickly. It is maintained within fixed limits by the control system and when it fails, the protection system takes over.

A schematic diagram of the feedwater control system is included in Figure 2.6. The mismatch signal between water level and its setpoint is passed through a proportional-integral control action of transfer function $G(1 + \tau_i s)/\tau_i s$ and a compensator of transfer function $(1 + \tau_{d'} s)/(1 + \tau_d s)$. The resulting signal is the first component demanding a feedwater flow change action. Also, the turbine load change translated into steam flow change signal by the transfer function $K^*/(1 + \tau_p s)$, passes through a filter of transfer function $1/(1 + \tau_v s)$ to become the second component of the feedwater flow change signal. The sum of these two components passes through a third order filter $1/(1 + \tau_e s)^3$. There is also a feedback effect of the feedwater flow change on the steam flow perturbing the steam generator, presented by the transfer function $(A - Bs)/(1 + Cs + Ds^2)$.

The system of differential equations simulating the feedwater flow control system is presented in Chapter 3.

CHAPTER 3

DESCRIPTION OF THE MODELS

3.1 Introduction

In Chapter 2, a description of the system under study was given. It consists of the reactor core, the steam generator and the reactor and feedwater control systems (see Figure 2.6, page 20). In order to simulate the various components of this system, one should use models after considering the main objectives of the study and the computer facilities available with their associated cost.

In this study, one of the objectives was to simulate the overall closed-loop system in real time on a minicomputer. The limited capabilities in memory size and execution speed of the minicomputer used (described in Chapter 7), dictated the use of simplified models to represent the various components simulated. However, the special interest in water level control necessitated the use of an adequately detailed steam generator model. Also, the simulation of all the components of the control systems limited the reduction of the size of the overall order of the system. To represent the reactor core dynamics however, a very simplified core model was used, which was sufficient to predict the hot leg temperature (very important in the steam generator water level computation) and the nuclear power for the simulation of the reactor control system. The real-time simulation of the overall system was possible, within the limits of the minicomputer capabilities.

In this chapter a brief description of the models used to simulate all the components of the system is given.

3.2 The Reactor Core Model

The model of the reactor system consists of a set of nine differential equations representing the reactor kinetics, the core heat transfer, the upper and lower plenums and the hot and cold leg temperatures. A linearized point kinetics model with an effective single delayed neutron precursor group is used to represent the reactor kinetics. To model the heat transfer, the entire fuel region is represented by one node with two coolant nodes coupled to it (Mann's method) (56). The primary pressure is assumed constant during the transients under study, because the feedback reactivity effect of pressure changes is much smaller than the effect of primary temperature changes. An inclusion of the pressure effect would also require modelling of the pressurizer, increasing the order of the model.

A schematic of the core model nodes is given in Figure 3.1. The model equations with their derivation and the data used are given in Appendix I.

3.3 The Steam Generator Model

The steam generator code simulating a U-tube natural recirculation steam generator is a linear code developed by Dr. A. R. Ali for his doctoral studies at The University of Tennessee (21). A few minor modifications were made to the initial version of the code by the French Designer Framatome (22) in order to improve agreement with a reference,

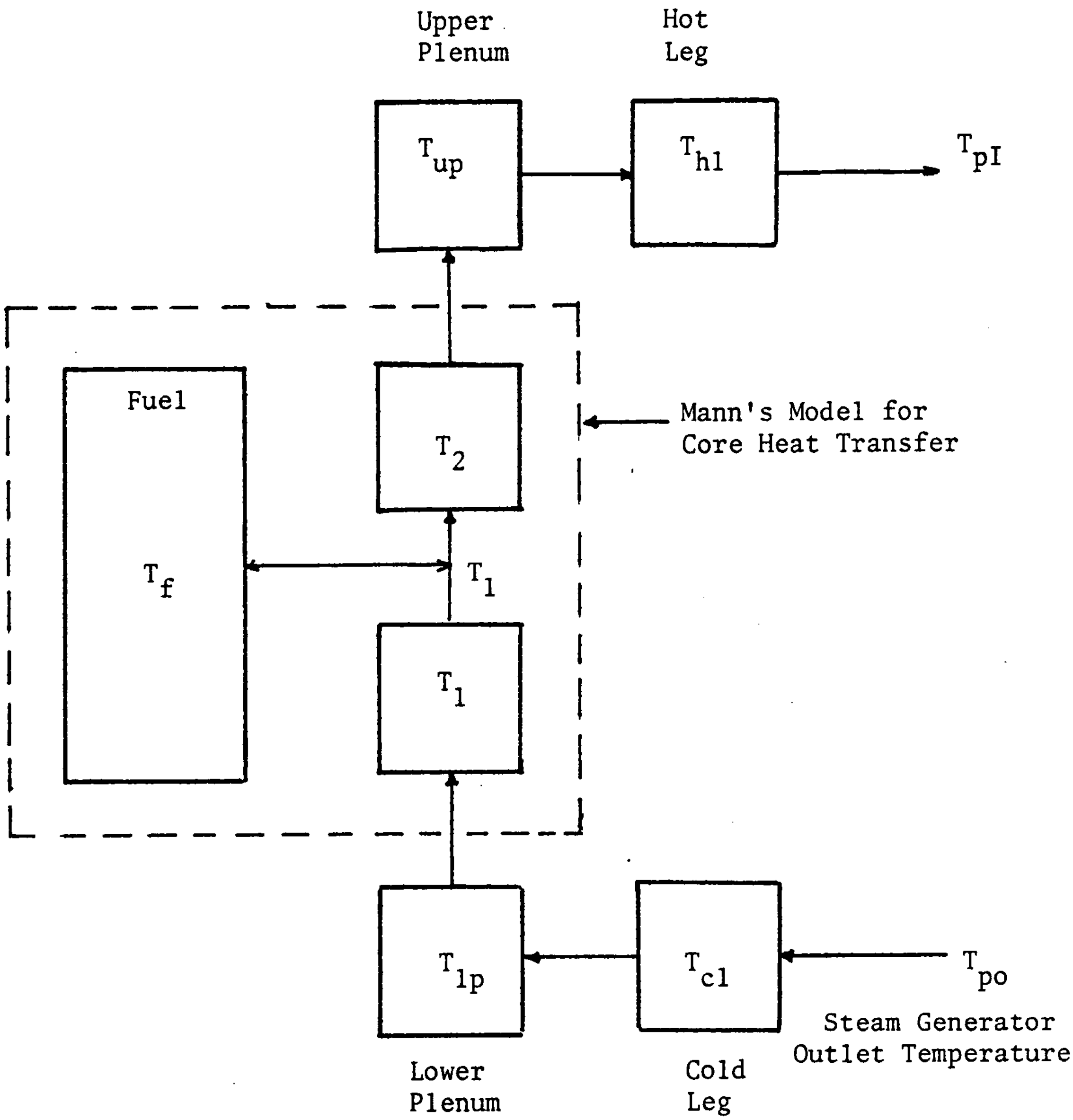

Figure 3.1 Schematic Diagram of the Core Model.

large, nonlinear, detailed code. The model consists of 15 differential and 4 algebraic equations, which are reduced to a system of 15 pure differential equations. The boundary between subcooled and boiling regions is a variable that is calculated explicitly by the code. A schematic diagram of the model's nodal structure is given in Figure 3.2.

From this figure one can distinguish: (a) The primary coolant loop, which consists of the inlet plenum node (PRI), the coolant nodes in the subcooled region (PR1, PR4), the coolant nodes in the boiling region (PR2, PR3), and the outlet plenum node (PRO). (b) The tube metal nodes corresponding to the primary coolant nodes, in the subcooled (M1, M4) and boiling (M2, M3) regions. (c) The secondary coolant loop, which consists of the downcomer (D), the subcooled node (S1), the boiling node (S2), the riser (S3), and the steam dome (S4).

The model equations with their derivation and the data used are given in Appendix II.

3.4 The Reactor Control System Model

The reactor control system design used at the power plant under study was furnished by the French Designer Framatome and the transfer functions of its various components can be seen in Figure 2.6, page 20. Following the same notion as in Figure 2.6 gives the corresponding differential equations. Since there are 24 differential equations describing the core and the steam generator, the reactor control system equations occupy the 25th-30th places in the overall system of equations, and they are given below. The state variables represent variations around the initial steady-state.

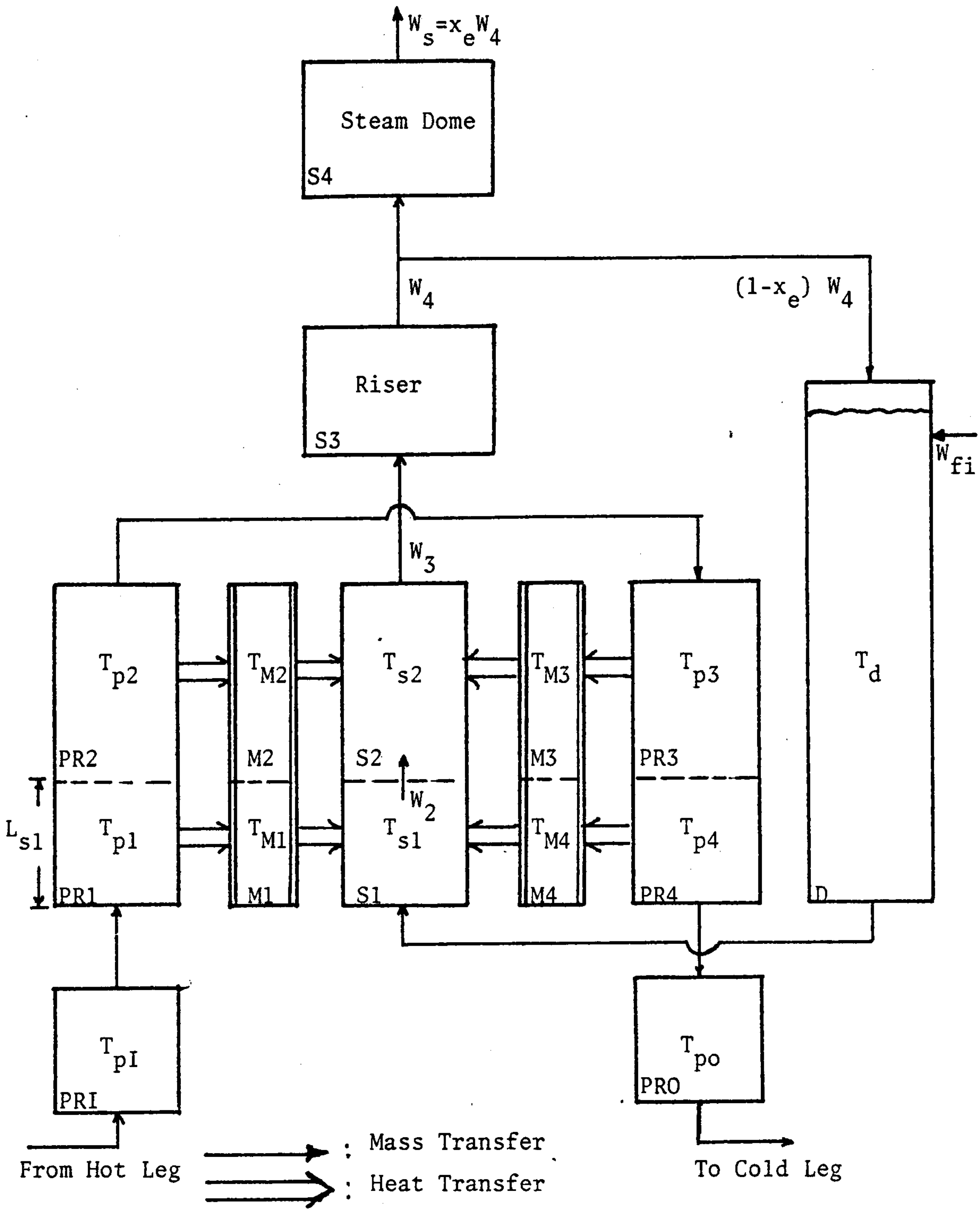

Figure 3.2 Schematic Diagram of the Steam Generator Model.

$$\frac{d\ Tavg}{dt} = \frac{0.5}{\tau_7} T_{h\ell} + \frac{0.5}{\tau_7} T_{c\ell} - \frac{1}{\tau_7} Tavg \tag{3.1}$$

$$\tau_2 \frac{d\ T\acute{a}vg}{dt} - \tau_1 \frac{d\ Tavg}{dt} = Tavg - T\acute{a}vg \tag{3.2}$$

$$\frac{dT\acute{a}v}{dt} = \frac{1}{\tau_3} T\acute{a}vg - \frac{1}{\tau_3} T\acute{a}v \tag{3.3}$$

$$\frac{dT\acute{r}ef}{dt} = \frac{ZKs}{\tau_5} Qtu - \frac{1}{\tau_5} T\acute{r}ef \tag{3.4}$$

$$\frac{dQp}{dt} + \frac{1}{\tau_6} Qp = \frac{dQ_N}{dt} - \frac{dQtu}{dt} \tag{3.5}$$

$$\frac{dQtu}{dt} = -\frac{1}{\tau_4} Qtu + \frac{1}{4} *(\text{load perturbation}) \tag{3.6}$$

The design values of the various parameters were not available. However, the values that were found to achieve a good reactor and steam generator water level control during the system simulation are presented in Chapter 7.

3.5 The Feedwater Control System Model

The feedwater control system in use today at the plant under study was employed, and the transfer functions of its various components can be seen in Figure 2.6, page 20. The differential equations deduced from these transfer functions, using the same notation as in Figure 2.6, are given below and they occupy the 31st-39th places in the overall system of equations. The state variables represent variations around the initial steady state.

$$\frac{dQv}{dt} = -\frac{1}{\tau_p} Qv + \frac{K^*}{\tau_p} *(\text{load perturbation}) \tag{3.7}$$

$$\tau_v \frac{dCQ_{e1}}{dt} = Q_v + Q_{v1} - CQ_{e1} \tag{3.8}$$

$$\frac{dCQ\acute{e}}{dt} = \frac{1}{\tau_e} L_e'' + \frac{1}{\tau_e} CQe_1 - \frac{1}{\tau_e} CQ\acute{e} \tag{3.9}$$

$$\frac{dCQe''}{dt} = \frac{1}{\tau_e} CQe'' - \frac{1}{\tau_e} Qe \tag{3.10}$$

$$\frac{dQv_1}{dt} = Qaux \tag{3.11}$$

$$D.\ \frac{dQaux}{dt} + B\,\frac{dQe}{dt} = A \cdot Qe - C \cdot Qaux - Qv_1 \tag{3.12}$$

$$\tau_d \frac{dLe''}{dt} - \tau_d' \frac{dL\acute{e}}{dt} = L\acute{e} - Le'' \tag{3.13}$$

$$\tau_i \frac{dL\acute{e}}{dt} + G \cdot \tau_i \frac{dL}{dt} = -G \cdot L + G \cdot (\text{Water level setpoint}) \tag{3.14}$$

The design values of the various parameters were not available. However, the values that were found to achieve a good feedwater control during the overall system simulation are presented in Chapter 7.

CHAPTER 4

PLANT TESTS

4.1 Introduction

In order to acquire a thorough knowledge of the dynamic behavior of a complex industrial process, like a nuclear power plant, it is important to perform dynamic tests which would reveal the various characteristics of the system's performance. These dynamic tests can be either of small amplitude, like a pseudorandom movement of the control rods, or of large amplitude, such as major perturbations in power demand. Tests of this later type are analyzed in this study.

4.2 Data Transmission Acquisition and Recording

Between each one of the sensors monitoring the physical process and the equipment (our data acquisition system) recording the various signals for the analysis purposes, there is a series of isolation amplifiers (IA). They insert a negligible amount of attenuation into the line for the incident signal and a large amount of attenuation into the line for the reflected signal. Thus, the sensor signals are protected against any alterations and they can be used reliably in the operation of the vital protection and control systems. A simple typical schematic of this is shown below:

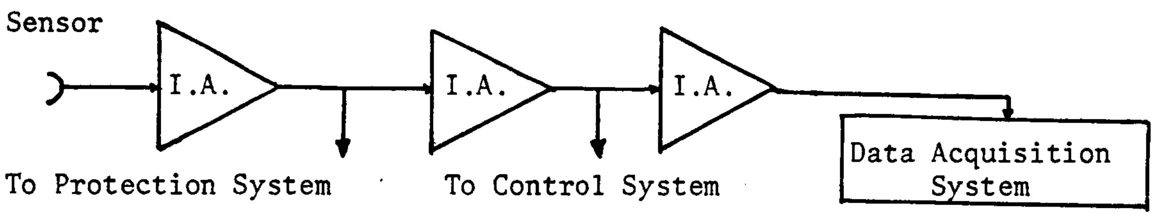

The data acquisition system used consists of 32 chains of signal conditioning connected to a 32-track analog tape recorder and two multi-track chart recorders which allow on-line verfication of the state of the test. The data acquisition system does not have any influence on the signals recorded, and it includes a stage for the rejection of the dc component when variations around a steady-state are to be recorded. A schematic diagram of the analog data acquisition and recording system is shown in Figure 4.1.

The operational limits for the voltage of each signal, corresponding to limits of the physical quantity being measured, are used. For example, for the water level signal, 0.4 volts corresponds to 0% level and 2.0 volts corresponds to 100% level. The gains on the amplifiers for each signal were preset to accommodate the voltages expected to occur during the tests.

During large power demand perturbations at low power, like the 30-20% step decrease, there is special concern about certain signals such as the steam flow and water level signals. Due to the very large perturbation, large peaks of noise may trigger the protection and control systems with undesirable consequences. To overcome this problem, the signal coming from the sensor is passed first through a low-pass filter:

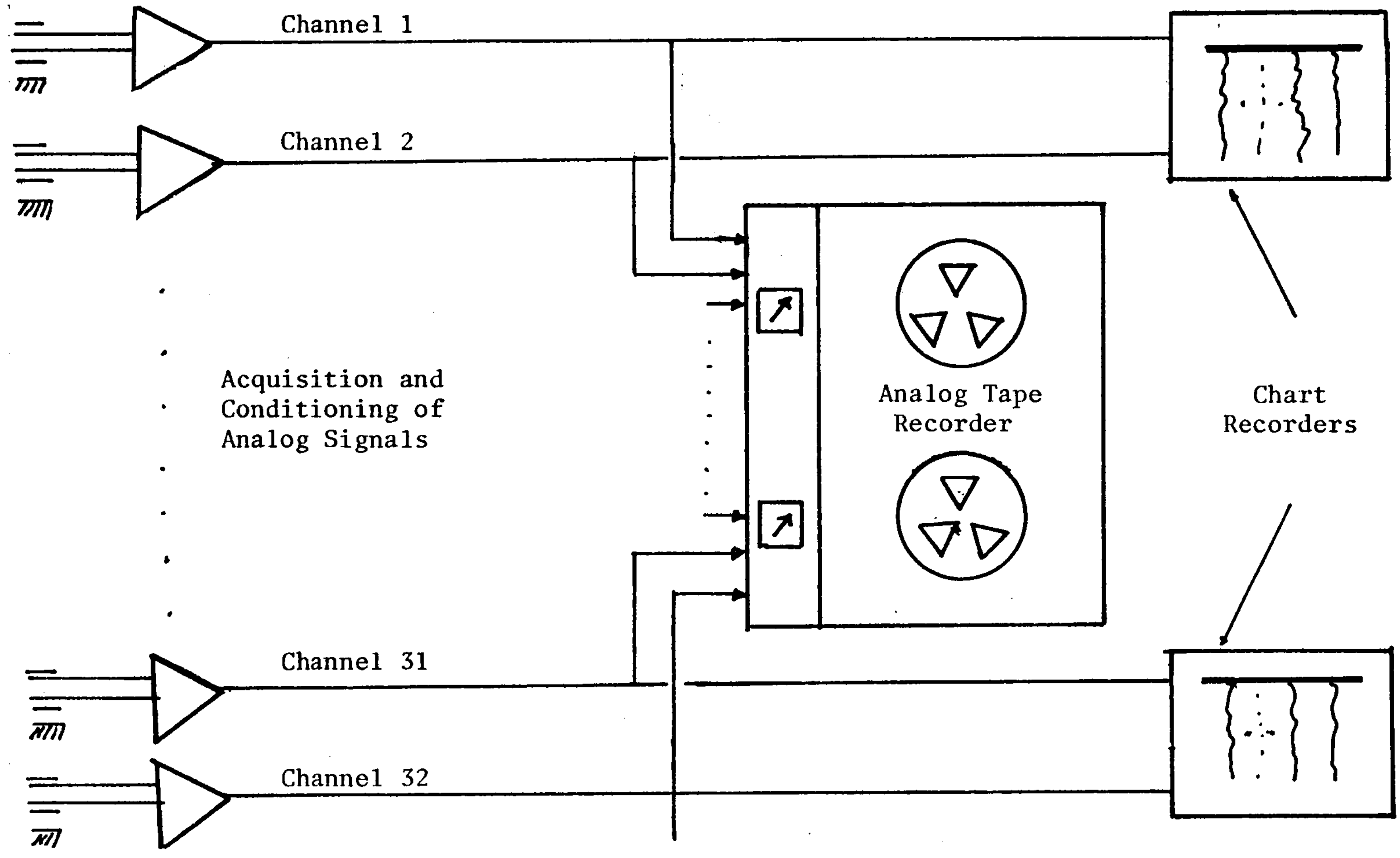

Figure 4.1 Schematic Diagram of the Data Acquisition and Recording System.

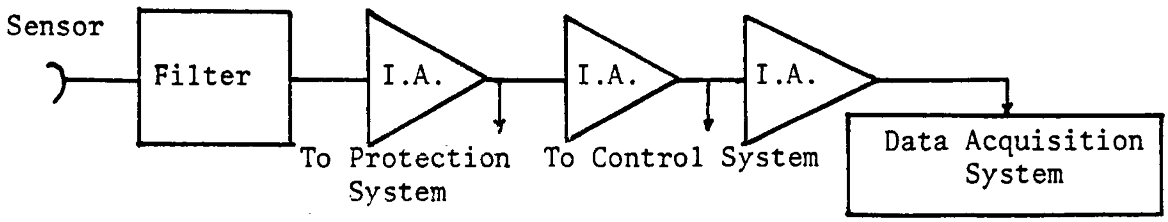

In the case of the transient at low power, the filters used reportedly had a 25 second time constant for the steam flow rate signal and a 30 second time constant for the water level signal. Since the heavily filtered steam flow signal does not represent the real behavior of the steam flow, a special effort must be made to reconstruct the nonfiltered signal, before it can be used as an input to our steam generator model. This effort is described in Chapter 6. The water level is an output of the steam generator model, and thus it is passed through a filter of the same magnitude, before it is compared to the experimental water level filtered signal.

During the test at low power, there was an additional problem encountered with the signal recording. There was a data-logging computer (to routinely record all the plant signals) with undesirable input characteristics. It acted as a low-pass filter on the signals recorded. It is shown schematically below:

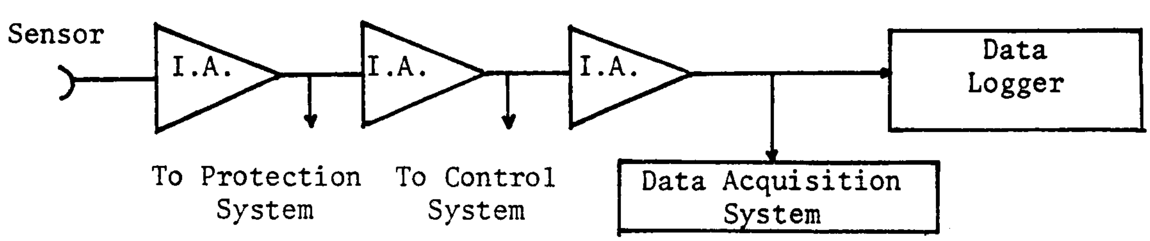

The effort to find the magnitude of this filtering effect is presented in Section 4.4.

4.3 Tests and Typical Data

The dynamic behavior of the core and the U-tube steam generator of a typical 900 MWe PWR was studied at full power and at a low power level, using the recorded transients of the physical quantities of interest (temperatures, pressures, etc.) after power demand step perturbations. Both tests under study were performed during the initial start-up of the reactor. The first test was a 30-20% step decrease in power demand, and the second test was a 100-90% step decrease in power demand. The absolute magnitudes of the two step perturbations are similar, but one should note that at low power the relative magnitude of the step perturbation is approximately 35% with respect to the initial steady-state power level. The use of linear models to analyze a perturbation of this magnitude is questionable, but the results of the analysis have shown the good response of the linear models used to a perturbation of this magnitude.

The signals necessary for the analysis of the core model are the two inputs: control rod reactivity and cold leg temperature, and the two outputs: nuclear power and hot leg temperature. The signals necessary for the analysis of the steam generator model are the four inputs: hot leg temperature, steam flow rate, feedwater flow rate, feedwater temperature, and the three measurable outputs: cold leg temperature, steam pressure, and water level. Thus, we need a total of nine different signals (shown in Figures 4.2 and 4.3 for the tests at full power and at low power, respectively).

Publication of the physical magnitude of these signals and of the time scale was prohibited by the owner of the power plant. However,

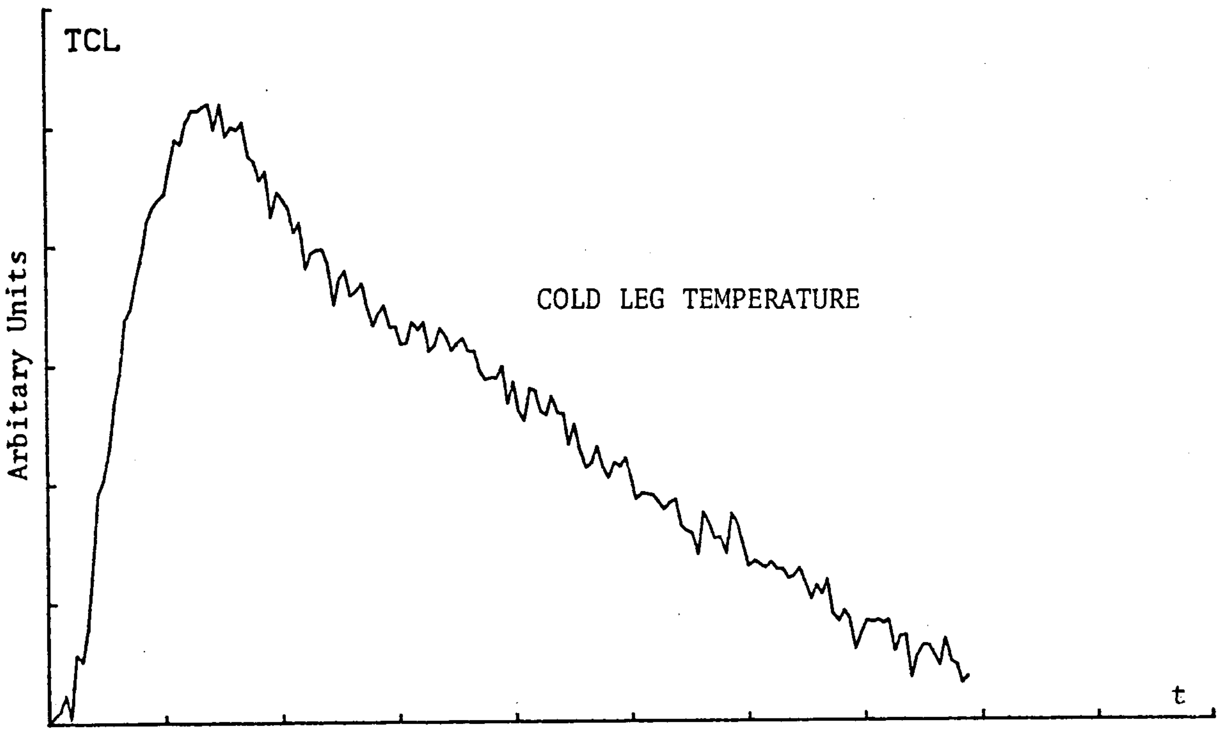

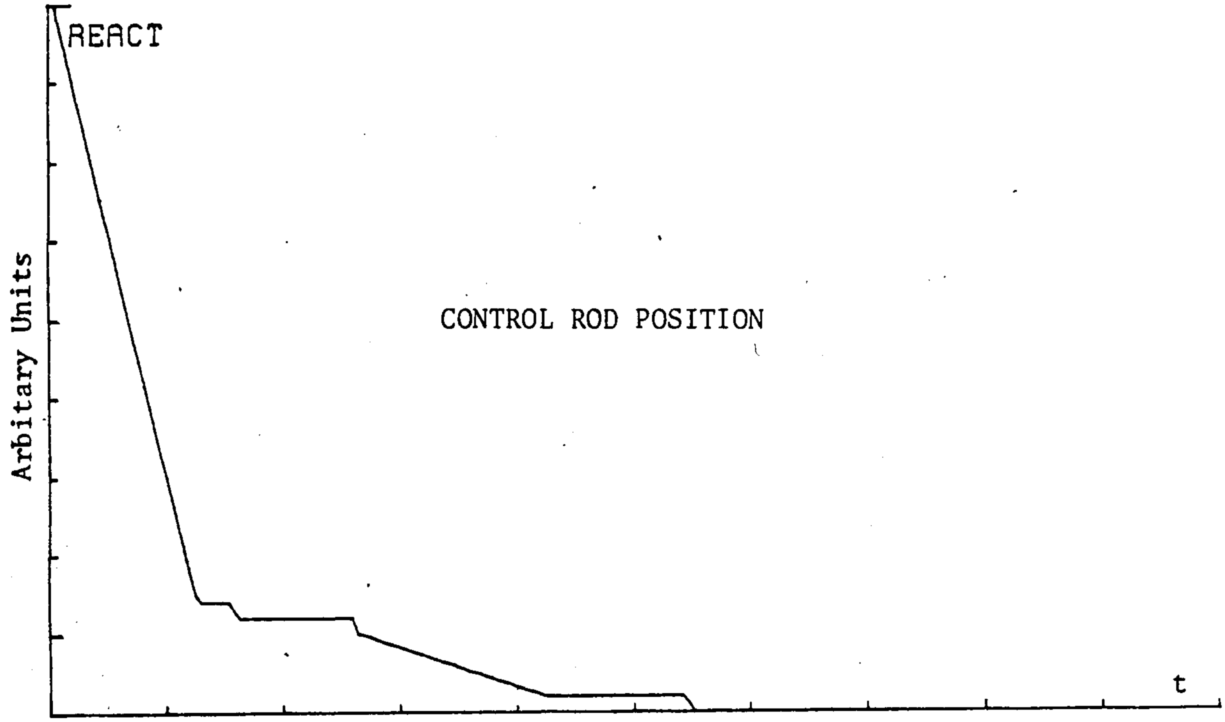

Figure 4.2 Test Signals for a 100-90% Power Demand Step Perturbation.

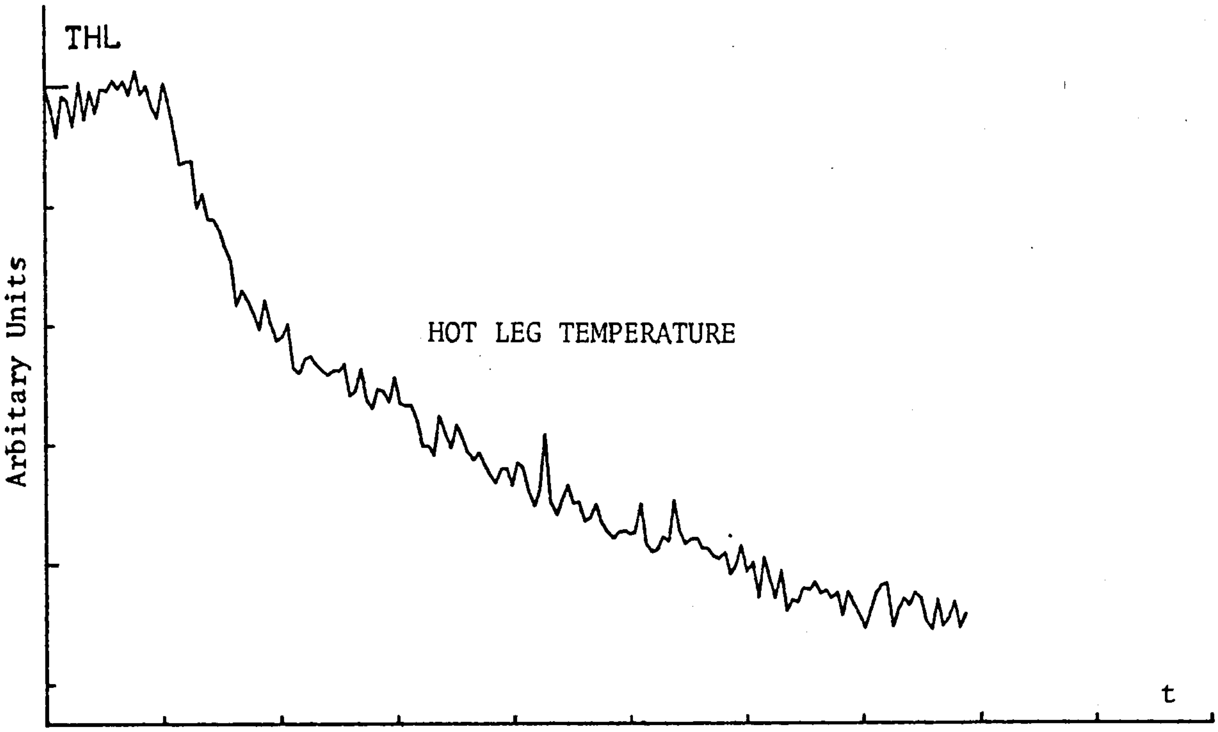

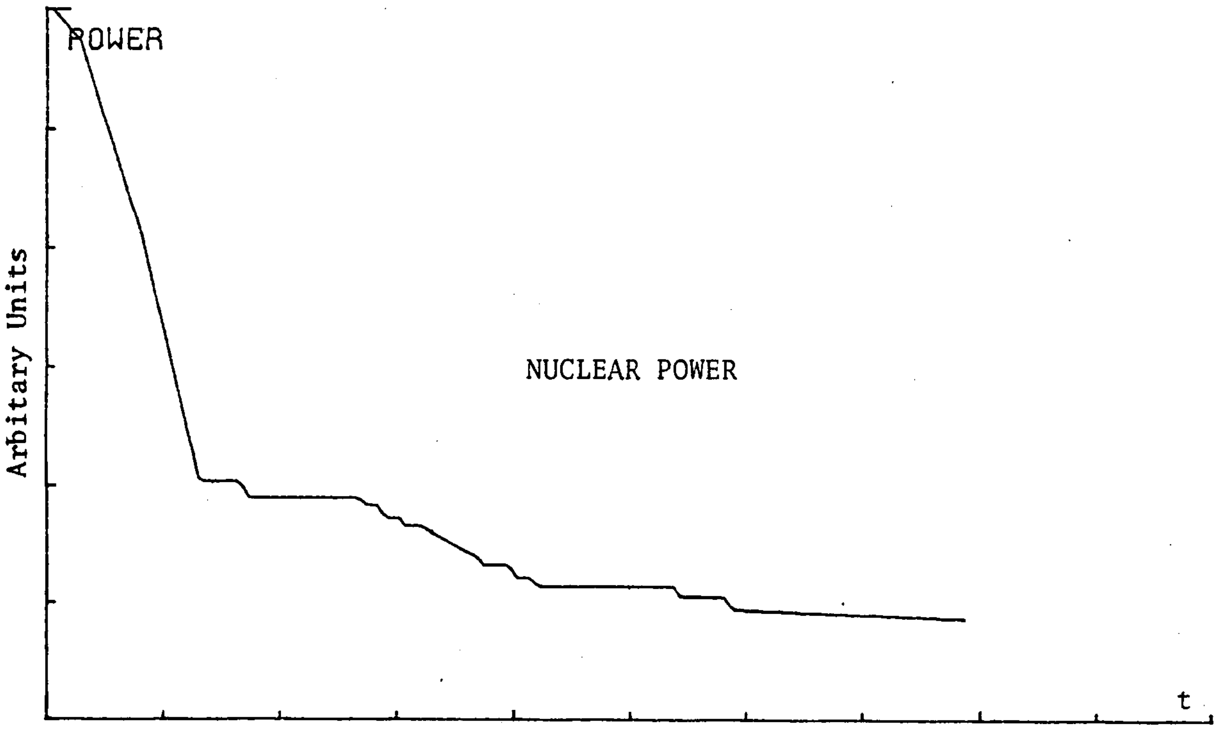

Figure 4.2 (Continued)

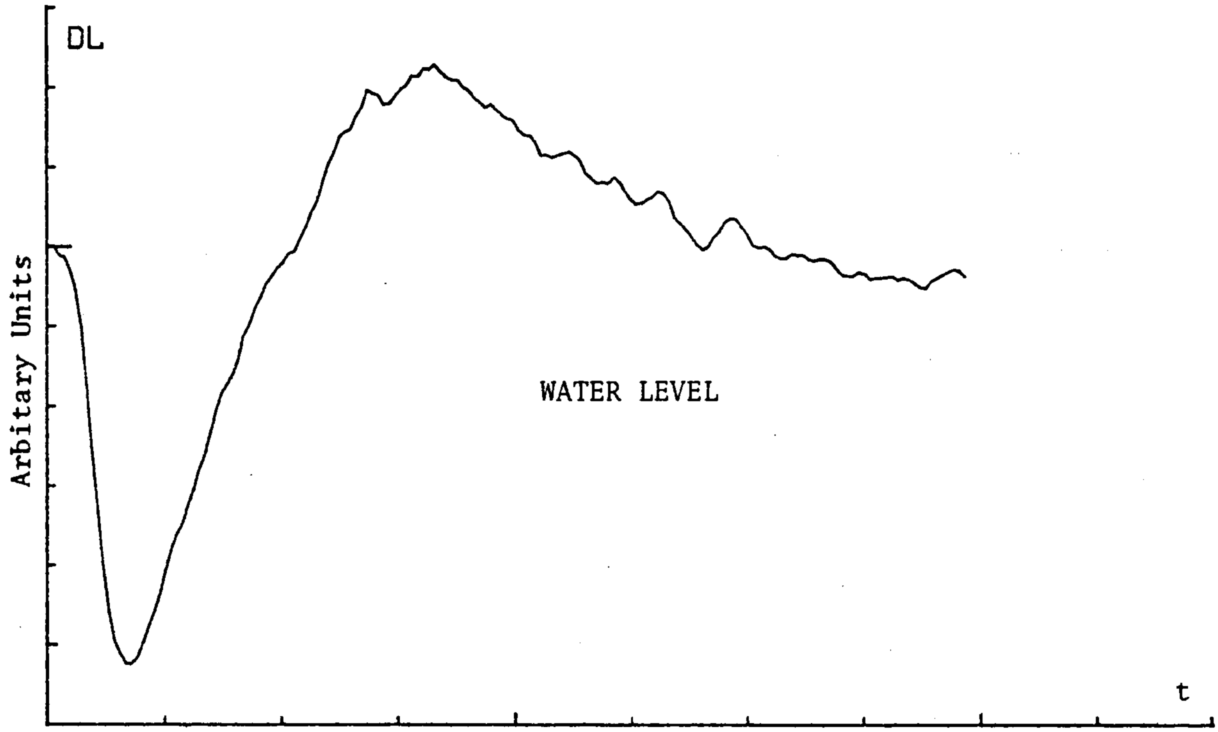

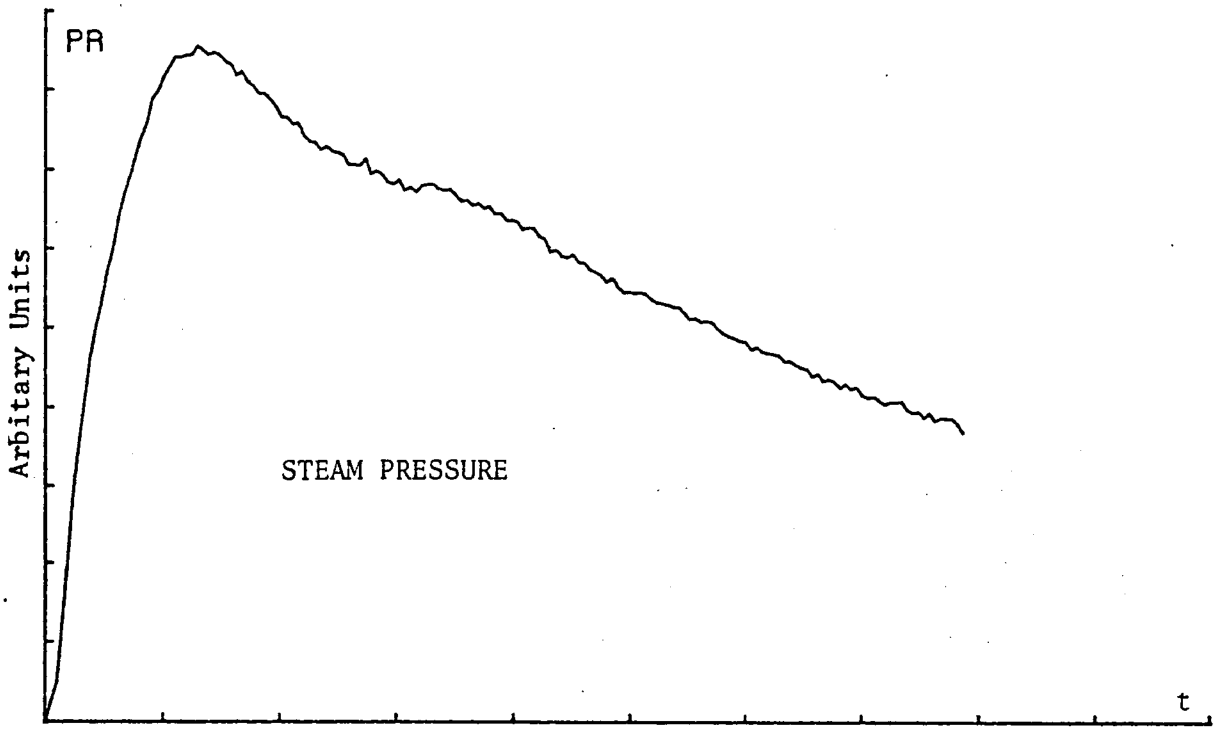

Figure 4.2 (Continued)

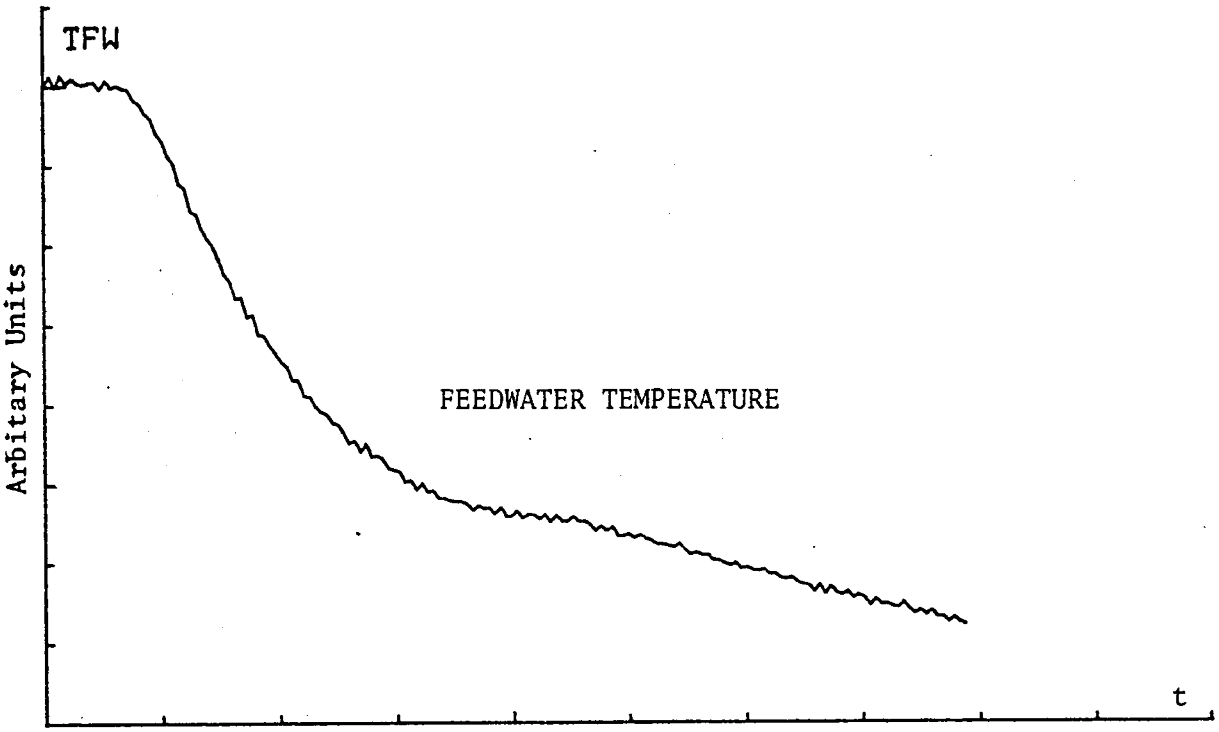

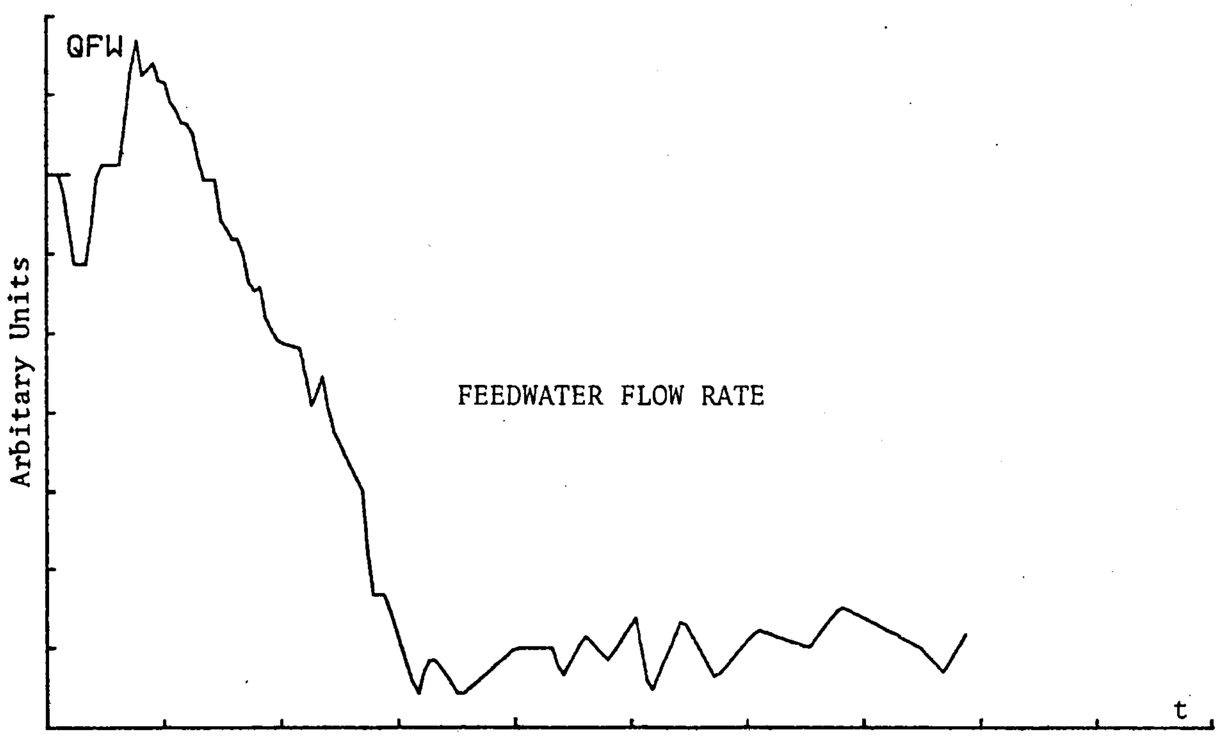

Figure 4.2 (Continued)

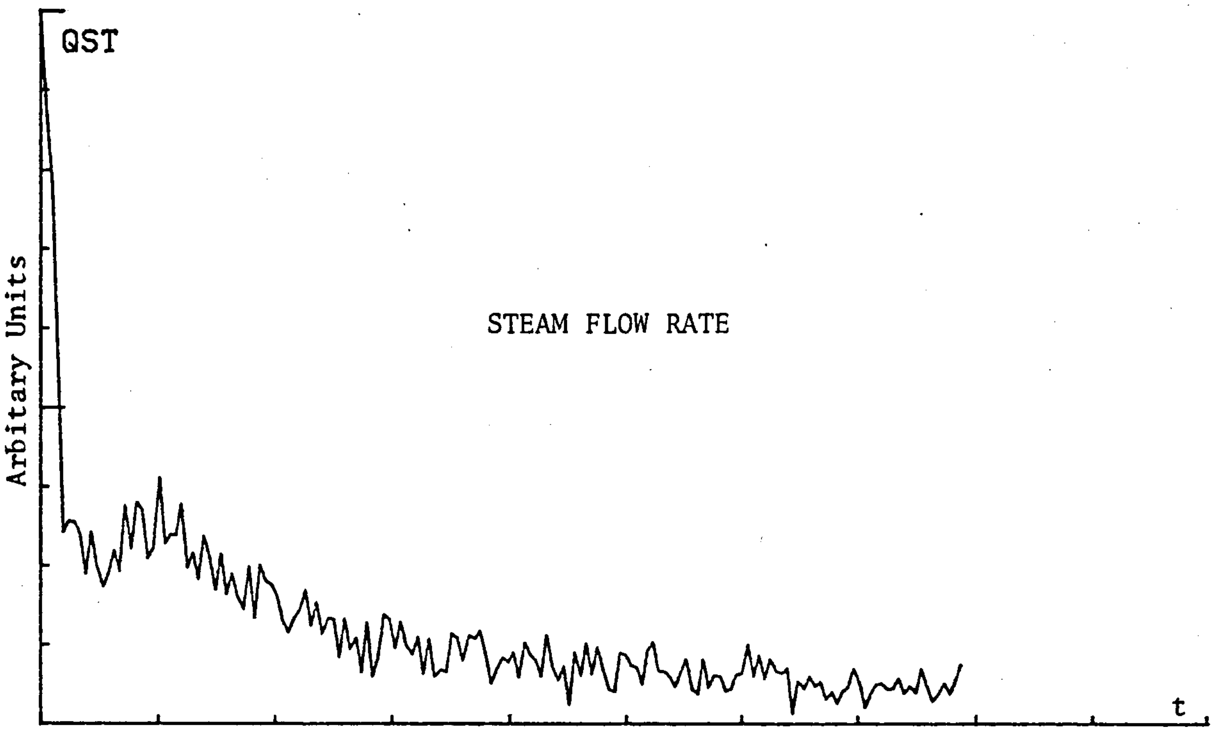

Figure 4.2 (Continued)

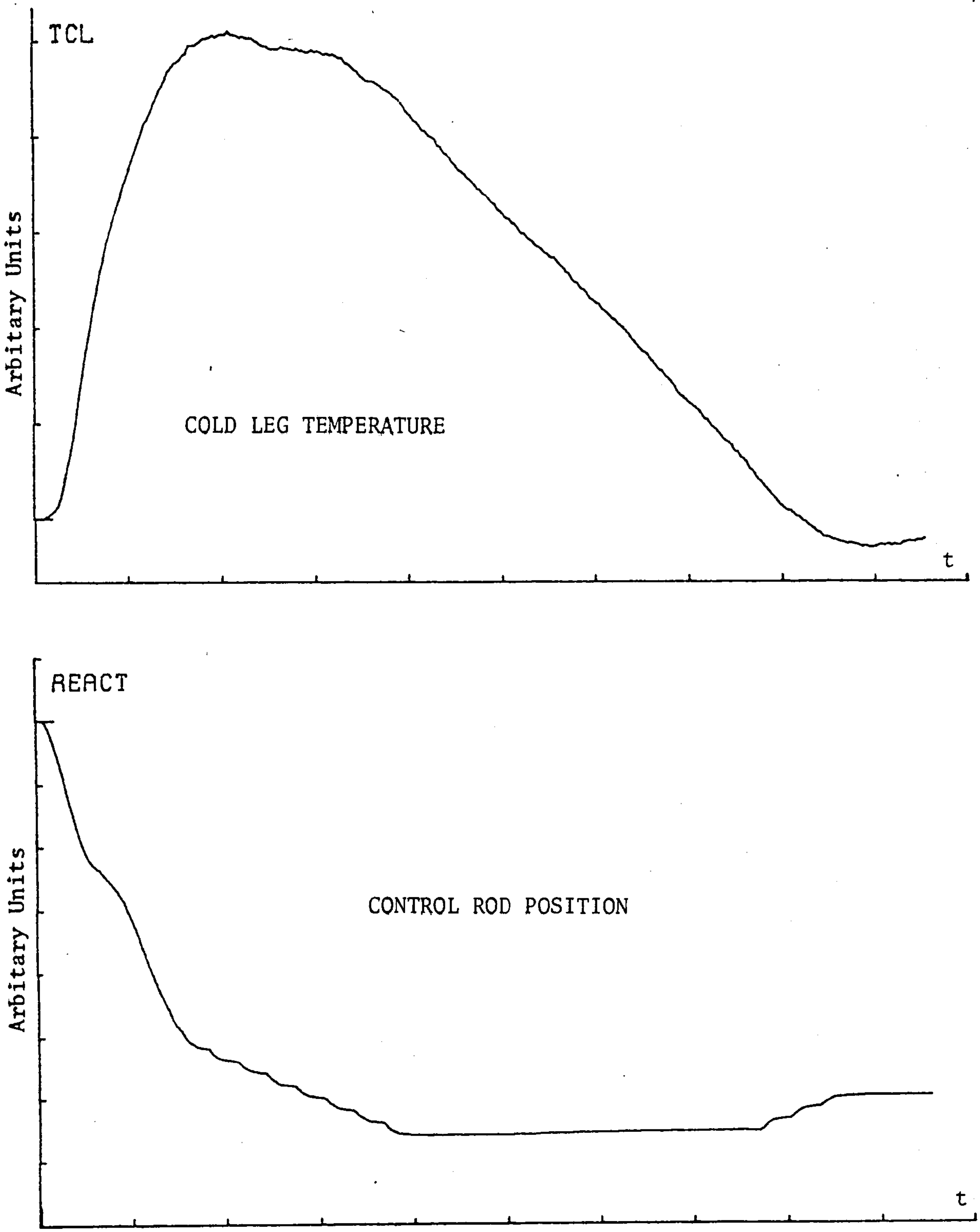

Figure 4.3 Test Signals for a 30-20% Power Demand Step Perturbation.

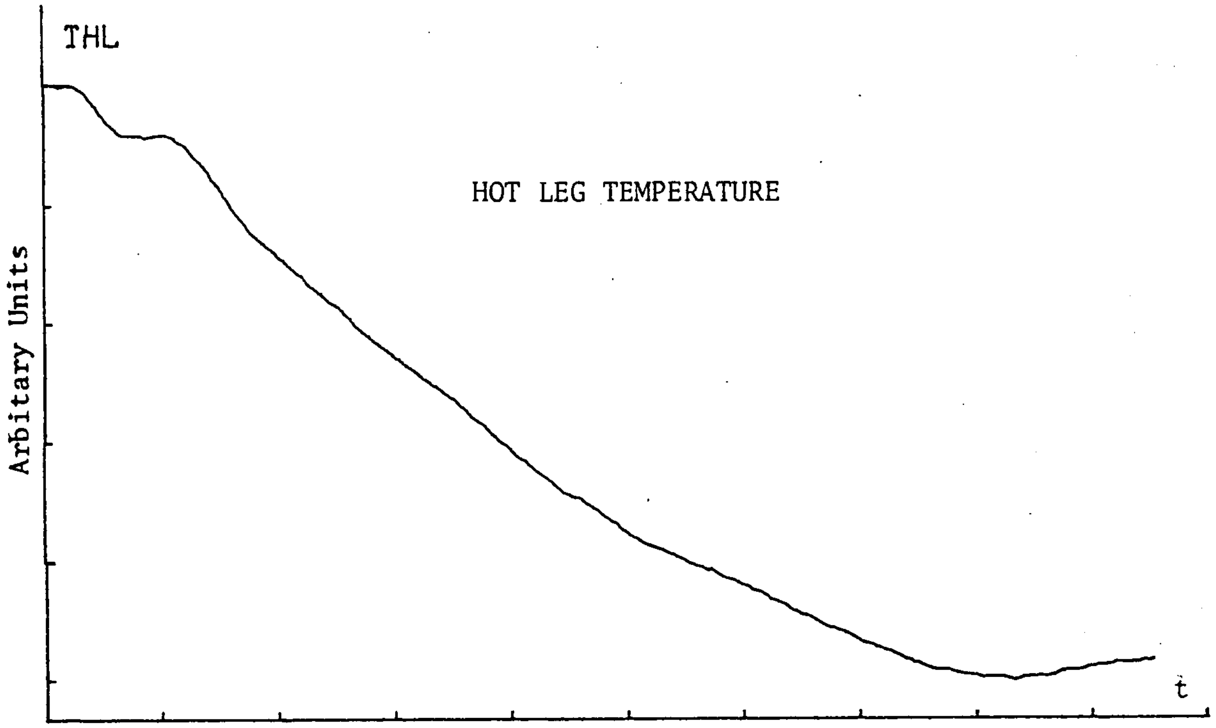

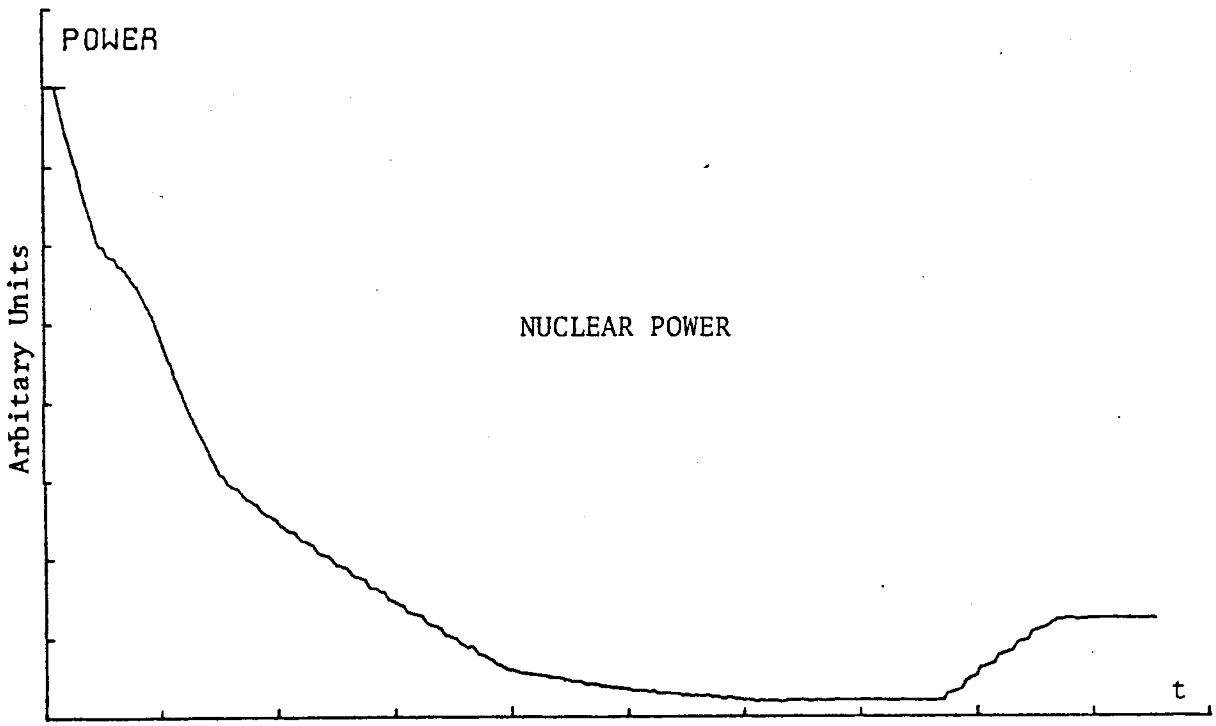

Figure 4.3 (Continued)

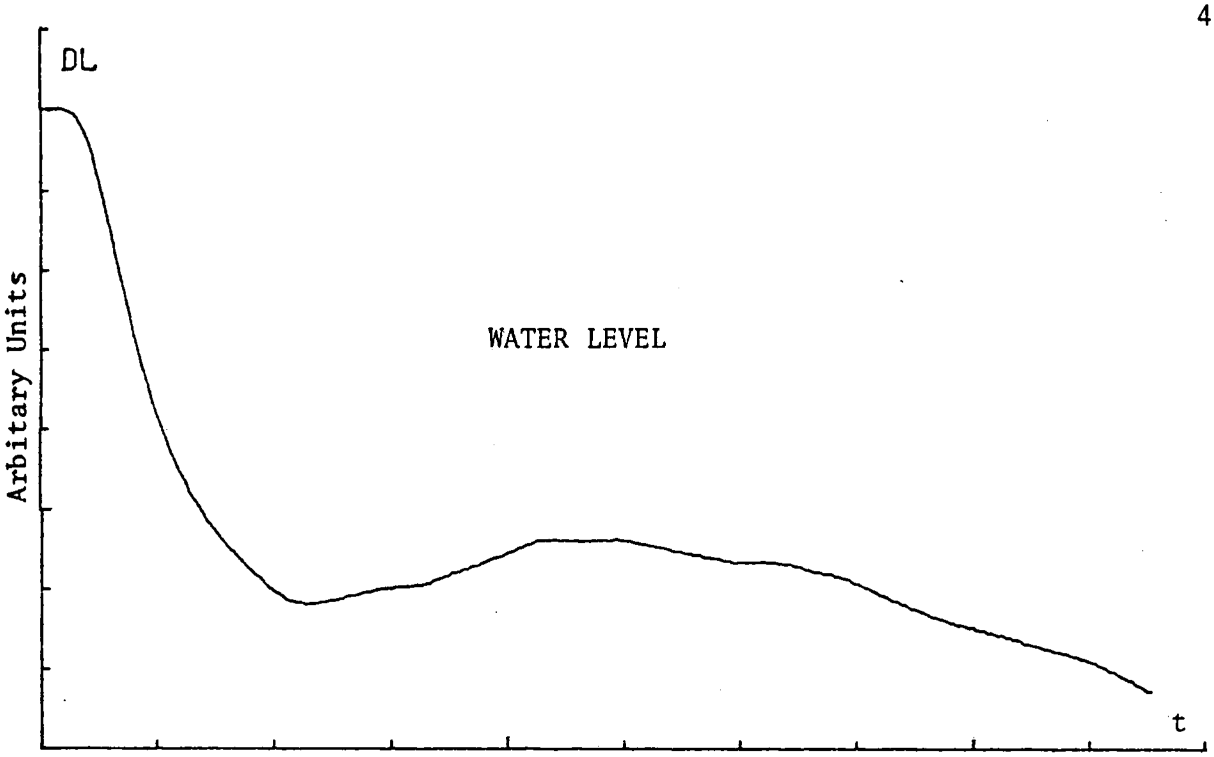

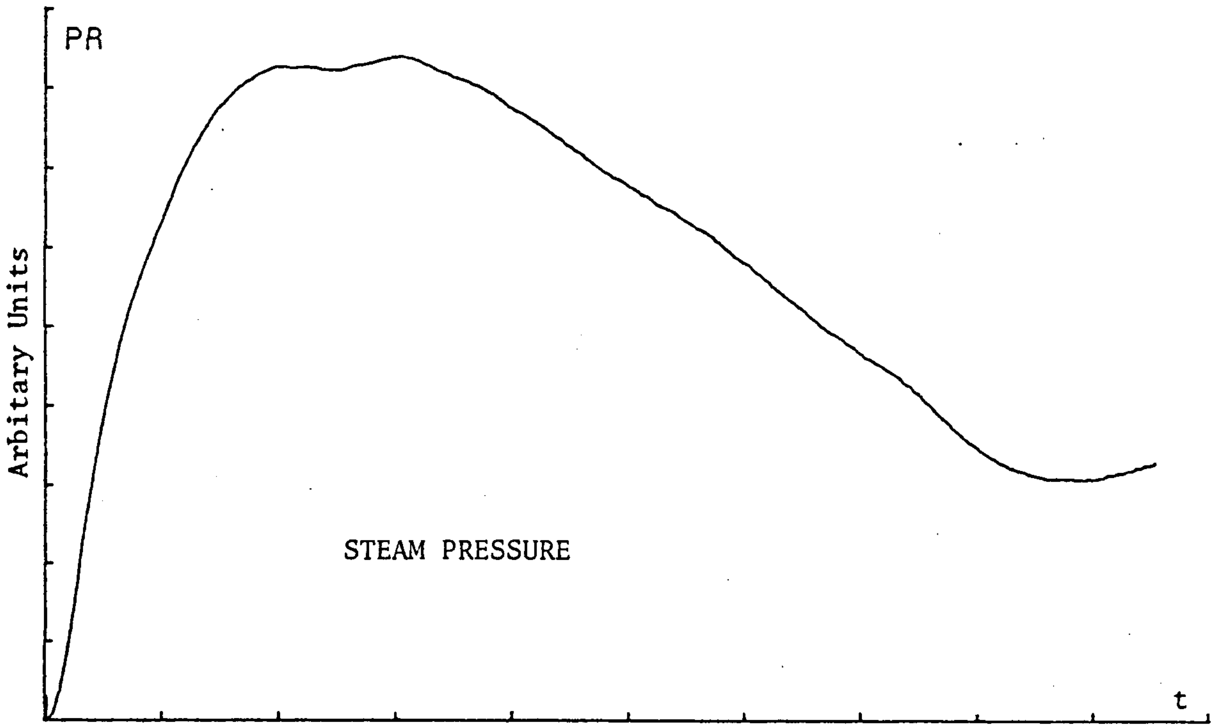

Figure 4.3 (Continued)

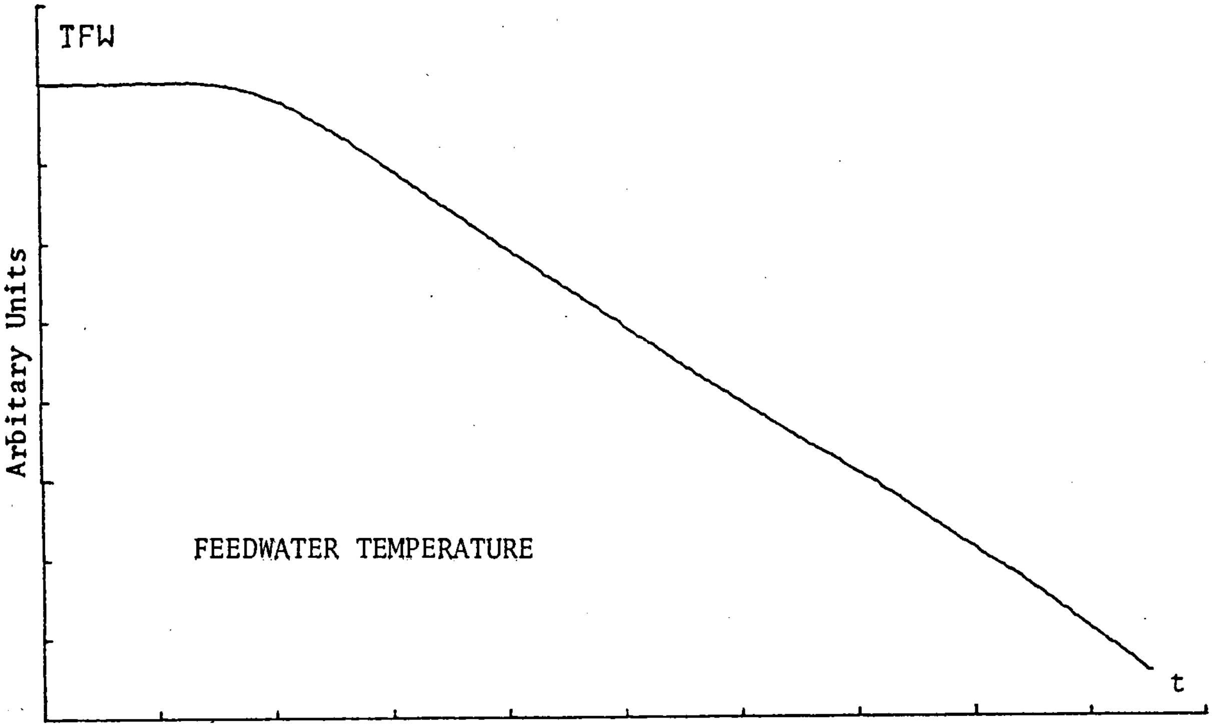

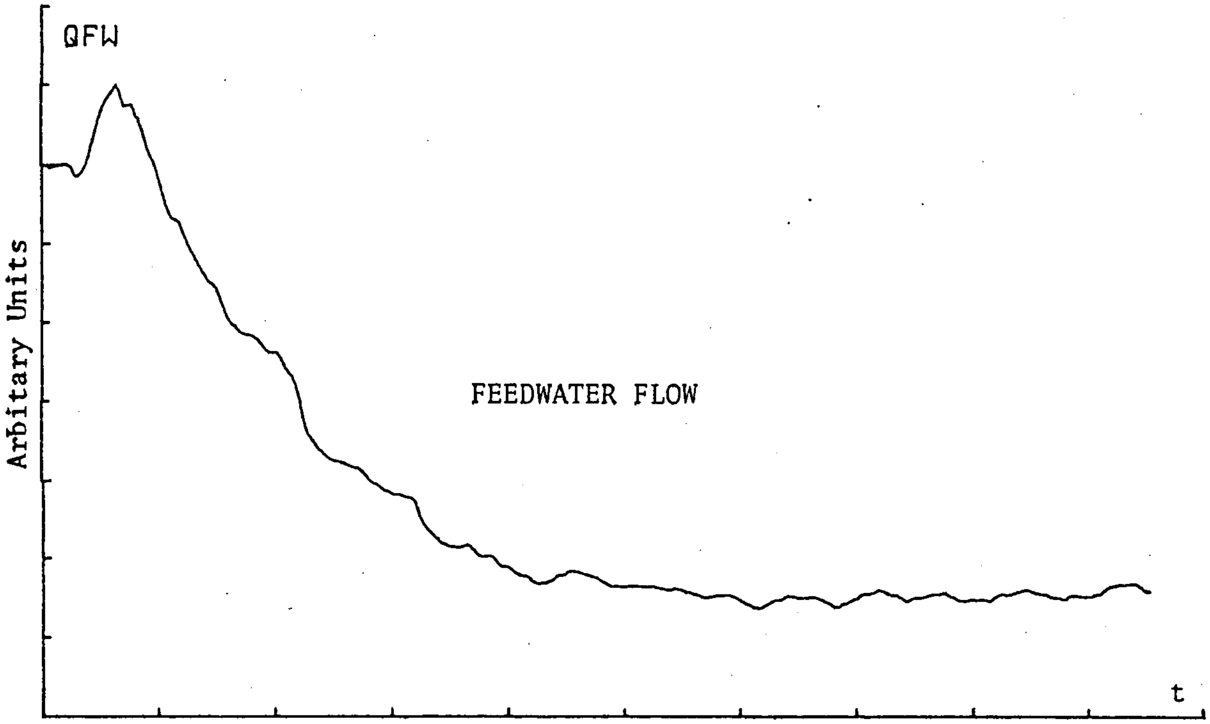

Figure 4.3 (Continued)

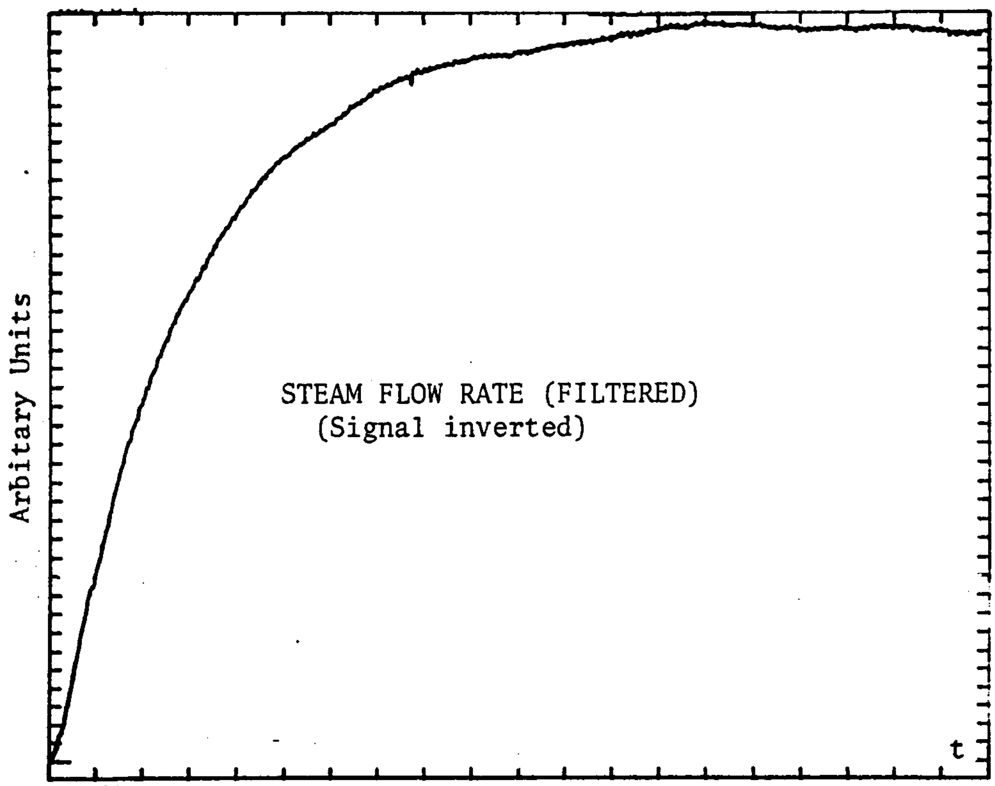

Figure 4.3 (Continued)

their time duration is of the order of a few minutes, and it was considered that this time duration was sufficient to represent the dynamic behavior of the core and the steam generator after the power demand step perturbations discussed above.

4.4 Noise Analysis of the Signals Used

As was discussed in Section 4.2, the data-logger connected to the data acquisition chain during the test at lower power acted as a filter on the signals being recorded. Thus, it was necessary to find the magnitude of this effect, before these signals could be used in any identification study.

This was done by analyzing the noise of a temperature signal during a steady-state condition with the data-logger connected. The Power Spectral Density (PSD) of the signal noise was obtained. The filtering process was modeled with a third order transfer function, and its input noise was assumed to be white. Thus, the PSD of the input is assumed constant so that the dynamics of the PSD of the output represents the dynamics of the process. Then, fitting of the theoretical and experimental PSDs was performed to find the time constant introduced. Very good textbooks exist on Noise Analysis, for example, Bendat and Persol (23) and Uhrig (24), but for the sake of completeness a brief outline of the theory behind this particular study will be given here.

Noise can be defined as being the random fluctuations of sensor output about the mean value, and noise analysis is a statistical analysis of the noise in order to extract information about the system for diagnostic and surveillance purposes. The spectral density analysis used in this study is one of the procedures that can be followed.

The random variable represented by the noise signal is assumed to be stationary (i.e., its statistical characteristics do not change with time). Furthermore, let us consider taking N individual measurements (records), called an ensemble of records, and form the ensemble average by calculating the average value of the random variable x(t) at any time t = t* over all the records, i.e.

$$< x(t^*) > = \lim_{N\to\infty} \frac{\sum_{i=1}^{N} x_i\,(t^*)}{N}$$

For a stationary process the ensemble averages remain constant regardless the choice of the time instant t*. Let us also consider the time average of a single sample record, $x_i(t)$, i.e.

$$x_i(t) = \lim_{T\to\infty} \frac{1}{2T} \int_{-T}^{T} x_i(t)\,dt$$

which should be the same for any i. We will assume that the stationary process under study is also ergodic, i.e., the common value for the ensemble average at any time < x(t) > must be equal to the common value for the time average of any record $\overline{x_i(t)}$ (23). Now we can compute the power spectral density, $S_{xx}(f)$, which is the average power per unit frequency evaluated for a particular frequency f. The procedure for a digital computation of $S_{xx}(f)$ is as follows (23):

1. Obtain the signal $x_k(t)$ for duration T, where k is the index of the ensemble record under study.

2. Construct the Fourier Transform of $x_k(t)$:

$$X_k(f,T) = \int_o^T x_k(t)\, e^{-j2\pi ft} dt$$

and find its conjugate $X_k^*(f,T)$.

3. Construct the vector product

$$S_{xx}(f,T,k) = \frac{1}{T} X_k^*(f,T)\; X_k(f,T)$$

4. Obtain the expected value

$$E[S_{xx}(f,T,k)] = \frac{1}{N} \sum_{k=1}^{N} S_{xx}(f,T,k) \equiv S_{xx}(f,T)$$

which for sufficiently large values of T is the power spectral density $S_{xx}(f)$. The Fourier Transform, X_k, is estimated using Fast Fourier Transform digital computer procedures.

The power spectral densities were calculated with and without the logging computer and the results are shown in Figure 4.4. One can clearly see the effect of having the computer connected to the sensor output signals.

We model the whole filtering process by a transfer function of third order (assuming also white noise input):

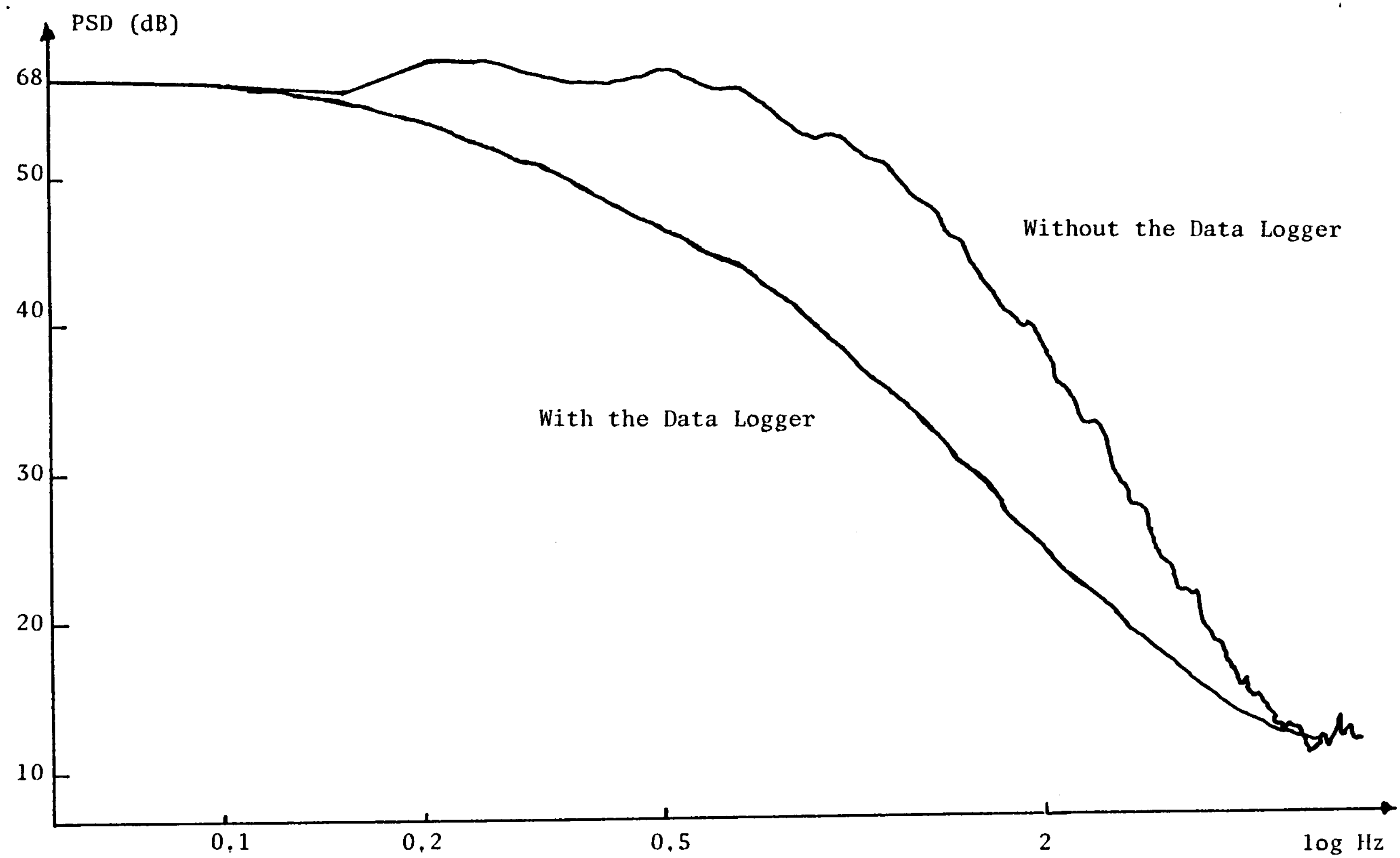

Figure 4.4 Comparison of PSD's With and Without the Data Logger.

$$H(s) = \frac{a_1}{s+b_1} + \frac{a_2}{s+b_2} + \frac{a_3}{s+b_3}$$

The magnitude of the frequency response was found, and spectrum fitting was tried with the power spectral density that was calculated experimentally, as was described above. The problem reduces to a six-parameter identification problem (a_1, a_2, a_3, b_1, b_2, b_3) with the error criterion being the square of the difference between the two spectra, as shown in Figure 4.5. The Simplex method described in Appendix III and used later in the study for the model identification work, is employed for the optimization search, and the final fitting of the spectrum is shown in Figure 4.6. When the optimal values for a_1, a_2, a_3, b_1, b_2, and b_3 are substituted in the transfer function and its step response is calculated, Figure 4.7, we obtain the time constant associated with the filtering process, and it was found to be three seconds. Thus, during the core and steam generator parameter identification (Chapter 6), the outputs of the models are modified by a filter with a three-second time constant before they are compared with the experimental (also filtered with three-second filter) outputs.

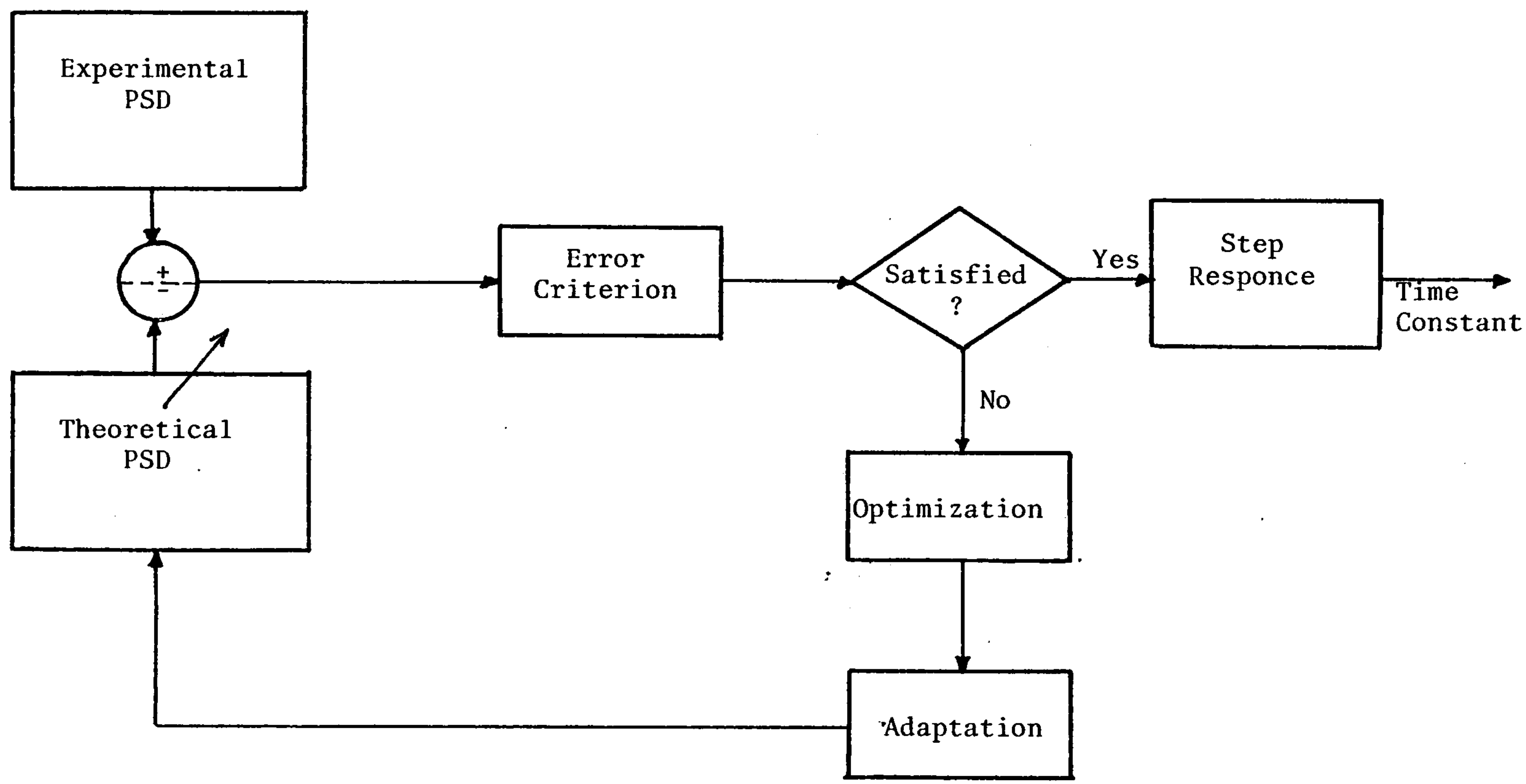

Figure 4.5 Schematic Diagram of Power Spectrum Fitting Method.

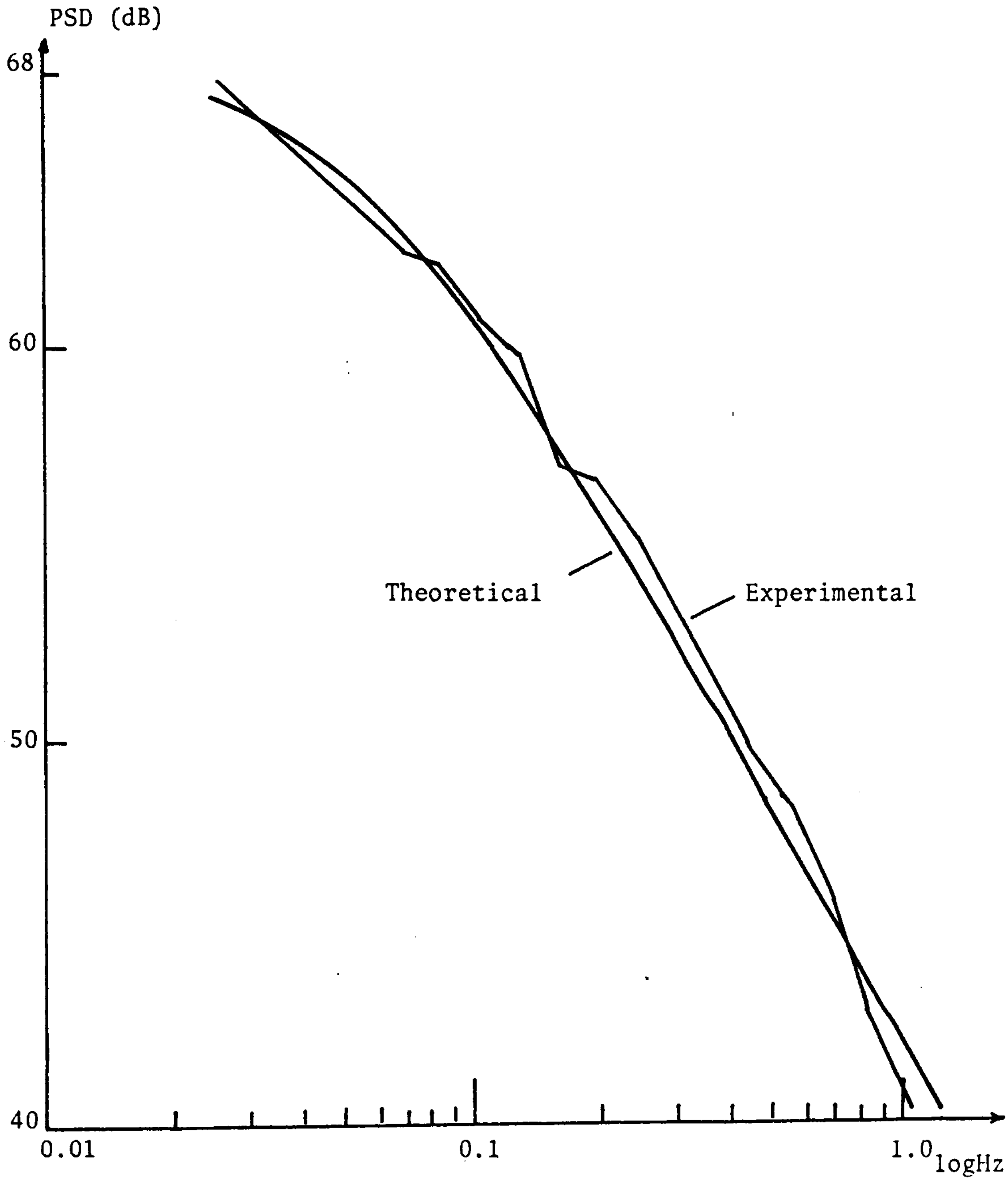

Figure 4.6 Power Spectrum Fitting.

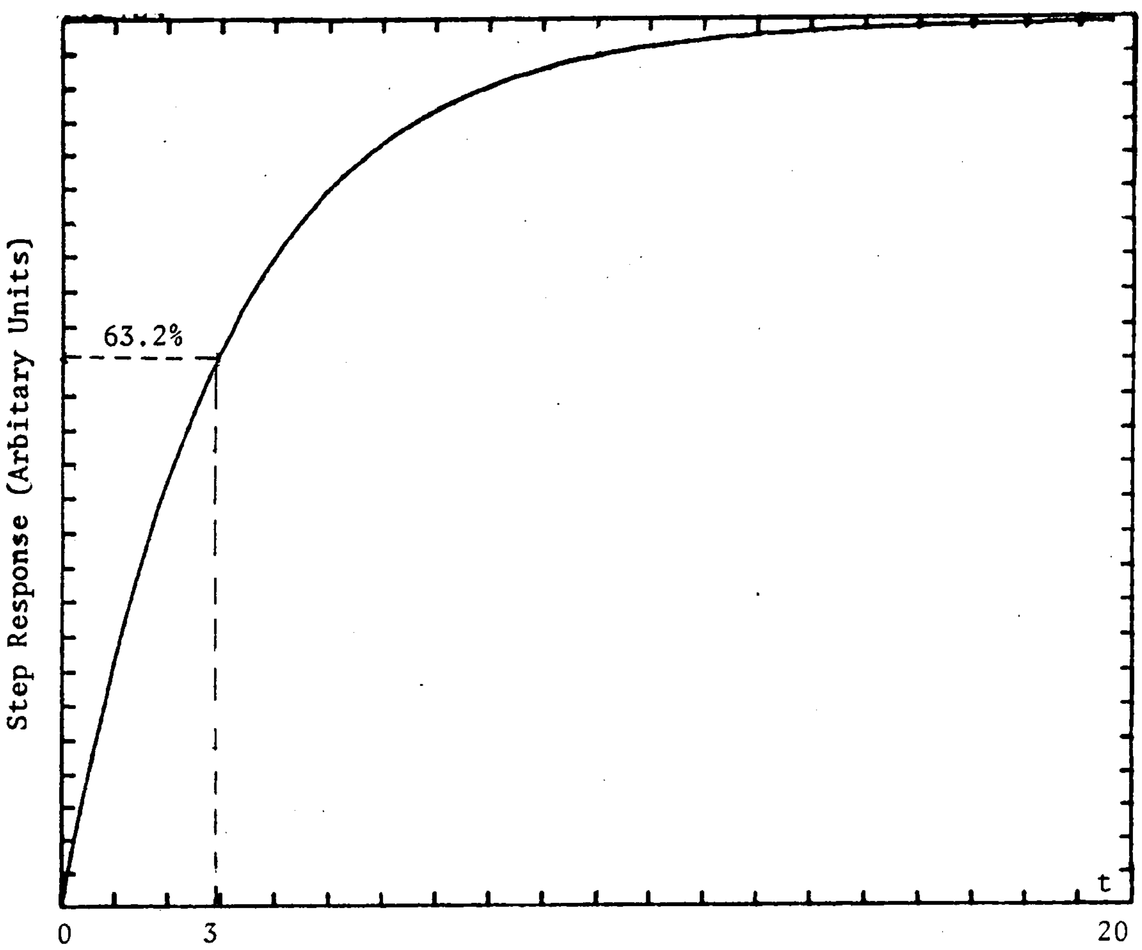

Figure 4.7 Step Response of the Third Order Transfer Function H(s).

CHAPTER 5

SENSITIVITY ANALYSIS OF THE STEAM GENERATOR MODEL

5.1 Introduction

The difference between experiment and model prediction is due to uncertainties in the mathematical model itself and in the values of the various parameters used. Analysis of the effects of the various assumptions made during the development of the mathematical model is quite involved, and there is no systematic procedure for finding the sensitivity of the predicted performance to model changes. However, sensitivity analysis of the model dynamic performance to parameter changes is straightforward and requires little extra effort.

Sensitivity analysis is very useful, especially when model parameter identification work is to be undertaken. It can furnish valuable information on the importance of some key, nonmeasurable parameters to the model dynamic performance. This information is necessary to determine the parameters which should be included in the identification scheme.

The sensitivity analysis of the steam generator model performance to three parameters (primary coolant specific heat capacity Cp_1, change in the primary to secondary overall heat transfer coefficient (U) and initial steam exit quality (X_{eo}) was undertaken at full power and at low power level, and the results are presented in this chapter. The choice of the parameters studied is not unique, since additional parameters could have been included in this sensitivity analysis, as well as in the parameter identification discussed in Chapter 6. However, within the scope and the time-frame of this study, only the effects of the three parameters mentioned above were considered.

Additional information included in this chapter is the effect of the feedwater inlet temperature on the dynamic performance of the model. It will be required in Chapter 7 for the interpretation of the overall system simulation performance (reactor core, steam generator, and control systems), where the feedback effect of the feedwater temperature is not included.

5.2 Effect of ±10% Changes in Key Physical Parameters

The results of the sensitivity analysis for each parameter studied are presented in this section, both for a test at full power (100-90% power demand step perturbation) and at a low power level (30-20% power demand perturbation). All three measurable outputs of the steam generator, i.e., primary outlet temperature, secondary pressure and water level are examined. The reference transients are plotted. The transients corresponding to +10% and -10% parameter changes are the points represented by the crosses and circles respectively. An effort is also made to give a plausible physical interpretation of the dynamic performance of the model for these parametric changes. Arbitary Units (A. U.) are used.

The effect of changes in C_{pl} can be seen in Figures 5.1 and 5.2. This effect is weaker during the early part of the transient due to the fact that the first part of the transient is determined primarily by the strong steam flow rate change. The product of primary flow

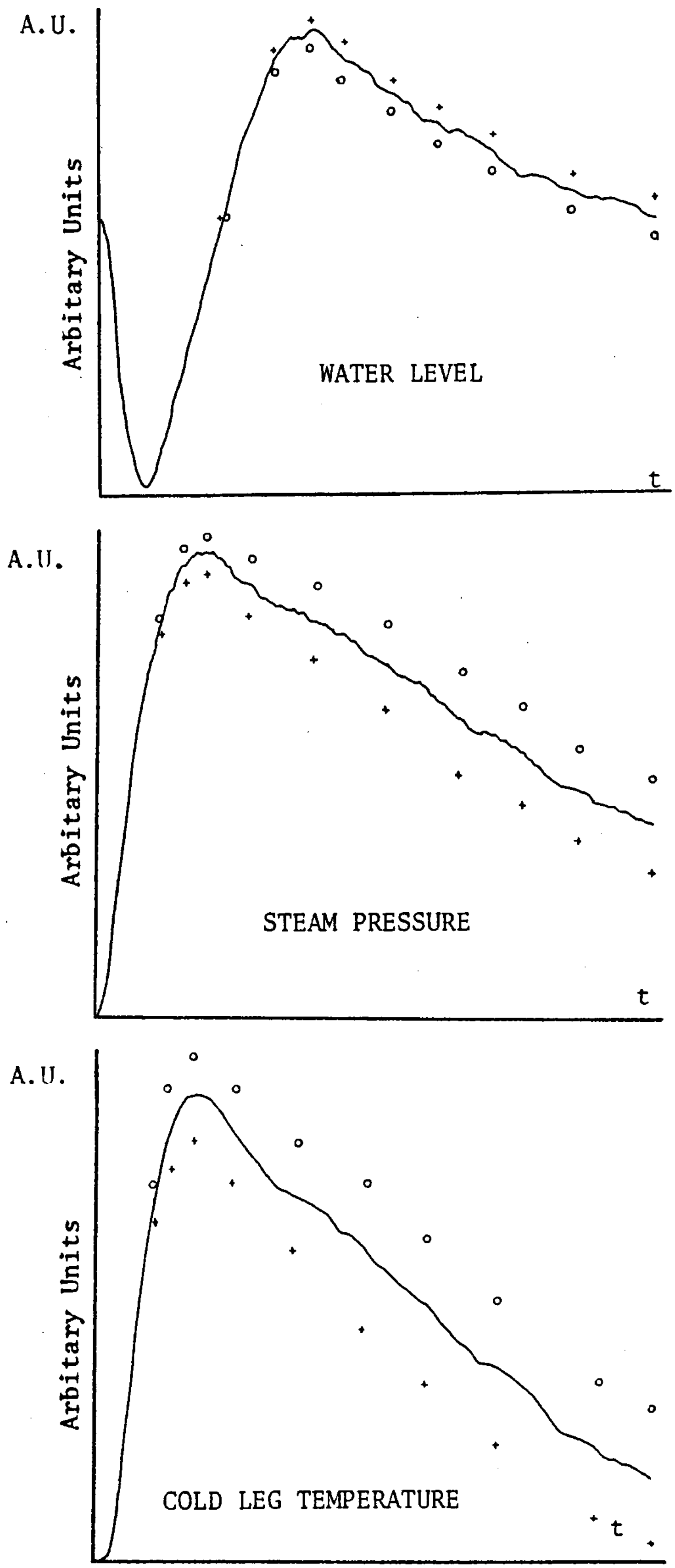

Figure 5.1 Effect of the Primary Coolant Specific Heat During a 100-90% Power Demand Step Perturbation (+:+10%,°:-10%).

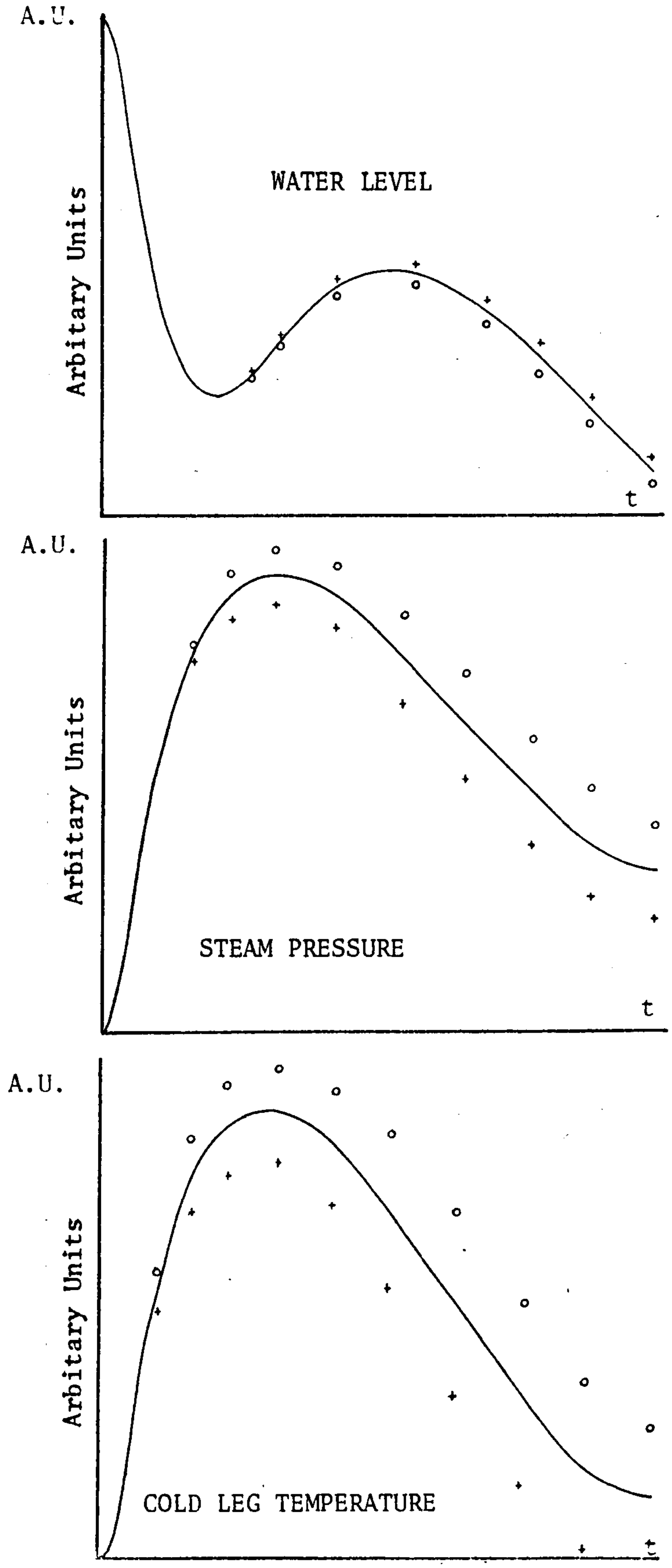

Figure 5.2 Effect of the Primary Coolant Specific Heat During a 30-20% Power Demand Step Perturbation (+:+10%,°:-10%).

rate, specific heat capacity, and temperature difference determines the amount of heat carried by the primary coolant. Thus, an increase in C_{p1} results in a decrease in the primary temperature, for the same perturbation on the secondary side, and vice-versa. This decrease in the primary temperature results in a decrease in the secondary coolant temperature and thus a decrease in the secondary pressure. However, the decrease in the primary outlet temperature is larger than the one in the pressure due to its direct relation with C_{p1}. The decrease in the steam pressure results in an increase in the water level. The reason is that an increase in steam pressure results in shrink or collapse of steam bubbles in the steam-water mixture and thus an increase of its density and a decrease in the water level. The opposite happens during a steam pressure decrease.

The effects of changes in the overall primary to secondary heat transfer coefficient U, are shown in Figures 5.3 and 5.4. The sudden increase in the steam pressure, due to the strong steam flow decrease, increases the saturation temperature Ts(t) immediately. The primary to secondary heat flux Qps(t) decreases, and this results in an increase in the primary coolant temperature Tp(t), according to

$$\delta Qps(t) = UA(1 + EZ)\ (\delta Tp(t) - \delta Ts(t))$$

where EZ denotes fractional changes in U. For an increase in U, i.e., EZ positive, the decrease in Qps(t) becomes even stronger and results in a smaller increase in the saturation temperature and consequently in the steam pressure, compared to the EZ = 0 case. This introduces a small

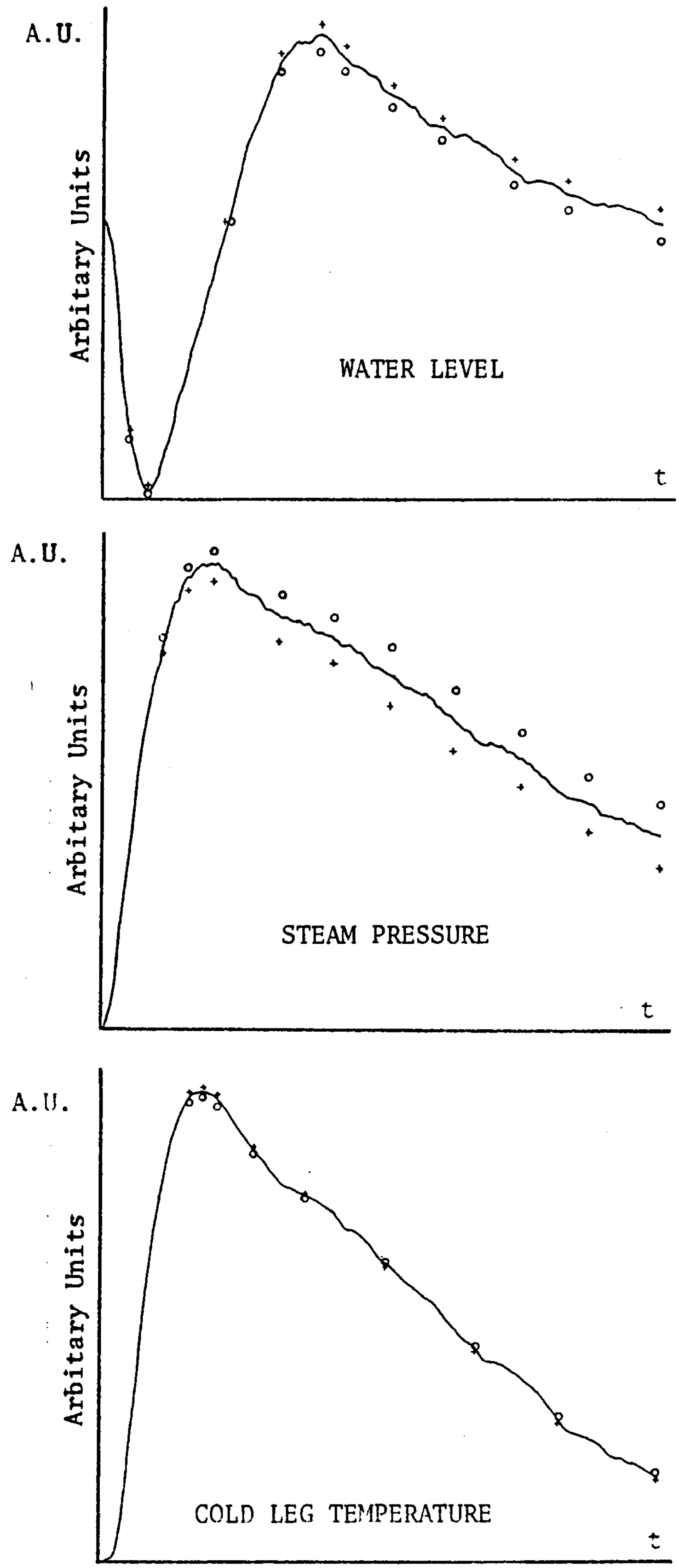

Figure 5.3 Effect of the Primary to Secondary Heat Transfer Coefficient During a 100-90% Perturbation (+:+10%,°:-10%).

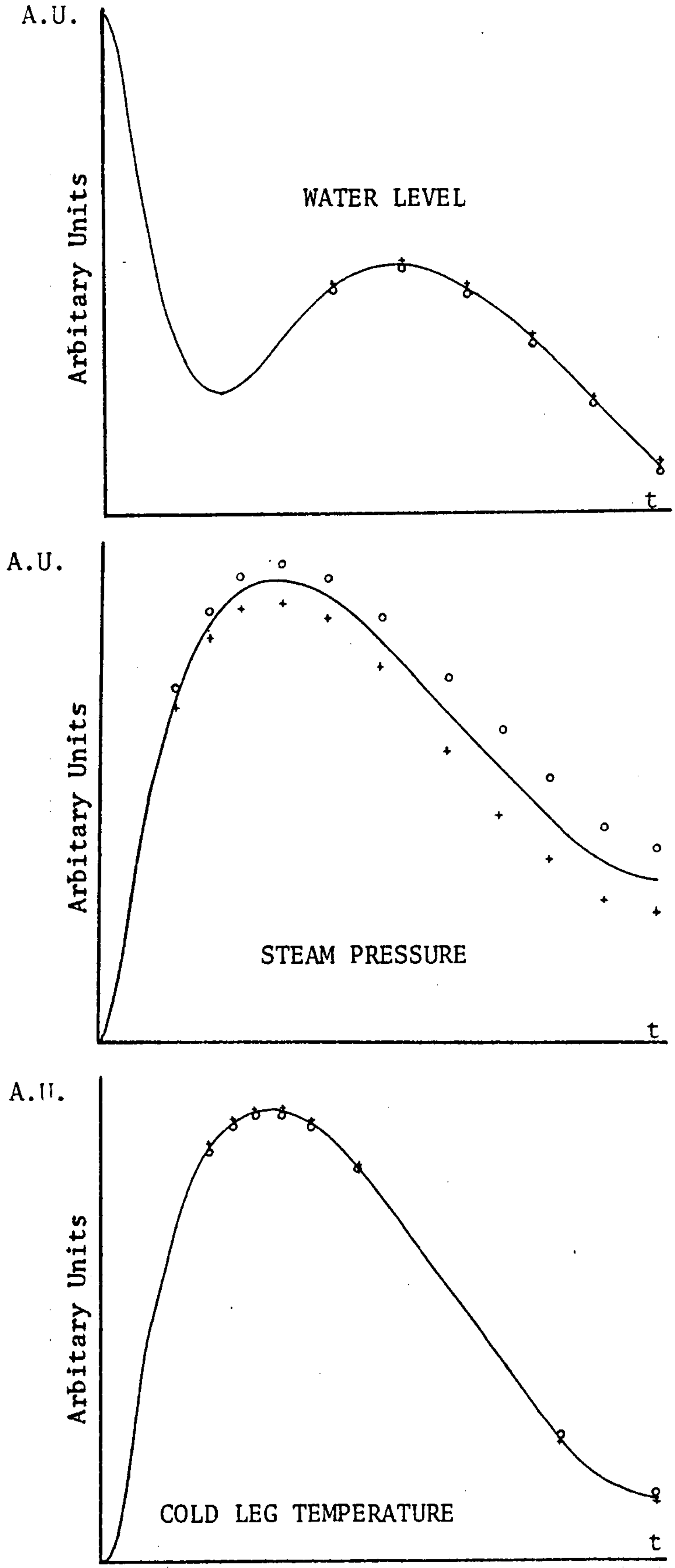

Figure 5.4 Effect of the Primary to Secondary Heat Transfer Coefficient During a 30-20% Perturbation (+:+10%,°:-10%).

further increase, during the first part of the transient, in the primary temperature, and a small further decrease in it during the later part of the transient. The water level shows an increase due to the decrease in steam pressure. When we introduce a decrease in U, i.e., EZ negative, the same phenomena take place, with an opposite direction in the changes of the different physical quantities.

The effect of changes in the initial steam exit quality (X_{eo}) are shown in Figures 5.5 and 5.6. In order to give a plausible physical interpretation of the dynamic performance of the model, both at full power and at low power, for a given change in X_{eo}, one should take into account the corresponding changes in the steam content of the steam-water mixture, and in the recirculation ratio

$$W_r = \frac{1-X_{eo}}{X_{eo}} W_s$$

where W_s is the exit steam flow rate. At full power, $X_{eo} = 0.2$ (approximately) while in our low power (30%) case $X_{eo} = 0.05$ (approximately). Thus, we can see that for a 10% increase in X_{eo} for example, the decrease in the recirculation ratio in absolute magnitude is much stronger (with respect to the steam flow rate and thus feedwater flow rate) at low power than at full power. Because of this, at a low power level, we observe a relative decrease in the water level, and thus a relative decrease in steam pressure and in primary outlet temperature. However, at full power, the corresponding decrease in W_r is several times weaker, with respect to the feedwater flow, than in the low power case. Thus, we observe rather the effect of the lower steam content in

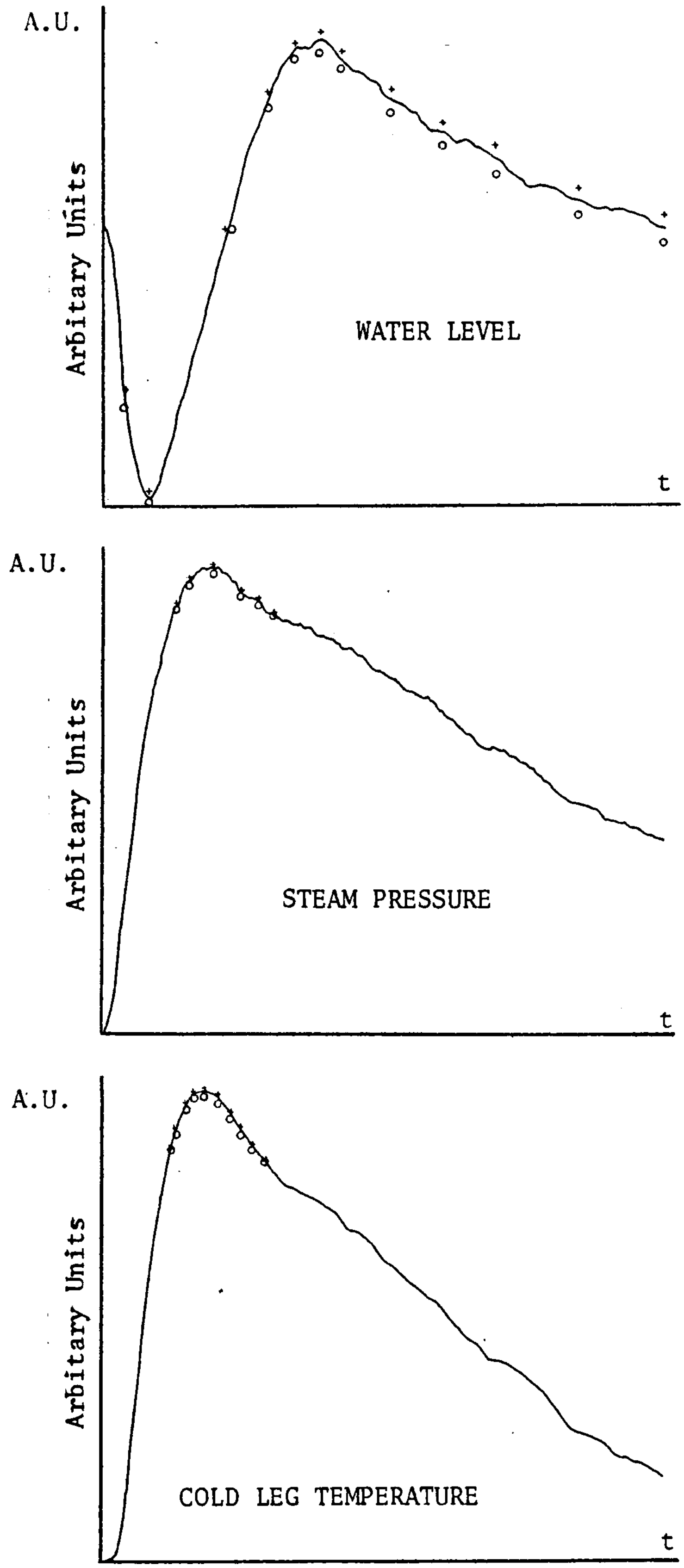

Figure 5.5 Effect of the Initial Steam Exit Quality During a 100-90% Perturbation (+:+10%, °:-10%).

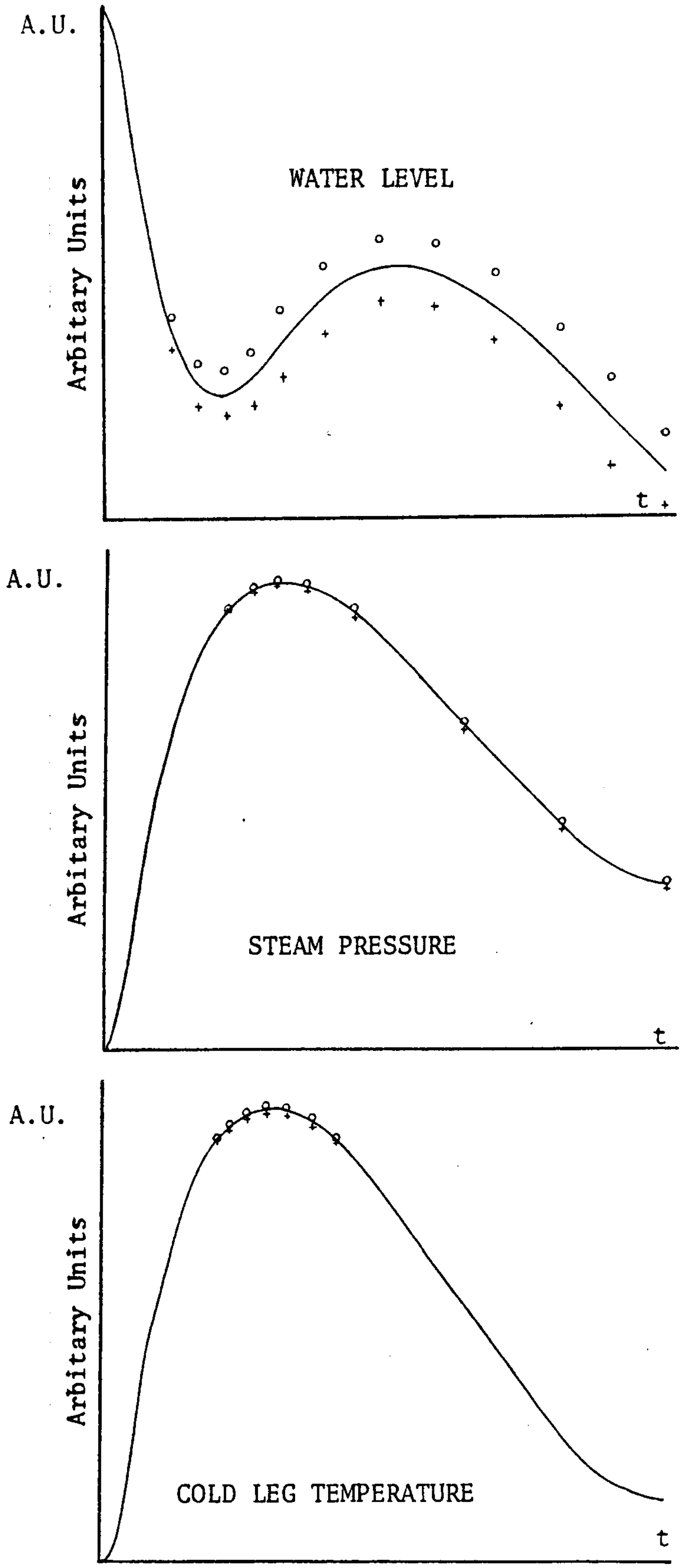

Figure 5.6 Effect of the Initial Steam Exit Quality During a 30-20% Perturbation (+:+10%, °:-10%).

the steam-water mixture, which is a weaker demonstration of the shrink phenomenon, i.e., an increase in the water level and corresponding increases in the steam pressure and in the primary exit temperature. The reverse phenomena occur for a -10% change in X_{eo}.

5.3 Effect of the Feedwater Temperature

The four inputs to the steam generator model are: (a) primary inlet temperature, (b) exit steam flow rate, (c) feedwater flow rate, and (d) feedwater temperature. In Chapter 7, the simulation of the steam generator, in a closed loop with the reactor core and the associated reactivity and feedwater control systems, is presented, but the feedback effect of the feedwater temperature is not included. Thus, in order to interpret and evaluate the results of that study, the effects of the feedwater temperature on the steam generator dynamic response must be known.

The two steam generator transients under study, at full power and at low power, were simulated by setting the feedwater temperature perturbation equal to zero, and the resulting responses of each output, represented by circles, were compared to the reference transients plotted in the same figure. The results can be seen in Figures 5.7 and 5.8.

In order to give a plausible physical interpretation of these results, one should note that the change in the feedwater temperature, during both transients studied (see Figure 4.2, page 36 and Figure 4.3, page 41), is negative and it starts only 40-60 seconds after the beginning of the transients. The fact that we do not take into account a decrease in the feedwater temperature, means that the saturation temperature, and

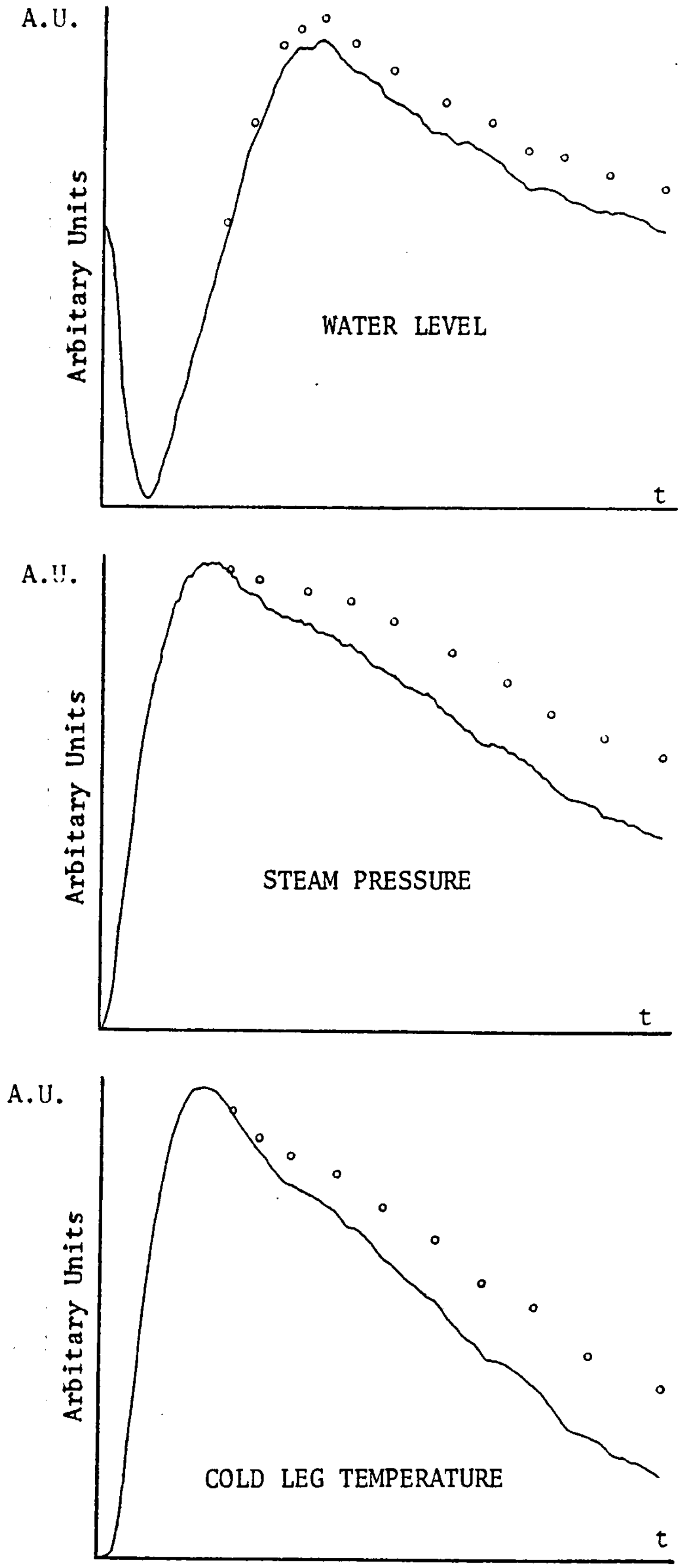

Figure 5.7 Effect of the Feedwater Temperature During a 100-90% Perturbation ($^\circ$:T_{fw}=0).

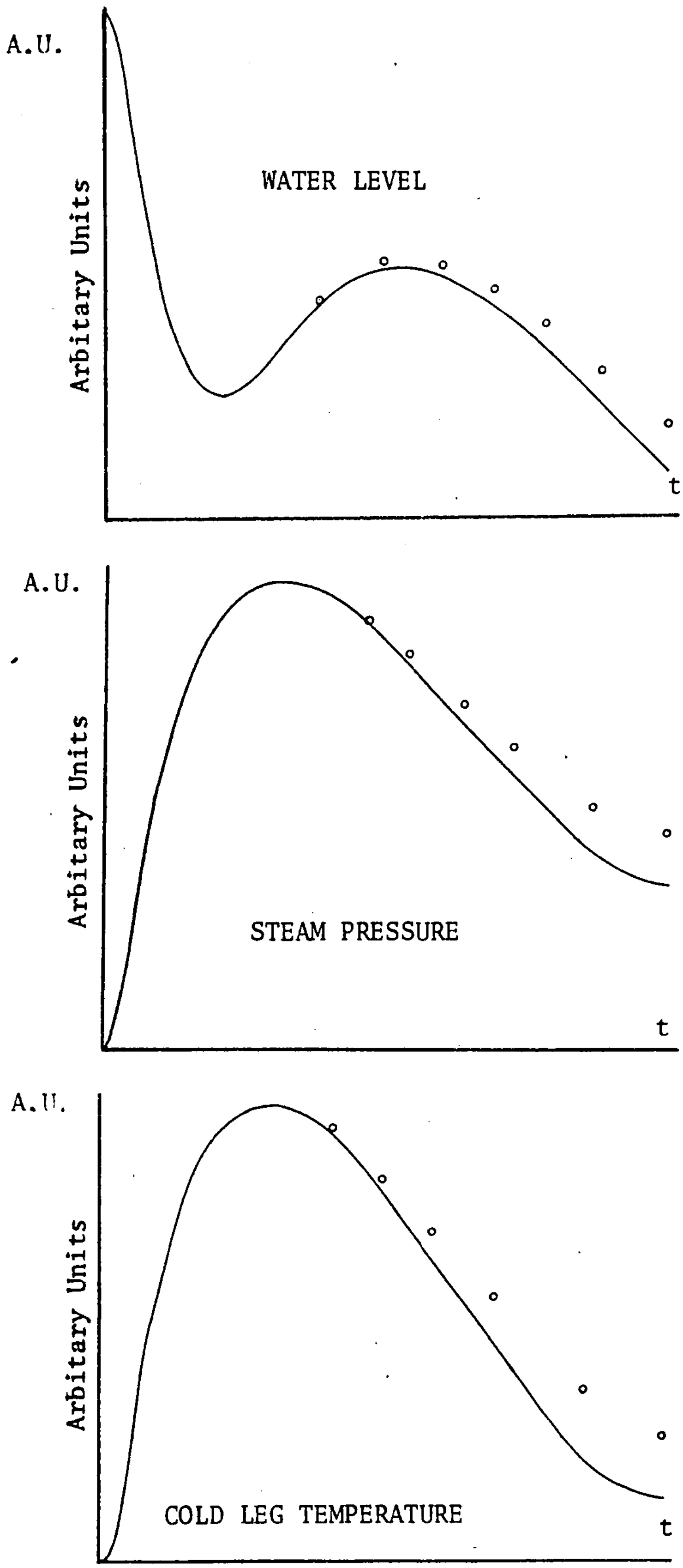

Figure 5.8 Effect of the Feedwater Temperature During a 30-20% Perturbation (°:T_{fw}=0).

thus the steam pressure, will increase. Due to the increase in saturation temperature, the steam content of the steam-water mixture will increase and thus the overall effect on the water level would be an increase, despite the increase in the steam pressure.

CHAPTER 6

MODEL VALIDATION

6.1 Introduction

The models used in this study to simulate the reactor core and the steam generator are linear, low-order, physical models. Because of the linearity of the models and the simplifying assumptions made and the complexity of the nonlinear physical process, there will always be some disagreement between experiment and model prediction. However, before using these models, especially for control design purposes, special care must be taken to minimize this disagreement.

This is achieved by adjusting the numerical values of certain physical parameters that are not known precisely. An optimization scheme is used to search for the optimal parameter values by minimizing the error between experiment and model prediction.

The uniqueness of the optimization search is examined using simulated transients as reference "experimental" transients. Thus, the exact values are known beforehand, and the uniqueness can be checked by performing the identification starting from different initial parameter estimates, and expecting the search to converge always to the same, exact, values.

The optimal parameter values found by performing the identification with plant test transients are then adopted and confidence is gained that the models represent satisfactorily the physical process studied.

The reactor core model and the steam generator model validation effort, at full power and at low power, are described in this chapter.

6.2 Validity of the Model

A valid physical model must describe correctly the physical process involved using coherent a-priori estimates of the parameter values. Even with nonoptimal parameter values a valid model will still reproduce the main characteristics of the dynamic behavior of the physical process being modeled. Any disagreement with the experiment must be of such magnitude and importance that most of it could be accounted for by inaccurate knowledge of the values of certain parameters, while a part of it will always exist due to the simplified nature of the model.

Thus, before any parameter identification work is undertaken, we can check roughly the validity of a model using the best a-priori estimates of the parameter values. This was done for the core and the steam generator models at full power and at low power, and the results can be found in Figures 6.1-6.4. The experimental signals used as inputs to the isolated core and the isolated steam generator models were presented in Chapter 4, while the data used are given in Appendices I and II.

We can see from these Figures 6.1-6.4 that at both power levels studied, the core and steam generator models predict the main dynamic characteristics of the physical processes they simulate. The form of the transients is approximately the same while their peaks occur exactly at or within a few seconds from the right time moment. The quantitative

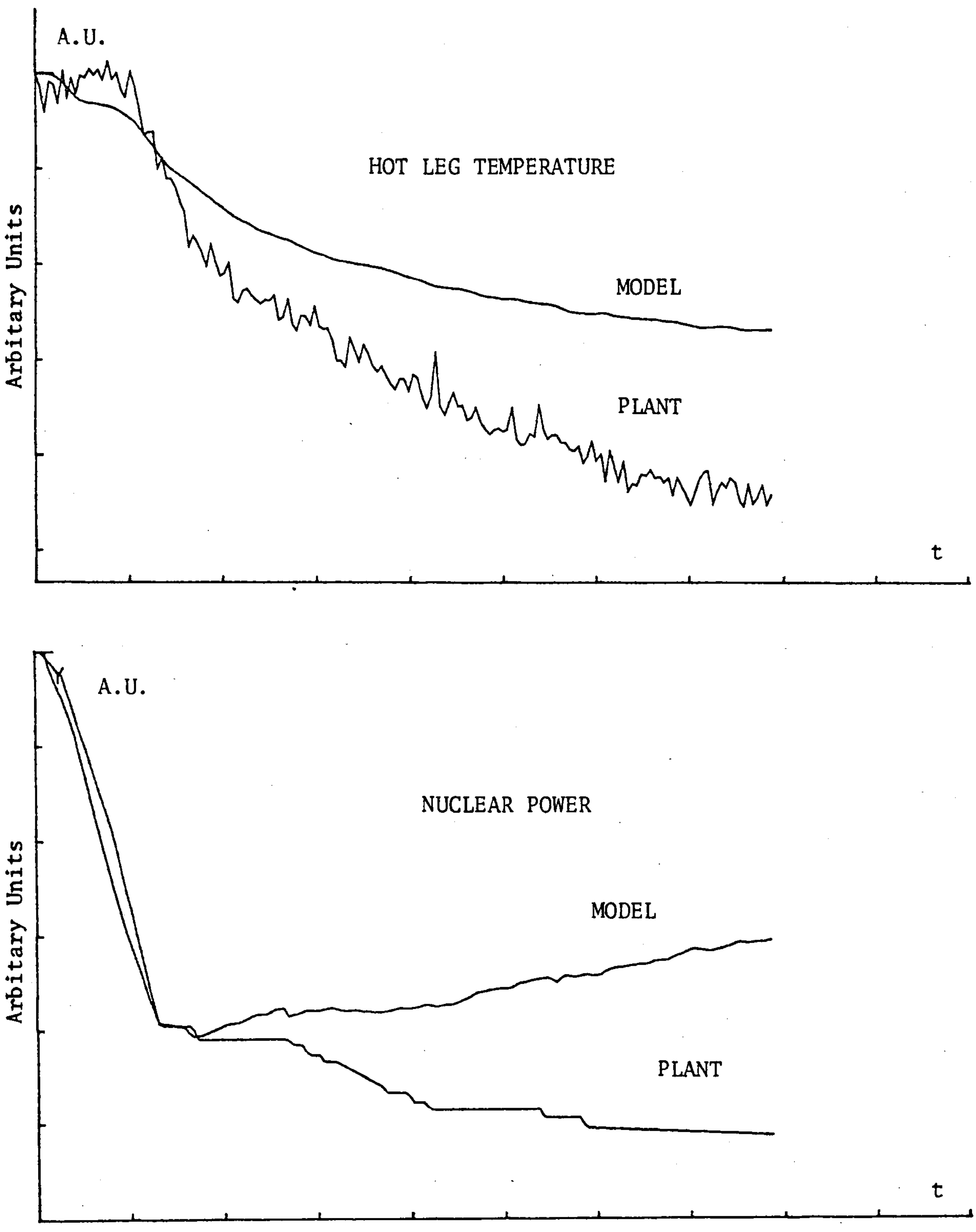

Figure 6.1 Core Model Initial Response to a 100-90% Power Demand Perturbation.

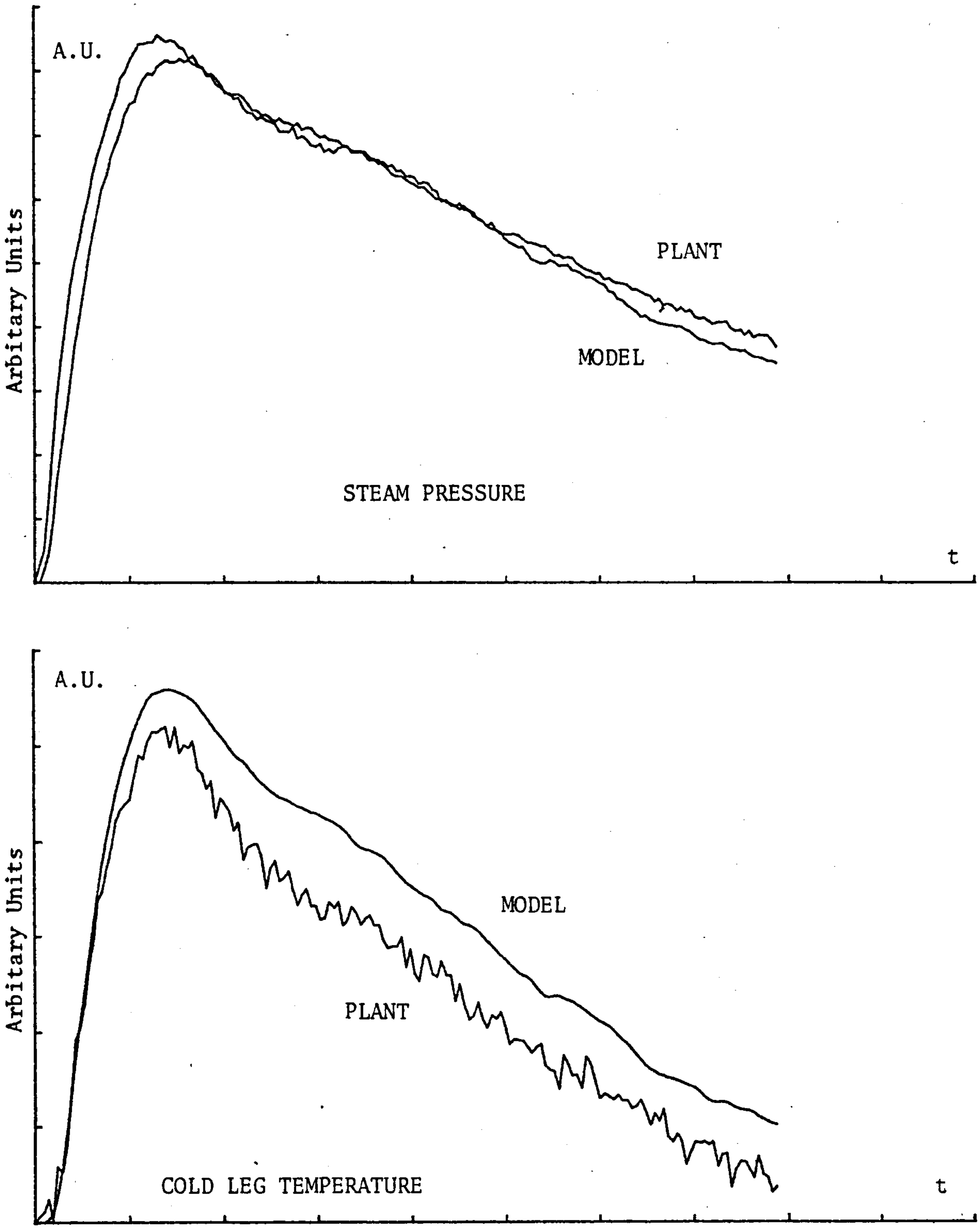

Figure 6.2 Steam Generator Model Initial Response to a 100-90% Power Demand Perturbation.

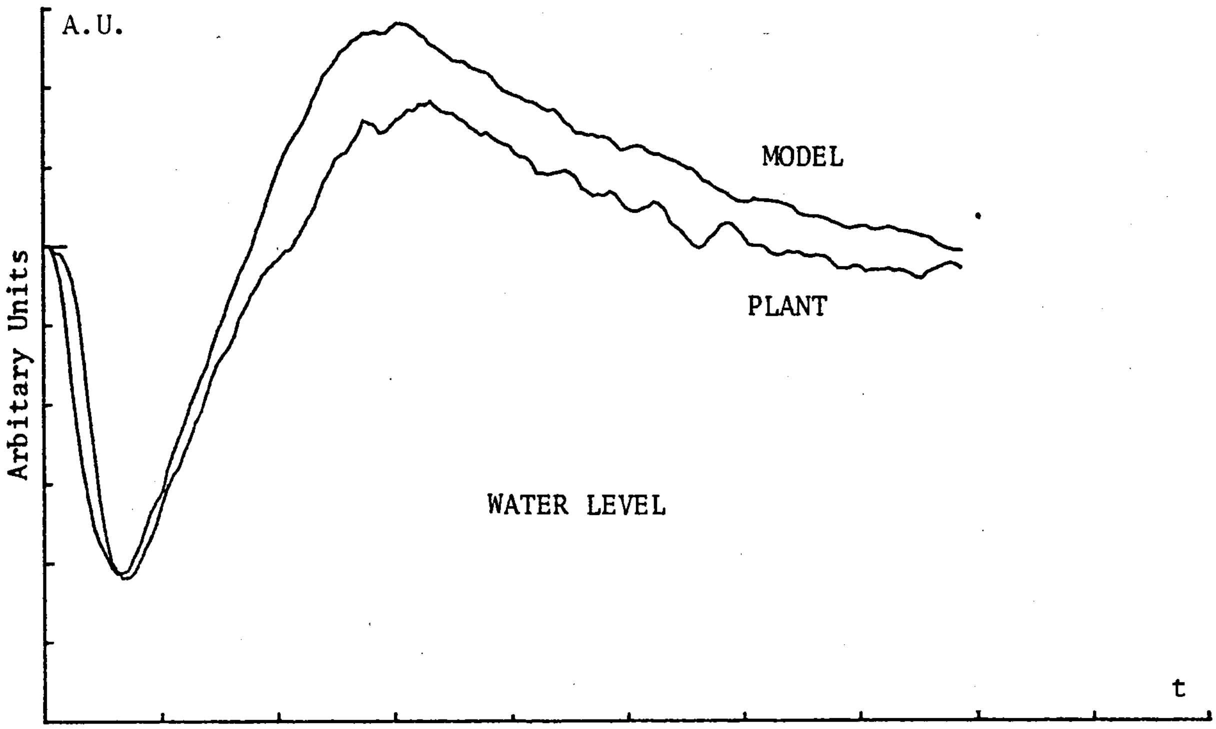

Figure 6.2 (Continued)

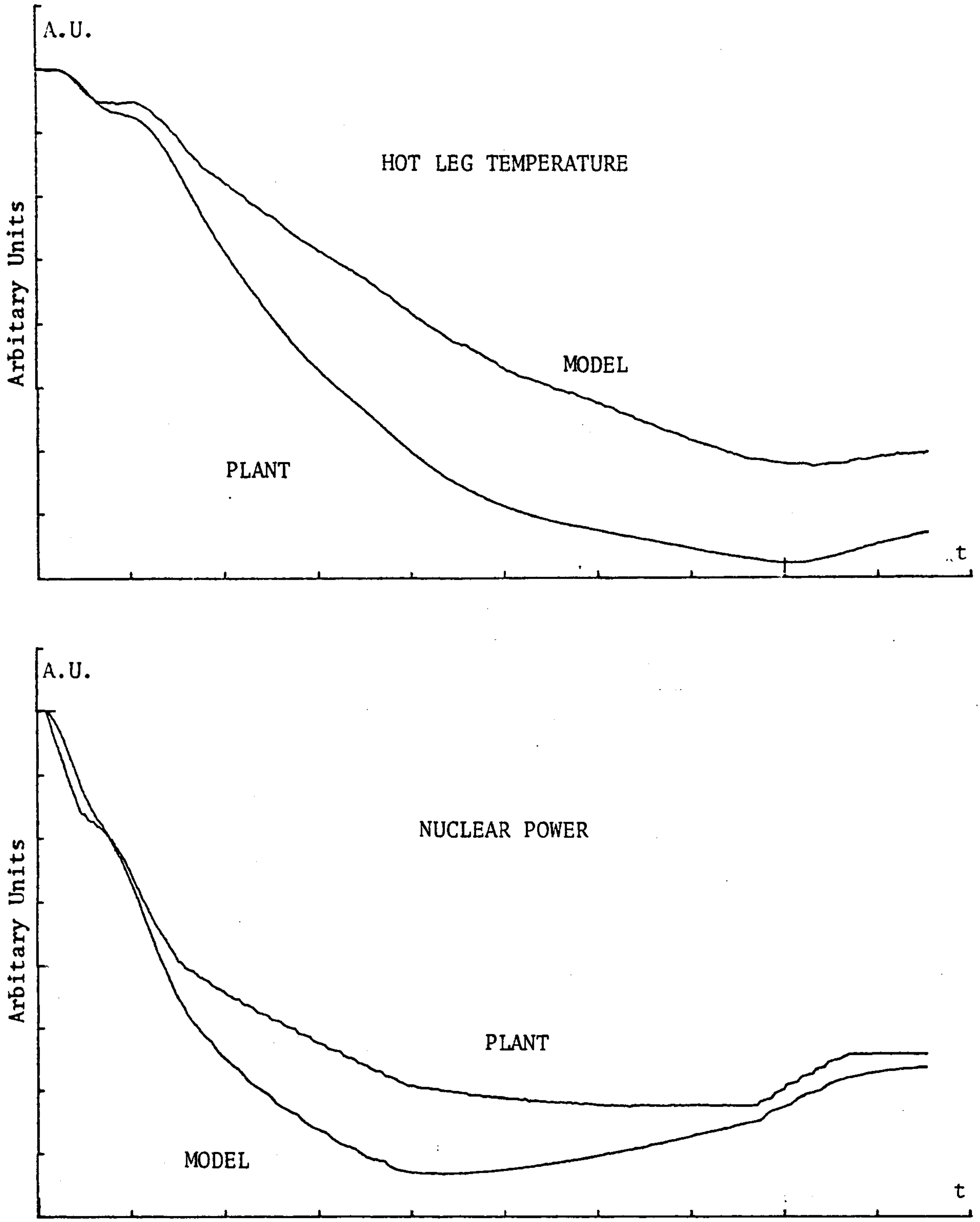

Figure 6.3 Core Model Initial Response to a 30-20% Power Demand Step Perturbation.

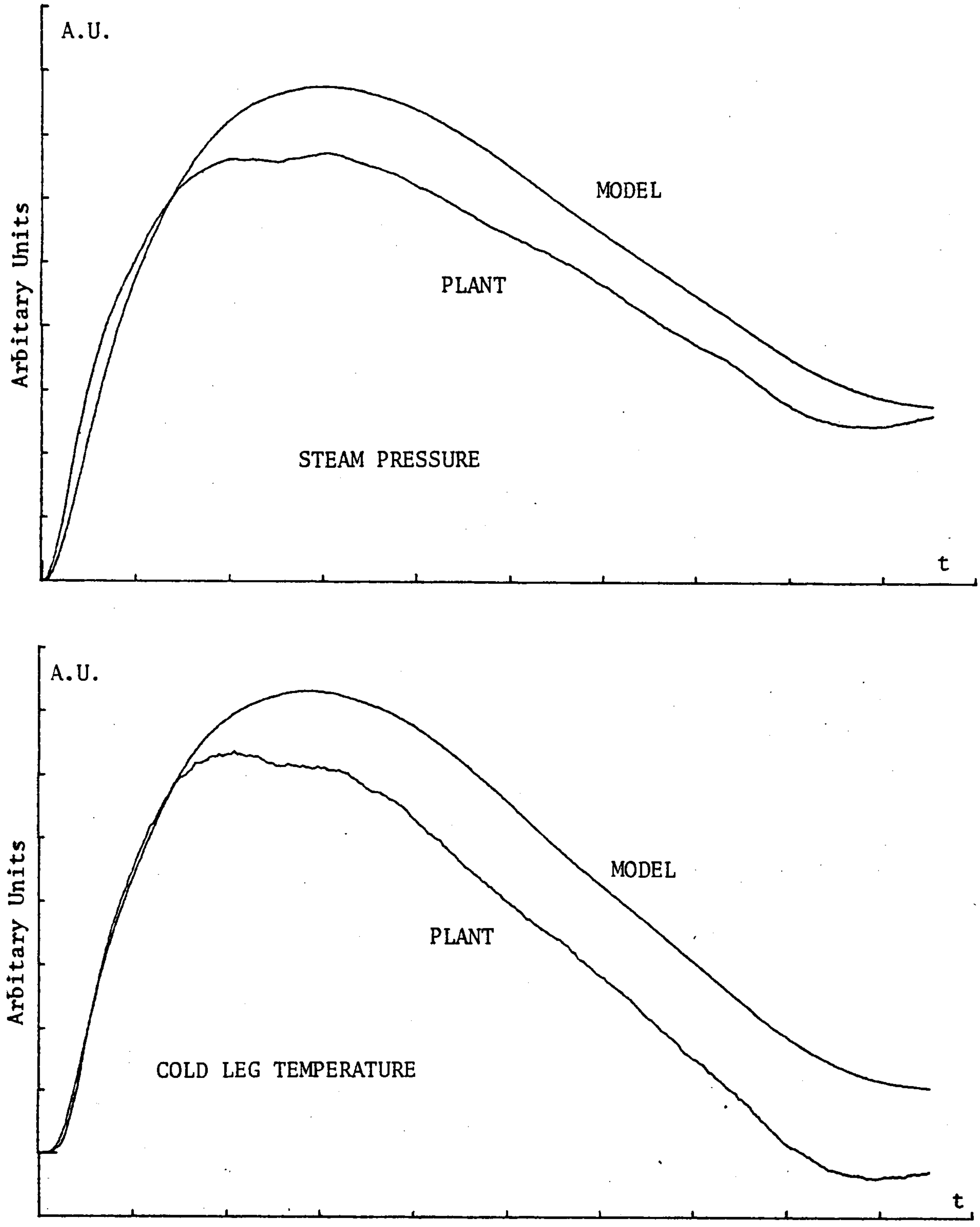

Figure 6.4 Steam Generator Model Initial Response to a 30-20% Power Demand Step Perturbation.

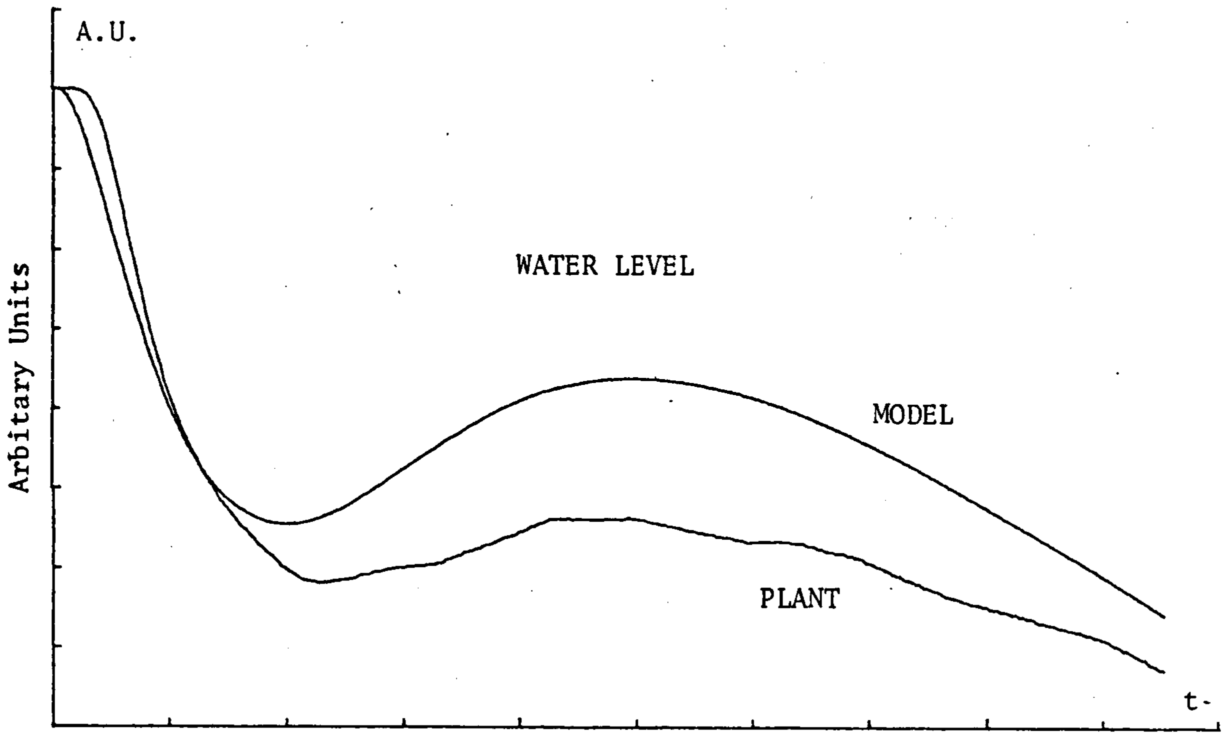

Figure 6.4 (Continued)

agreement between experiment and prediction is already good for some signals, especially at the end of the transients, which corresponds approximately to the new steady-state.

However, big differences exist for some signals, especially with the core model predictions. At this point we can comment that this could be due to the very approximate initial parameter values used in the core model, since the plant operating conditions corresponding to the set of available data were unknown. We expect that the core parameter identification could adjust the values of certain key parameters, such as the reactivity feedback coefficients, and improve the agreement between experiment and model prediction.

From the sensitivity analysis of the steam generator model presented in Chapter 5 (Figures 5.1-5.6, pages 56-63), we can note that small changes in the values of certain parameters could account for much of the disagreement observed in Figures 6.2 and 6.4. For example, from Figure 6.2 we can see that the water level prediction is higher than the experiment, but from Figure 5.5, page 62, we can note that a -10% in X_{eo} would lower, and thus improve, the water level prediction for the entire transient and have an excellent agreement at the end of the transient. Similar remarks could be made on the water level from Figure 6.4 and Figure 5.6, page 63, and also on the primary outlet temperature and the steam pressure transients by comparing the initial agreement and the sensitivity to the various parameters. Thus, we expect that the identification procedure could find the combination of parameter changes that would optimize the agreement for the three steam generator outputs.

6.3 Model Parameter Identification

For some time, there has been an increasing interest in system parameter identification. In the case where the system under study is an industrial process, like a nuclear power plant, this interest has arisen from the need to obtain a better knowledge of the plant in order to design improved control schemes and thus achieve lower operating cost and increased efficiency. The parallel development of digital computers has allowed the undertaking of similar tasks, since the high-order mathematical models describing the complex physical processes studied, and the iterative schemes of the various optimization methods involve a great deal of computation.

All solutions to parametric identification problems consist of finding the minimum of a cost function that defines the error as a function of the parameters to be optimized. It must be such that both positive and negative errors contribute in a positive sense to the criterion value. Thus, it is taken to be the sum of the squares of the differences, for each time step, between the experimental outputs and the model predicted outputs when using the same inputs as were used in the experiment, i.e.

$$S = \sum_{i=1}^{N} \left(\sum_{j=1}^{M} (y_{ej} - y_{mj})^2 \right)_i$$

where,

N = Number of time steps

M = Number of outputs

y_e = Experimental output

y_m = Model predicted output.

The parameter values are modified using an algorithm that minimizes the error. This is repeated until adequate agreement between experiment and prediction is obtained, taking into account the constraints on the parameter value changes. A schematic of the principle of the model-adjustment method is shown in Figure 6.5.

6.4 The Simplex Optimization Method

The optimization algorithm that can minimize the error criterion can be chosen from several available methods. These methods can be distinguished as (a) direct-search methods and (b) gradient methods. The direct search methods do not require an explicit evaluation of the gradient of the error, whereas the gradient methods are based on the assumption that the gradient can be determined. There are several references on surveys of optimization techniques like Box, Davies and Swann (25), Wilde (26), Bekey and McGee (27), Wilde and Beightler (28), Kowalik and Osborne (29), Powel (30), Dixon (31), Eykhoff (6).

The method used in this study is the simplex method of Nelder and Mead (32) for function minimization. It was chosen because of the previous experience gained in its use by the author and its good performance in similar problems. It is a direct-search algorithm, and its detailed description of the algorithm is given in Appendix III.

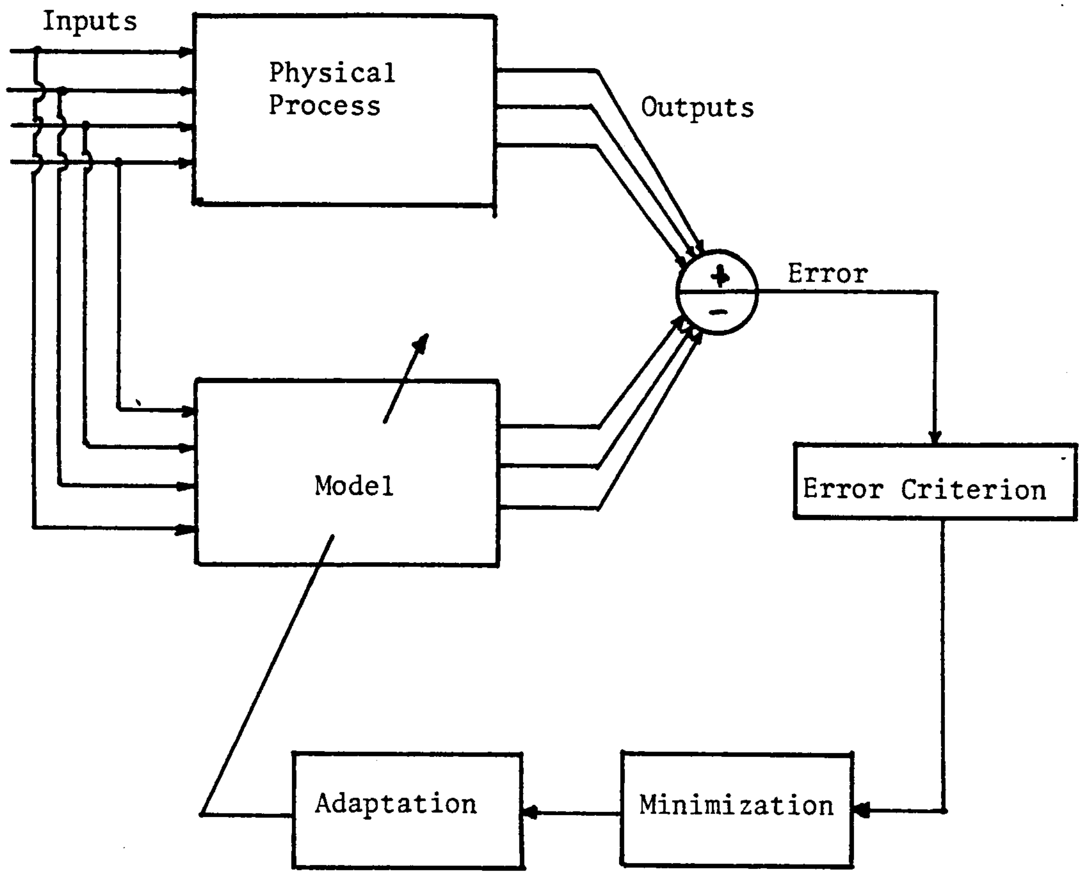

Figure 6.5 Principle of the Model-Adjustment Method.

6.5 Reconstruction of the Nonfiltered Steam Flow Signal

From Figure 6.5 can be seen that we need experimental signals for all the inputs and the outputs of the physical process in order to perform the model parameter identification. The test data and the model used are the main sources of error. Thus, good quality experimental data is essential. However, problems associated with the data acquisition system, as was discussed in Chapter 4, result in distortion of the signals recorded. Special effort must be taken to determine the nature and extent of such signal distortion.

The problem that was encountered with the steam flow rate signal at the low-power level test is typical. The existence of a 25-second filter at the exit of the sensor, used to smooth out possible noisy overshots for protection and control considerations after a big power demand step perturbation at low power level, resulted in the collection of a signal (Figure 4.3, page 41) that does not represent the real behavior of the steam flow after such a step perturbation. Thus, special care must be taken to reconstruct the real, unavailable steam flow input, which must be used in the parameter identification work.

The reconstruction of the steam flow input can be done by approximating the true input for the time interval of interest, T, by a number of line segments. The number of line segments was chosen to be four. It was shown that by using less line segments, the resulting input did not represent satisfactorily a step perturbation in steam flow (the end of the first line segment corresponded to eight to ten seconds instead of two to three seconds). Using more line segments, the input found took the form of a saw.

Thus, using an input of the form shown in Figure 6.6, the problem is to identify the time moments t_1, t_2, t_3 and the amplitudes y_1, y_2, y_3, and y_4, so that when this signal passes through a 25-second filter, the output obtained is as close as possible to the filtered steam flow rate signal (Figure 4.3, page 41). This problem is a seven-parameter identification problem and it is solved using the simplex optimization method. The iterative scheme adopted is shown in Figure 6.7.

The reconstructed, approximate, nonfiltered steam flow signal and the agreement between experimental and theoretical filtered signals are shown in Figure 6.8. This signal was used as the true steam flow rate signal in the parameter identification at low power.

6.6 Core Parameter Identification

In this section the results of the core parameter identification at full power and at low power level are presented. The physical parameters that were chosen to be identified are the fuel and moderator reactivity feedback coefficients (α_f and α_c), the overall fuel-to-coolant heat transfer coefficient h_{fc}, and the heat capacity of the primary coolant ($(MC_p)_c$). They are all nonmeasurable quantities and there is uncertainty on their values. The rest of the core model parameters (see Appendix I) are the fuel heat capacity ($(MC_p)_f$) and the coolant residence time in the various parts of the primary loop (τ_{core}, τ_{up}, $\tau_{h\ell}$, $\tau_{c\ell}$, $\tau_{\ell p}$), and they are assumed to be constant and known.

In order to always have meaningful results from the identification procedure, constraints were set for the maximum allowable changes from the initial values of these parameters. The magnitudes of these

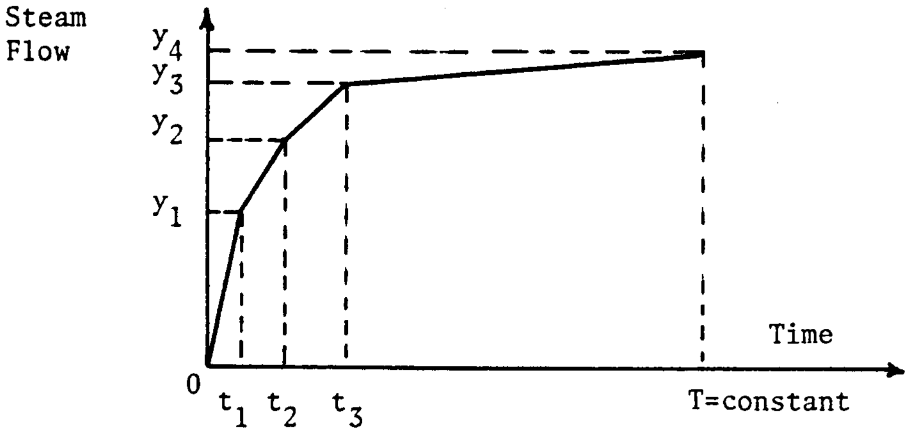

Figure 6.6 Schematic Diagram of the Approximate Form Used to Reconstruct the Nonfiltered Steam Flow Signal.

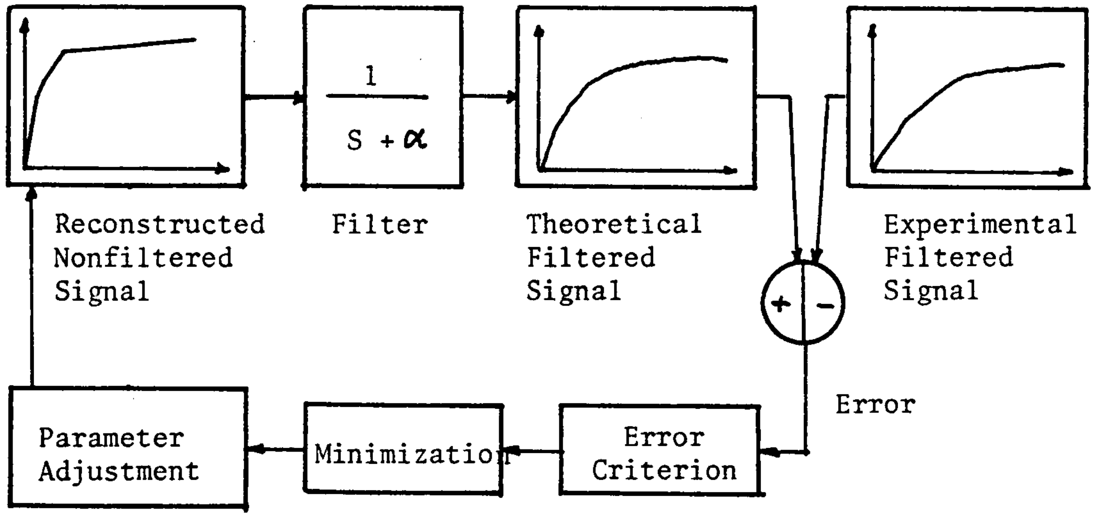

Figure 6.7 Schematic Diagram of the Iterative Scheme for the Reconstruction of the Nonfiltered Steam Flow Signal.

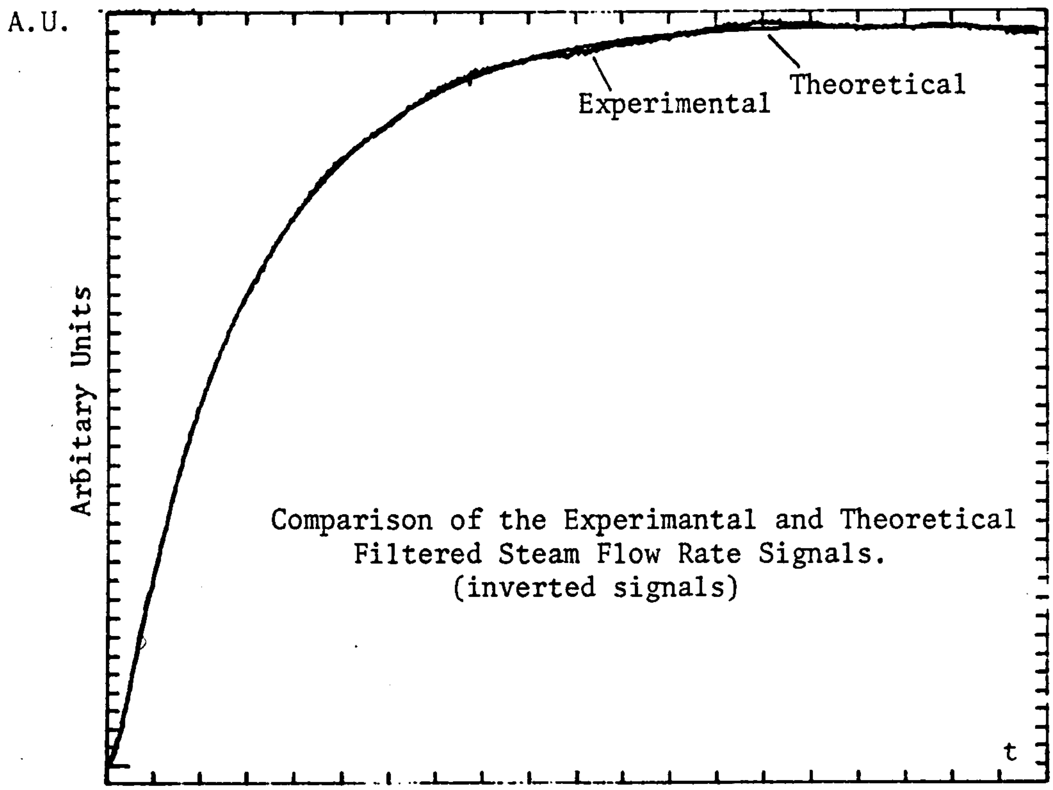

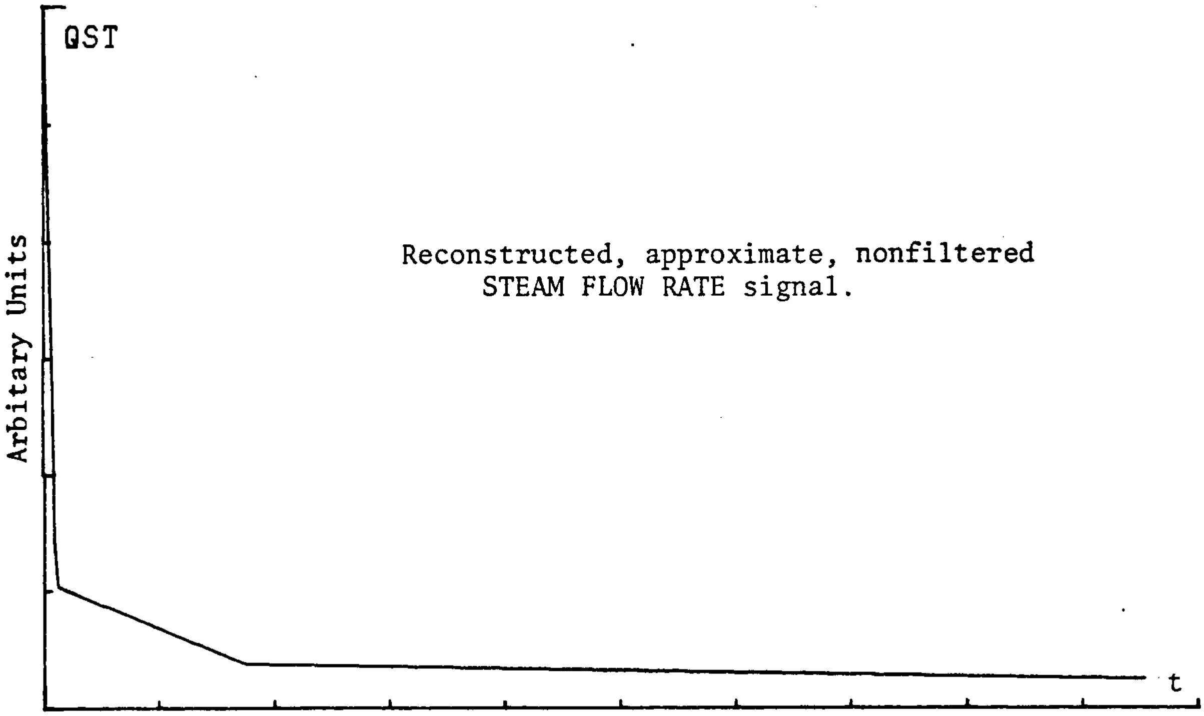

Figure 6.8 Reconstruction of the Nonfiltered Steam Flow Rate Signal at Low Power.

constraints were not chosen after precise calculations of the uncertainties associated with them due to the different physical phenomena. They were rather empirical choices in order to try the identification procedure within the scope of this study. For example, it was felt there should be a greater uncertainty on the value of α_c, due to its high dependence on boron concentration and power level, than on the value of α_f. Thus, a 50% constraint was chosen for α_c, a 10% constraint for α_f, and a 20% constraint was chosen for h_{fc} and $(MC_p)_c$.

The identification was repeated with the optimal values from the previous run used as initial parameter values until the cost function did not decrease. This is why the final changes in the α_c values were larger than its constraint. The agreement between experiment and core model prediction with the final optimal parameter values can be seen in Figure 6.9 at full power and in Figure 6.10 at low power (30%). The complete sets of data at both power levels, along with the core model equations, are given in Appendix I. The changes in the parameter values from the identification are given in Table 6.1.

As was discussed in Section 6.2, the initial parameter values used in the core model were very approximate, since the plant operating conditions (exact power level, Boron concentration) corresponding to the data available were unknown. Especially the value used for α_c, which depends greatly on the power level and the Boron concentration, was very inaccurate. Thus, we observe an 80% and 68% reduction of the initial value, at full power and at low power, respectively. However, the new optimal values appear to be reasonable, corresponding to a Boron concentration of approximately 1,000 ppm in the low power (30%) case and

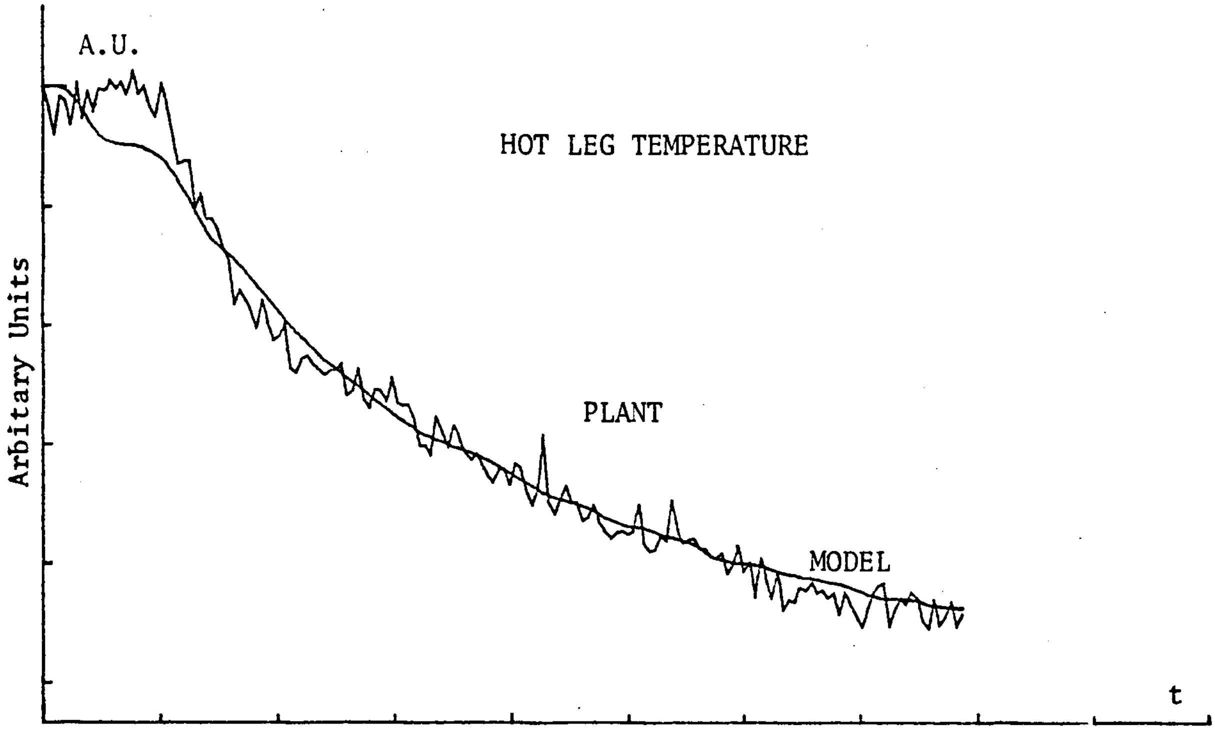

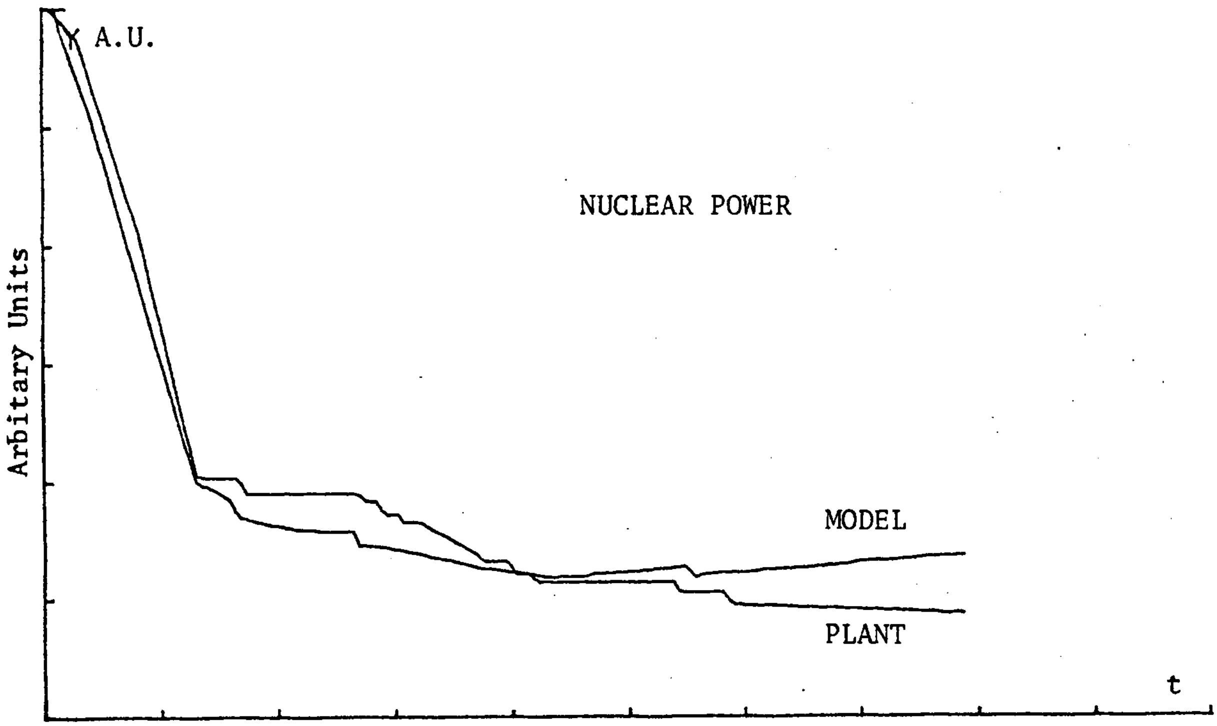

Figure 6.9 Core Model Optimal Response to a 100-90% Power Demand Step Perturbation.

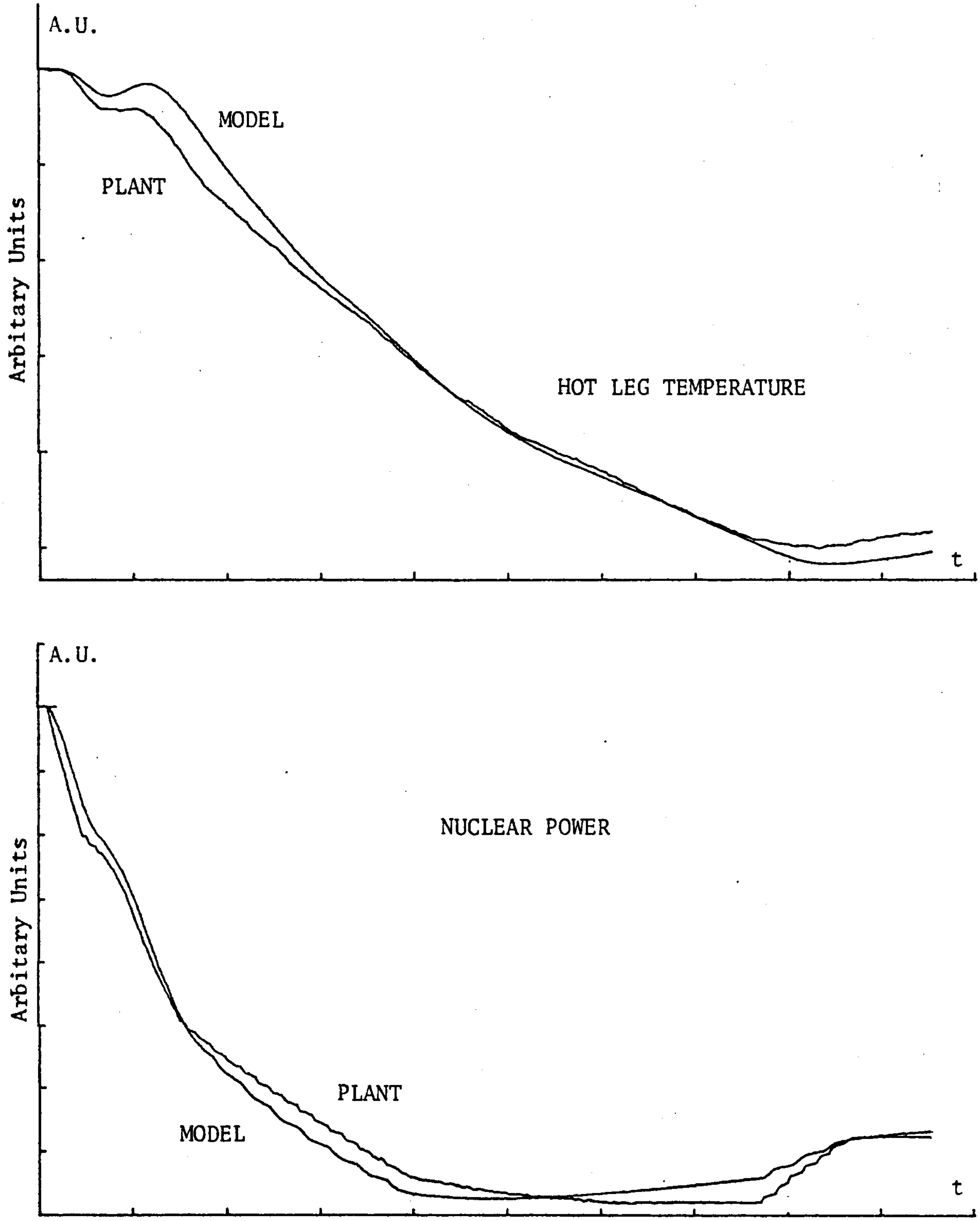

Figure 6.10 Core Model Optimal Response to a 30-20% Power Demand Step Perturbation.

Table 6.1

Core Identification Results

	Full Power			Low Power (30%)		
	Initial	Optimal	Final Change	Initial	Optimal	Final Change
α_f*	- 1.65	-1.52	- 8 %	- 1.52	-1.6	+ 5.3%
α_c*	-14.	-2.9	-80 %	-14.	-4.5	-68 %
h_{fc}**	205	236	15.1%	236	215	- 8.9%
$(MC_p)_c$***	$1.725 \cdot 10^4$	$1.665 \cdot 10^4$	- 3.5%	$1.5 \cdot 10^4$	$1.61 \cdot 10^4$	7.3%

*[pcm/°F] **[Btu/hr·ft²·°F] ***[Btu/°F·node]

approximately 1,300 ppm in the full power case (according to Westinghouse Reference Safety Analysis Report (33)). The Boron concentration recorded during the tests was 900 ppm at low power and 1,150 ppm at full power, and the corresponding α_c values would be about 2 pcm/°F higher in absolute magnitude than the optimal values found. However, the accuracy with which α_c is reportedly (33) calculated is within 2 pcm/°F, and thus the optimal values found by the identification were kept. The small changes in α_f and $(MC_p)_c$ seem also to be reasonable since they are slowly-varying functions with the power level. There is greater uncertainty with the exact value of h_{fc}, and thus the greater changes in h_{fc} observed in Table 6.1 are considered to be reasonable.

Furthermore, some additional cases were examined: (a) The identification was performed including the fuel heat capacity($(MC_p)_f$) as an additional identifiable parameter, and its value changed by only 0.8%, while the optimal values of the other parameters changed by about the same amount, with respect to the values found when $(MC_p)_f$ was not included in the identification. (b) Efforts to reduce the cost function even lower, by starting the identification again with the optimal values as initial values, did not succeed. It should be noted here that at the beginning of the identification the initial parameter values are changed randomly by 0-10% to start the search (see Appendix III). Despite these random changes to the initial (optimal in this case) values, the identification found the same optimal values quickly and converged to the same minimal value of the cost function. The consistent convergence to the same cost function value and the same optimal parameter values for several different initial a-priori estimates, and the physically reasonable optimal values found at full power and low power, were considered to be sufficient evidence that the optimal values found by the identification procedure were acceptably accurate, within the scope of this study.

However, methods exist that permit evaluation of confidence levels on the optimal parameter values found. The Normal Theory (34) for instance, could have been applied for this purpose and its outline is given below:

In the state variable form, the system under study is represented by the set of differential equations

$$\dot{x}(t) = Ax(t) + Bu(t) \tag{6.1}$$

where

x is the state vector

u is the perturbation vector

A is the (constant) system matrix

B is a constant matrix containing the coefficients of the perturbation vector.

In the discrete-time case, we have the equivalent system of difference equations

$$x_k = Dx_{k-1} + Eu_{k-1} \tag{6.2}$$

$$y_k = Cx_k \tag{6.3}$$

where

y is the vector containing the observable states

k is the time instant $t_k = k\Delta T$

ΔT is the sampling interval.

We also have the matrix relations

$$D = \exp(A\Delta T) = I + A\Delta T + \frac{(A\Delta T)^2}{2!} + \ldots \tag{6.4}$$

$$E = \exp((A\Delta t) - I)A^{-1}B = \Delta T(I + \frac{A\Delta T}{2!} + \frac{(A\Delta T)^2}{3!} + \ldots)B \tag{6.5}$$

If we denote by y_k* the measurement of the observable vector at k, then the quantity to be minimized is

$$S = \sum_{k=1}^{N} (y_k^* - CDx_{k-1} - CEu_{k-1})^T (y_k^* - CDx_{k-1} - CEu_{k-1}) \tag{6.6}$$

where N is the number of observation points.

Now assuming a normal distribution for the data, the joint probability density function of the measurements is given below:

$$p(y^*|\Theta) = \frac{1}{(2\pi\sigma^2)^{N/2}} \exp\left\{-\frac{1}{2}\sum_{k=1}^{N}(y_k^*-CDx_{k-1}-CEu_{k-1})^T\Gamma^{-1}(y_k^*-CDx_{k-1}-CEu_{k-1})\right\} \tag{6.7}$$

where

Θ is the vector containing the parameters to identify

Γ is the variance matrix.

Since the minimization is done in the least-squares sense, equation (6.6), the estimator of the parameter vector, $\hat{\Theta}$, is a least-squares estimator, and the Cramer-Rao inequality (34) holds for it, namely

$$\text{cov}\ \hat{\Theta} \geq M^{-1} \tag{6.8}$$

where

$$\text{cov}\ \hat{\Theta} = E_{y^*|\Theta}\{(\hat{\Theta} - \Theta)(\hat{\Theta} - \Theta)^T\} \tag{6.9}$$

is the covariance of the estimator and

$$M_\Theta = E_{y^*|\Theta}\left\{\left(\frac{\partial \log p(y^*|\Theta)}{\partial\Theta}\right)\left(\frac{\partial \log p(y^*|\Theta)}{\partial\Theta}\right)^T\right\} \tag{6.10}$$

is the Fisher information matrix.

The inequality (6.8) gives a lower bound for the estimator covariance, atainable theoretically for $N\to\infty$, and M_Θ has to be calculated using equations (6.10) and 6.7). Only the matrices D and E are functions of Θ, through their relationships to matrix A (equations (6.4) and (6.5)), since only the system matrix contains the parameters. Thus, M_Θ^{-1} can be computed, and its diagonal elements will give us the variance of the estimator, which could be used as a measure of the best estimation accuracy possible.

6.7 Steam Generator Parameter Identification

In this section the results of the steam generator parameter identification at full power and at low power are presented. The physical parameters to be identified are the primary coolant specific heat (C_{p1}), the steam exit quality (x_{eo}), the primary to metal heat transfer coefficient (HP), the tube metal heat conductance (UM), and the metal to secondary heat transfer coefficient, both for the subcooled region of the steam generator (HS1) and for the boiling region (HS2). They are all nonmeasurable quantities with uncertainties on their values. The choice of these parameters for a future identification work was initially made by the group of the French Designer Framatome, working within the framework of comparing this linear steam generator model with a large, detailed, nonlinear code, and it was retained in this study also. However, it should be noted that it is not a unique choice, and additional parameters may be included.

As with the core identification work, constraints were set for the maximum allowable changes in the initial values of these parameters. The magnitudes of these constraints were not chosen after a detailed study of the uncertainties associated with the corresponding parameter values. They were rather empirical choices in order to try the identification procedure. They were 10% for C_{p1}, and 20% for x_{eo} and for the heat transfer coefficients. Furthermore, all four components of the overall primary to secondary heat transfer process (UP, UM, HS1, HS2) were assumed to change by the same amount (EZ). Therefore, the steam generator identification is carried out on three parameters (C_{p1}, x_{eo}, EZ).

The agreement between experiment and steam generator model prediction with the optimal parameter values can be seen in Figure 6.11 at full power, and in Figure 6.12 at low power. The complete sets of data at both power levels, along with the steam generator model equations, are given in Appendix II. The changes in the parameter values from the identification are given in Table 6.2.

From the Table 6.2, we can see that x_{eo} changed much more than any other parameter. These changes are considered reasonable since the optimal values found and the initial values used are both close to the steam exit quality of a U-tube steam generator of these two power levels (see Kerlin (35), page 126). The small changes in C_{p1} are in accordance with the higher confidence on the value of this parameter, and the optimal values for the heat transfer coefficient stayed very close to the initial values calculated by a nonlinear detailed code (22).

6.8 Conclusion on the Validity of the Models Used

In section 6.2, page 69, we had seen that even with nonoptimal parameter values, the validity of the core and steam generator models is good (Figures 6.1-6.4, pages 70-75). Using the optimal values found by the parameter identification procedure, the agreement between experiment and model prediction has improved (see Figures 6.9-6.12, pages 85-96). The nuclear power and the hot leg temperature predictions of the core model have the same form with the experimental transients, and they are

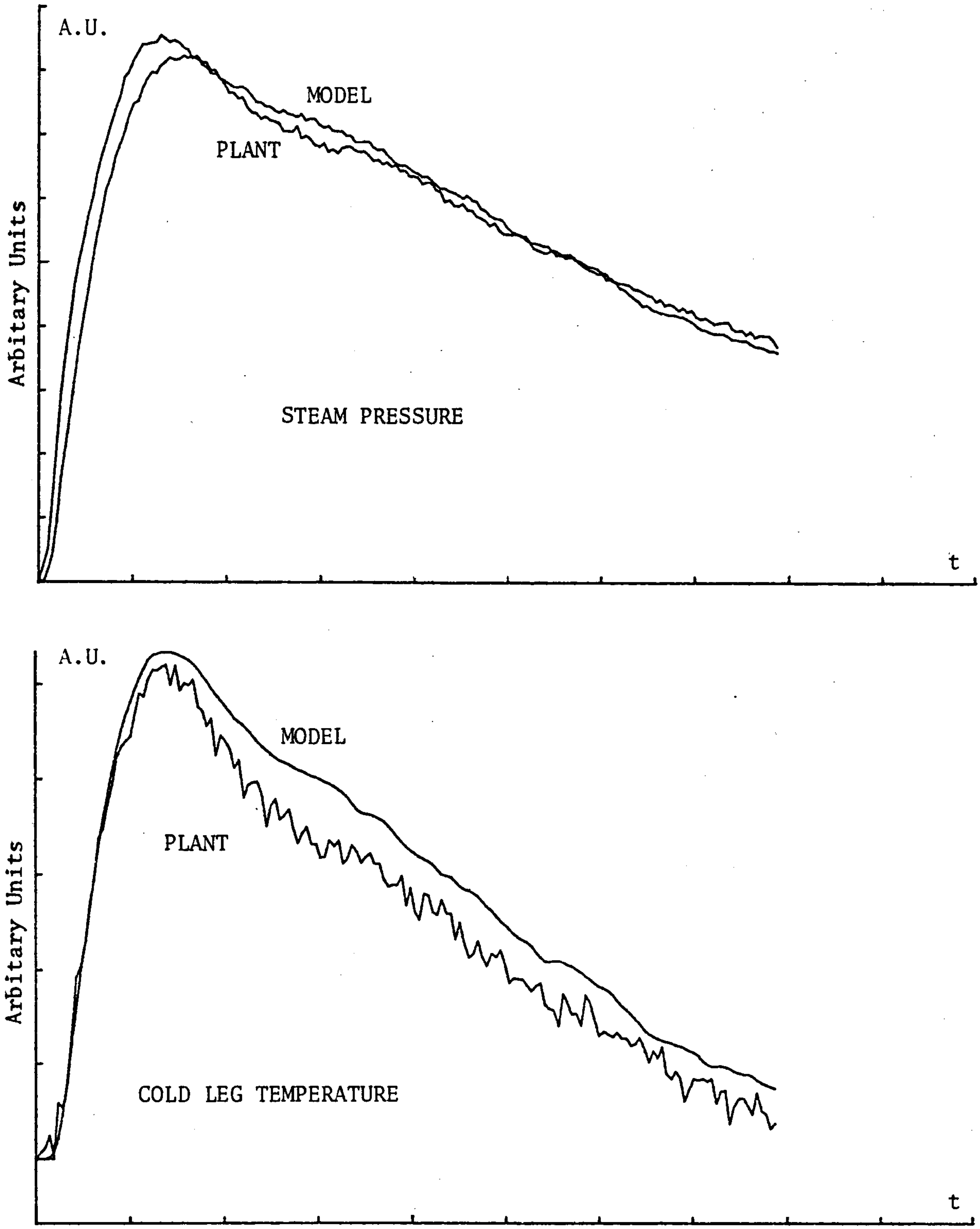

Figure 6.11 Steam Generator Model Optimal Response to a 100-90% Power Demand Step Perturbation.

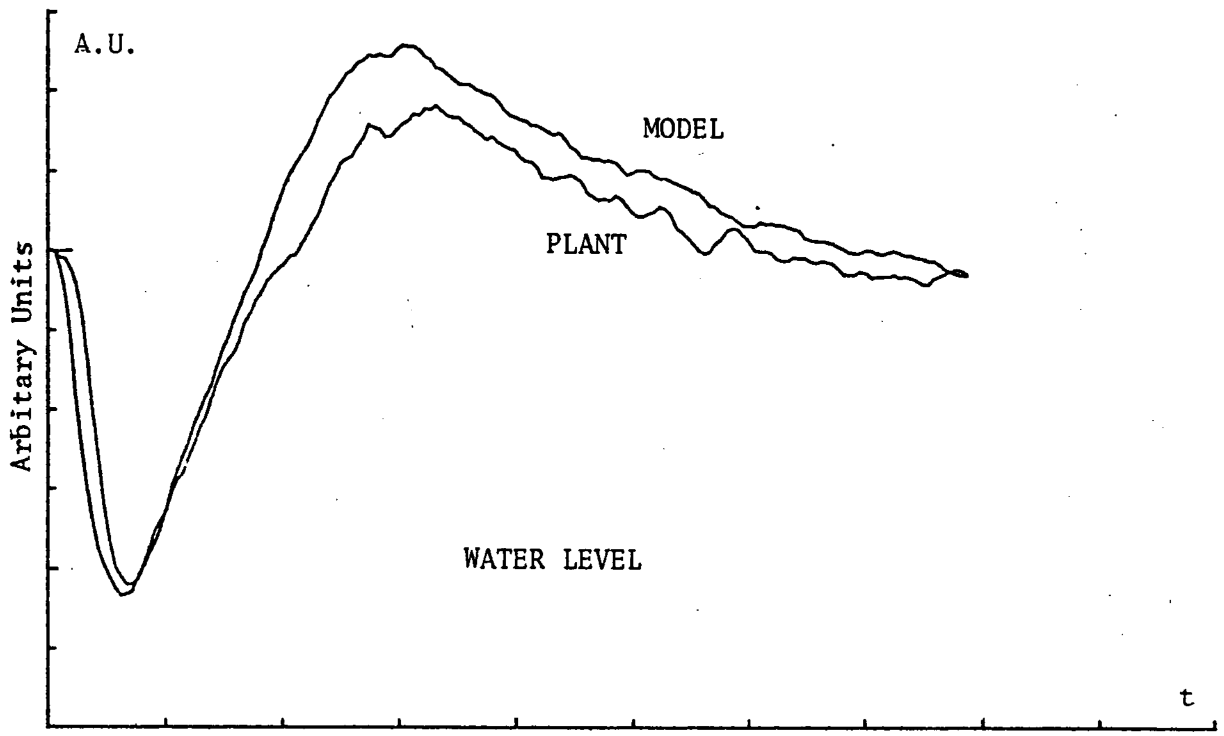

Figure 6.11 (Continued)

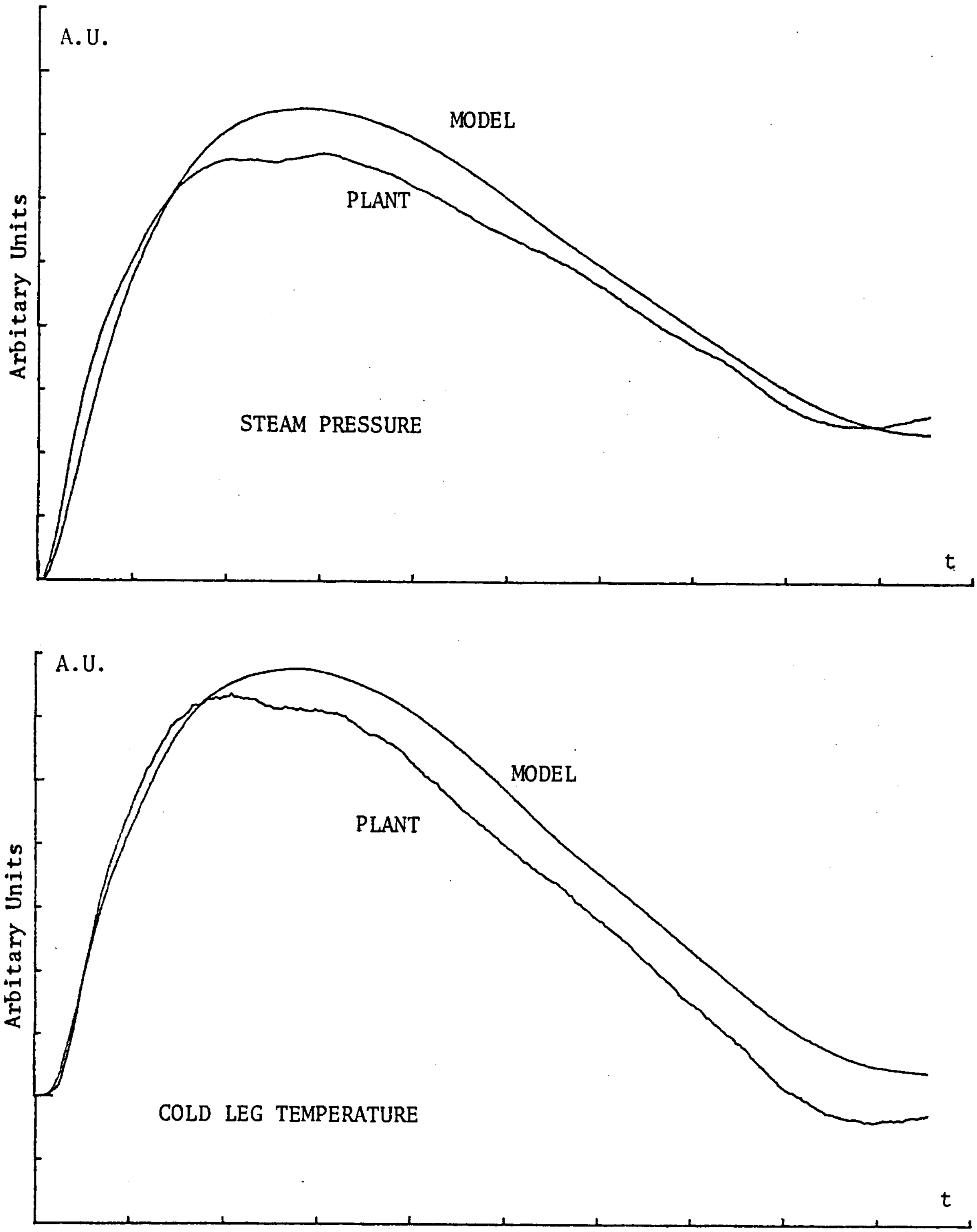

Figure 6.12 Steam Generator Model Optimal Response to a 30-20% Power Demand Step Perturbation.

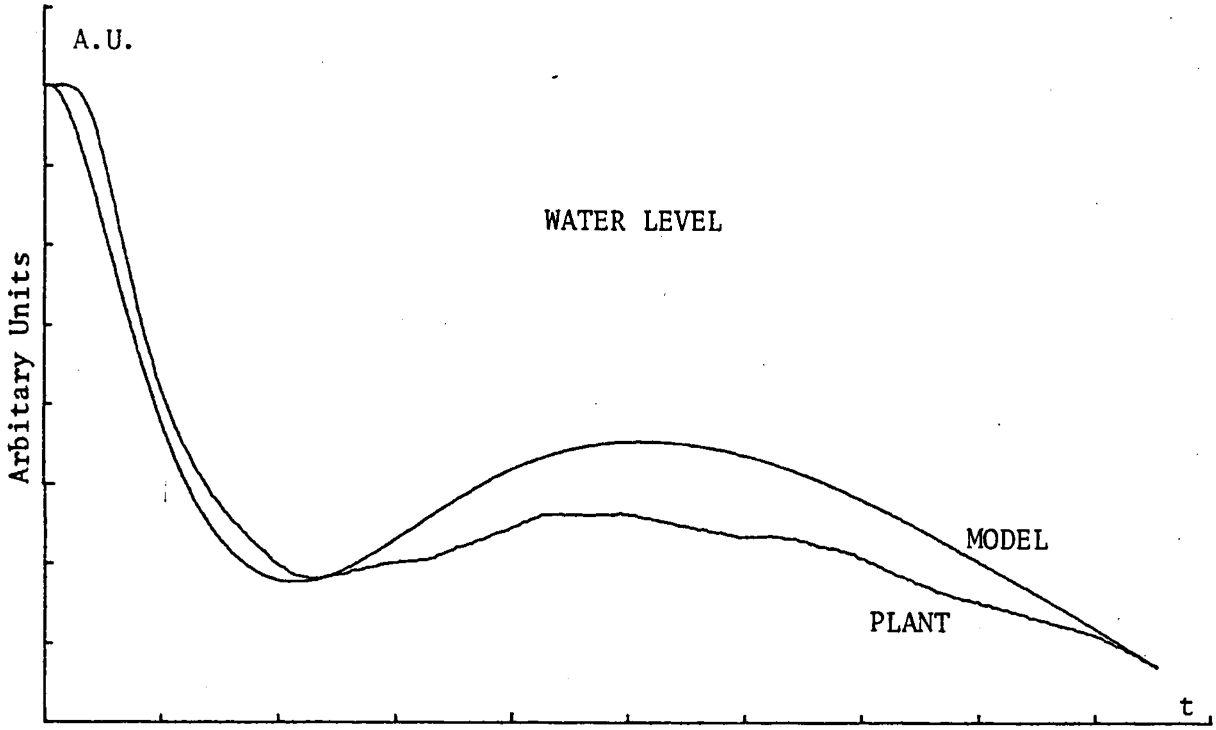

Figure 6.12 (Continued)

Table 6.2

Steam Generator Identification Results

	Full Power			Low Power		
	Initial	Optimal	Change	Initial	Optimal	Change
C_{pl}*	1.30	1.34	3 %	1.25	1.31	5%
x_{eo}**	0.21	0.19	-10 %	0.05	0.06	20%
EZ**	0.0	-0.066	- 6.6%	0.0	-0.04	-4%

*[Btu/lbm°F] **[Fraction]

only by a small percentage off the measured values (Figures 6.9 and 6.10). The time at which the peaks of the cold leg temperature, steam pressure, and the water level occur is exactly the same or within a few seconds of the measured time. At the end of the transients, which corresponds approximately to the new steady-state, we have very close agreement especially with the water level prediction, in which we are particularly interested in this study (see Figures 6.11 and 6.12).

Some of the reasons that may be responsible for the remaining disagreement observed in these figures could be (a) the simplified nature of the models, (b) the large size of the perturbations handled by linear models and (c) the nonoptimal values used for parameters not included in the identification.

However, for the purpose of simulating the reactivity control and feedwater control systems, it is felt that the agreement of the low-order linear models describing the core and steam generator dynamics with the experiment is good, and that we can proceed using them in the rest of the study, confident of their accuracy.

Furthermore, some additional cases were examined:

(a) The identification was performed only on two parameters (C_{pl} and EZ) with the initial value of x_{eo} being kept constant. The final changes in C_{pl} and EZ after this identification, both at full power and at low power, were identical to the ones found by the three-parameter identification. The final cost function value was higher since x_{eo} was kept constant. Thus, we are confident that the relatively larger changes in x_{eo} (see Table 6.2) did not overwhelm the search for the C_{pl} and EZ optimal values.

(b) The three-parameter identification on C_{pl}, x_{eo}, EZ was rerun with the metal to secondary heat transfer coefficient in the subcooled region (HS1) constant. This gave the same results as previously. This could mean that changes in UP, UM, and HS2 are much more important than changes in HS1.

(c) Efforts to reduce the cost function even lower, by starting the identification again with the optimal values as initial values did not succeed. The minimal value of the cost function and the optimal parameter values found were the same. The consistent convergence to the same cost function value and the same optimal parameter values for several different initial estimates, and the physically reasonable optimal values found at full power and low power, were considered to be sufficient evidence that the optimal values found by the identification procedure were acceptably accurate, within the scope of this study. However, one could possibly evaluate confidence levels on the optimal parameters found, using the procedure outlined in Section 6.6.

CHAPTER 7

OVERALL SYSTEM SIMULATION

7.1 Introduction

In previous chapters, the effort to obtain good quality plant test data, and the model parameter identification using this data, was presented for the reactor core model and the steam generator model at full and at low power. Thus, these two models can now be used to represent the coupled core-steam generator system for control purposes. The reactor control and feedwater control systems that close the loop (see Figure 2.6, page 20) are presented in Chapter 2 and the corresponding differential equations can be found in Chapter 3. There are 39 differential equations in total representing the dynamics of the closed loop system, and a listing of the 39 state variables, in the same order as they appear in the state vector, is given in Table 7.1. Special care was taken to simulate the nonlinear control rod motion, so that the reactor core outputs, nuclear power and hot leg temperature, which influence the responses of the control system and the steam generator, are as close as possible to responses obtained in a real plant test after the same perturbation.

The perturbations introduced are step changes in the power demand setpoint, as in the case of the plant tests. In order to evaluate the performance of the simulated control system, the same magnitude of step perturbations as in the plant tests were introduced, i.e., a 100-90% power demand perturbation and a 30-20% power demand perturbation.

Table 7.1

The State Variables of the Overall System (39×39)

1.	Q_N	Nuclear power
2.	X	The precursor state variable
3.	T_f	Fuel temperature
4.	T_1	Primary coolant temperature in the core (1st node)
5.	T_2	Primary coolant temperature in the core (2nd node)
6.	T_{up}	Upper plenum temperature
7.	$T_{h\ell}$	Hot leg temperature
8.	$T_{\ell p}$	Lower plenum temperature
9.	$T_{c\ell}$	Cold leg temperature
10.	T_{pI}	Primary coolant temperature in the steam generator inlet plenum
11-14.	T_{pi},i=1-4	Primary coolant temperature in node n° i.
15-18.	T_{mi},i=1-4	Metal temperature in node n° i.
19.	T_{po}	Primary coolant temperature in the steam generator outlet plenum
20.	L	Steam generator water level
21.	L_{s1}	Nonboiling length
22.	P	Steam pressure
23.	x_e	Steam exit quality
24.	T_d	Downcomer temperature
25.	Tavg	Hot leg-cold leg average temperature
26	Tavǵ	Tavǵ after a compensator
27.	Táv	Tavǵ filtered
28.	Tref	Change in reference temperature setpoint
29.	Q_p	Power mismatch
30.	Q_{tu}	Turbine power
31.	Q_v	Steam flow demand by the turbine
32.	CQ_{e1}	Filtered total steam flow signal for feedwater control
33-34	CQ_e',CQ_e''	Intermediate state variables for the 3rd order filter
35.	Q_e	Feedwater flow
36.	Q_{v1}	Steam flow correction
37.	Q_{aux}	Auxiliary state variable = dQ_{v1}/dt
38.	L_e''	Final water level feedback signal for feedwater control
39	L_e'	Water level feedback signal for feedwater control

These simulations were executed on the minicomputer described in the next section. Two integration methods were used, the matrix exponentiation method and a fourth-order Runge-Kutta method in order to check the results and compare the techniques. The matrix exponentiation technique, allowing real-time simulation on the minicomputer, was retained for the rest of the study. Various values were used for the parameters of the control system components to identify values that correspond to control performance as close as possible to the one exhibited during the plant tests.

7.2 The Computing Facility Used (36)

The computations required in this study were implemented on a SOLAR-16-40 minicomputer made by the Societé Europêene de Miniinformatique et Systémes in France. This medium size computer has the following specifications for the central unit processor:

--16 bit word size

--625 to 875 nanoseconds for memory cycle time

--64k words memory size.

The execution time for the most important operations are listed below:

--load register from memory	5.5 microseconds
--store register into memory	6.4 microseconds
--binary addition	2.2 microseconds
--binary multiplication	51 microseconds

Using a 32 bit hardware floating point operator, the execution time for the basis arithmetic operations is as follows:

--binary multiplication	3.5 microseconds
--binary division	6.4 microseconds
--floating multiplication	5.2 microseconds
--floating division	5.3 microseconds
--floating addition	10.3 microseconds

The peripheral equipment of the computer gives great flexibility for the input-output handling. It consists of:

--A moving head disc unit: this unit consists of a 5M bytes fixed disc and a removable disc with the same capacity, with a transfer rate of 156k words/second and a maximum access time equal to 70 milliseconds.

--A graphical CRT display unit, Tektronix model 4012. This unit is connected to a hardcopy system to reproduce the plots displayed on the screen.

--A teletype mode ASR 33.

--A card reader with a transfer rate of 400 cards/minute.

--An incremental digital plotter Tektronix model 4662. The configuration of the equipment is shown in Figure 7.1.

7.3 Method Used for the System Integration

The matrix state equation representing the system to be integrated is of the general form:

$$\dot{\underline{x}}(t) = A\underline{x}(t) + B\underline{u}(t) \tag{7.1}$$

where A is the (39 × 39) system matrix with constant coefficients, B is the (39 × 2) constant matrix containing the coefficients of the forcing

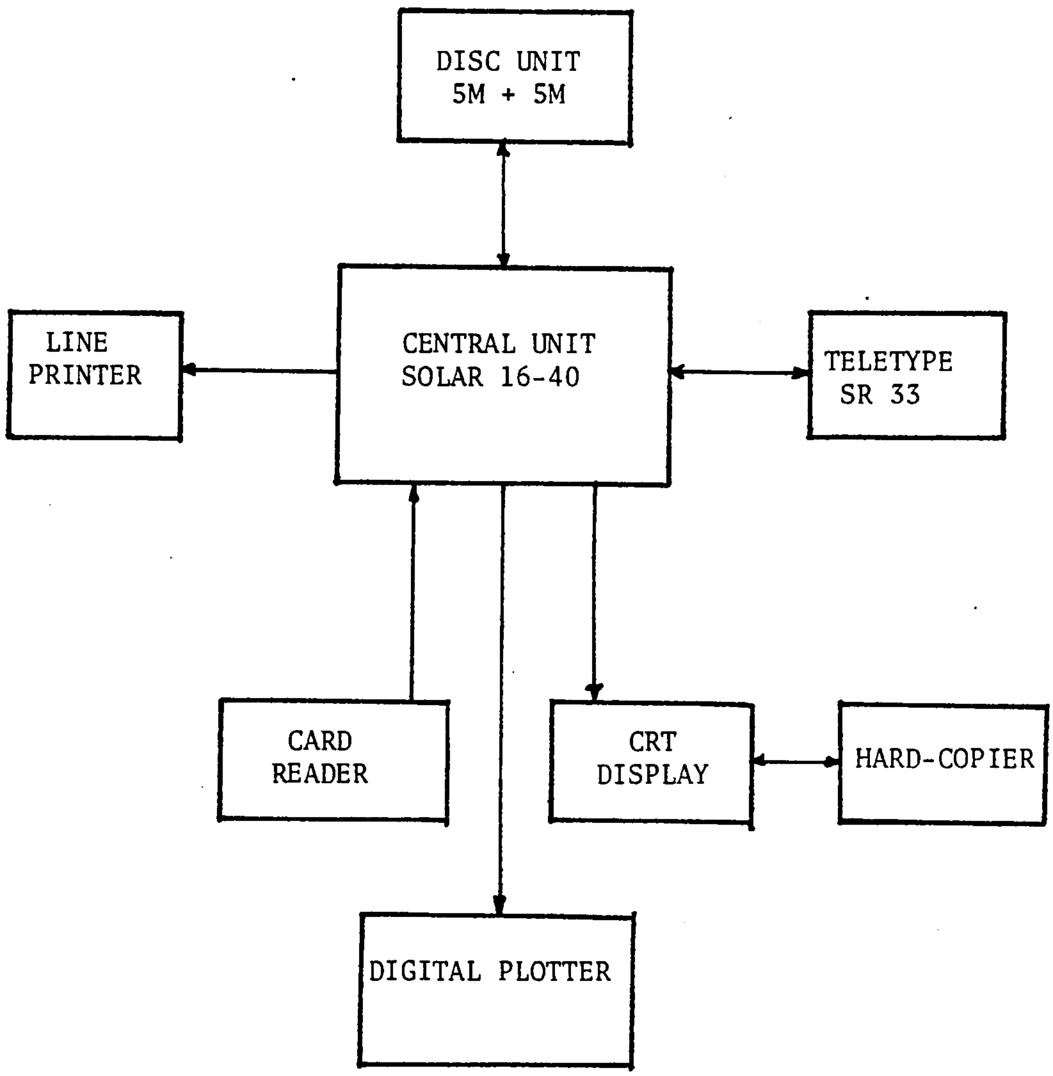

Figure 7.1 Configuration of the Solar 16-40 Minicomputer.

vector u, which consists of the control rod reactivity perturbation and the power demand perturbation. Since the state variables represent variations from the initial equilibrium, the initial condition on the state vector $\underline{x}$ is

$$\underline{x}(0) = 0 \ . \tag{7.2}$$

In order to solve equation (7.1) on a digital computer we need the equivalent matrix difference equation, obtained by integrating (7.1) and assuming that the forcing vector u is constant during the integration time step. The recursive solution obtained is

$$x(k+1) = D \cdot x(k) + E \cdot u(k) \tag{7.3}$$

with the matrix relations (6.4) and (6.5) for matrices D and E.

Several numerical problems are associated with the matrix exponential calculations. The power series approximation will be valid only if (37):

(1) The series converges

(2) The numerical computation does not lose significance due to overflow, roundoff and truncation errors.

In order to satisfy the two previous conditions, the initial sampling time interval ΔT is first reduced automatically to ΔT^* by a convenient power of two such that $\max_{ij} |A_{ij} \Delta T^*| < 1$, to insure the convergence of the power series expansion. To avoid roundoff errors, the step size is further reduced.

This procedure takes into account the significant digits of the floating point arithmetic computations (7 digits for single precision, 14 digits for double precision).

The system matrix A is a sparse matrix, and in practice many industrial processes are characterized by dynamic models with sparse state variable matrices. Thus, during the calculation of matrices D and E special care is taken to eliminate computations with zero elements. In general, throughout this work, matrix by matrix and matrix by vector products were optimized to save both computation time and memory space, and all programs were written in Fortran IV language.

The duration of the control rod step, corresponding to the fastest control rod motion possible (72 steps/minute) is 0.83 seconds, and thus we need an integration step shorter than this value. A value of $\Delta T = 0.2$ seconds was chosen because it allowed good resolution for the control rod movement, numerical stability, and real-time simulation of the system. With this integration step the matrix exponentiation code used six terms in the calculation of matrices D and E in equations (6.4) and (6.5).

In order to verify the accuracy of the integration provided by the matrix exponentiation method described above, a Runge-Kutta method (38) of the fourth order was used to integrate equation (7.1) for the same perturbations. It was found that the maximum integration step ΔT to give a numerically stable solution with this method was 0.008 seconds, and the solution was exactly the same (to the fourth significant digit) as the matrix exponentiation method using a $\Delta T = 0.2$ seconds. Since the matrix exponentiation method requires a much shorter time step, it was adopted as the integration technique to be used.

7.4 Control Systems Performance

The load following dynamics of the closed loop system (see Figure 2.6, page 20) were simulated at full power and at low power by introducing power demand step perturbations of the same magnitude as the ones introduced during the plant tests (Chapter 4), so that an evaluation of the performance of the control systems used could be made.

It should be emphasized that the main objective in these simulations is to obtain a satisfactory control of the steam generator water level. A good prediction of the primary loop dynamics though is also desirable. To this effect, the nonlinear control rod motion (Figure 2.8, page 21) was modeled together with the nonlinear gains involved (see Figure 2.7, page 21) in the power mismatch control chain. However, the control rods are assumed to move in a step-wise manner (instantaneous step transitions), and the digital simulation with an integration step of $\Delta T = 0.2$ seconds could introduce errors in the timing of the rod motion in response to its driving signal. These two factors and the use of a simplified core model could introduce inaccuracies in the prediction of the primary loop dynamics, which would cause inaccuracies in the prediction of quantities in the secondary loop. All these should be considered when comparing the simulated transients with actual test transients.

Since a large step perturbation was introduced on the secondary side, the steam generator water level control is not affected significantly by possible inadequacies of the primary loop modeling discussed above. However, the feedwater temperature feedback mechanism was not modeled and thus its effect, discussed in Chapter 5, must be taken into account when evaluating the performance of the overall system simulation. Because of that, higher secondary pressures could be predicted (see Figures 5.7 and 5.8, pages 65-66) and thus higher primary coolant temperatures, which in turn would cause lower nuclear power predictions because of the moderator negative feedback effect. The power mismatch control channel would then be affected and so will the error temperature signal that drives the control rods. Figures 7.2 and 7.3 (for the full power and low power case, respectively) illustrate the effect of the various assumptions made and discussed above, on the performance of the system simulation in a load following transient. A discussion of the results shown in these figures follows; the experimental transients are also shown on the same figures.

At full power, the approximate step decrease in steam flow rate and the resulting control action of feedwater flow rate change are considered to be in good agreement with the experimental transients. The behavior of the steam generator water level transient shows good control of the water level. The difference with the experimental transient could be attributed at the early part of the transient to possible limitations of the steam generator model used, as can be seen from the model validation work (see Figure 6.11, page 93), and at the later part of the transient to the constant feedwater temperature assumption, as can be seen from the sensitivity analysis (see Figure 5.7, page 65). The constant feedwater temperature assumption is also a plausible explanation (see Figure 5.7) for the differences observed in the secondary pressure and primary exit temperature. Primary exit temperature errors would

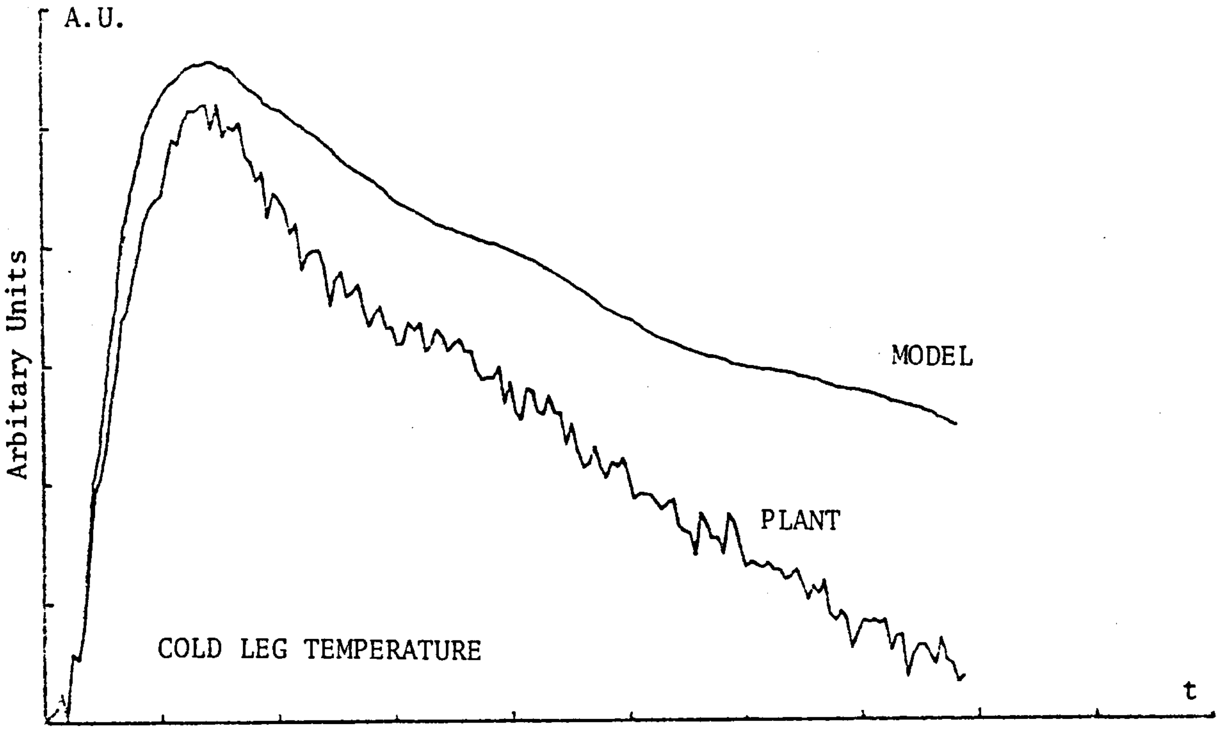

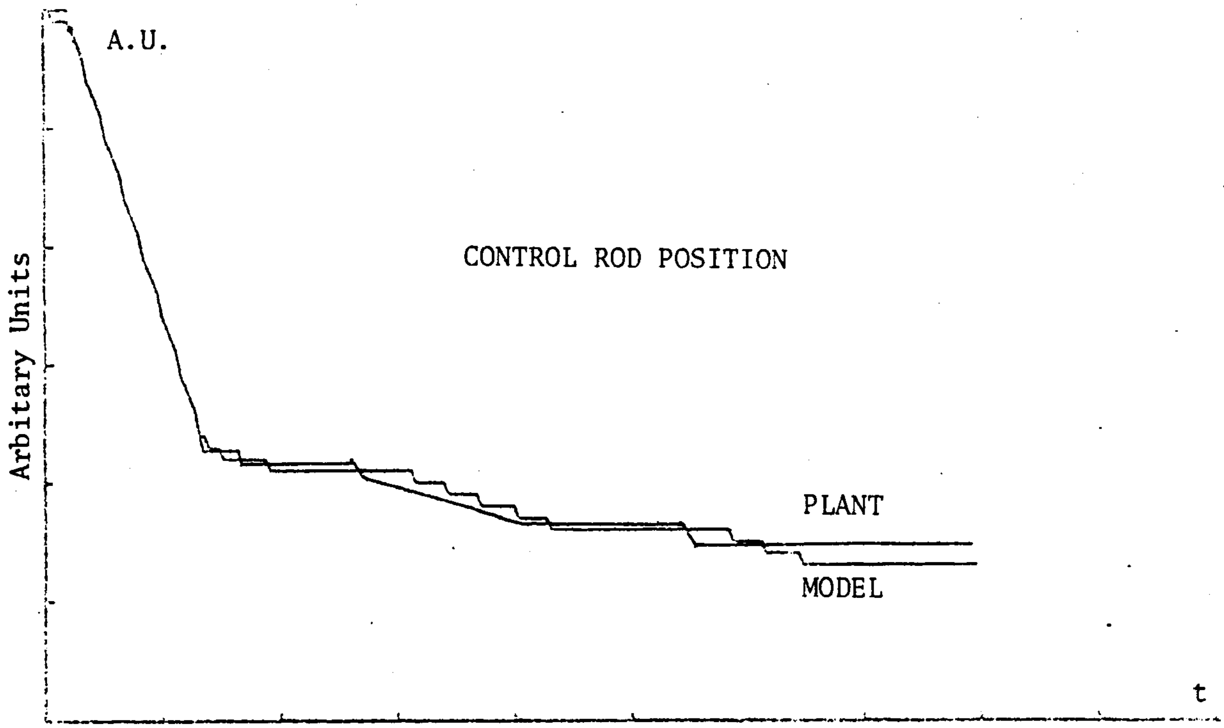

Figure 7.2 Performance of the Overall System Simulation for the 100-90% Power Demand Step Perturbation.

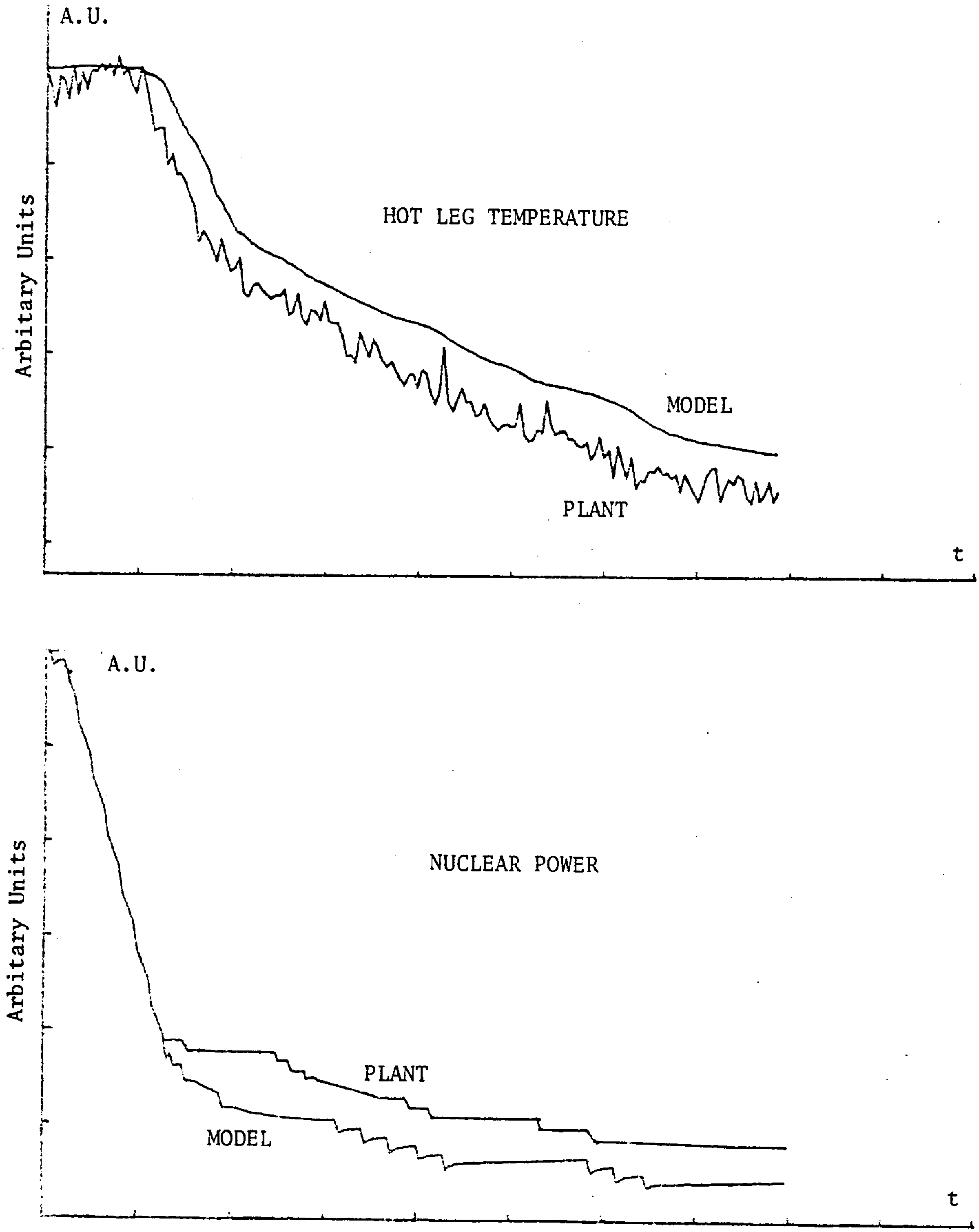

Figure 7.2 (Continued)

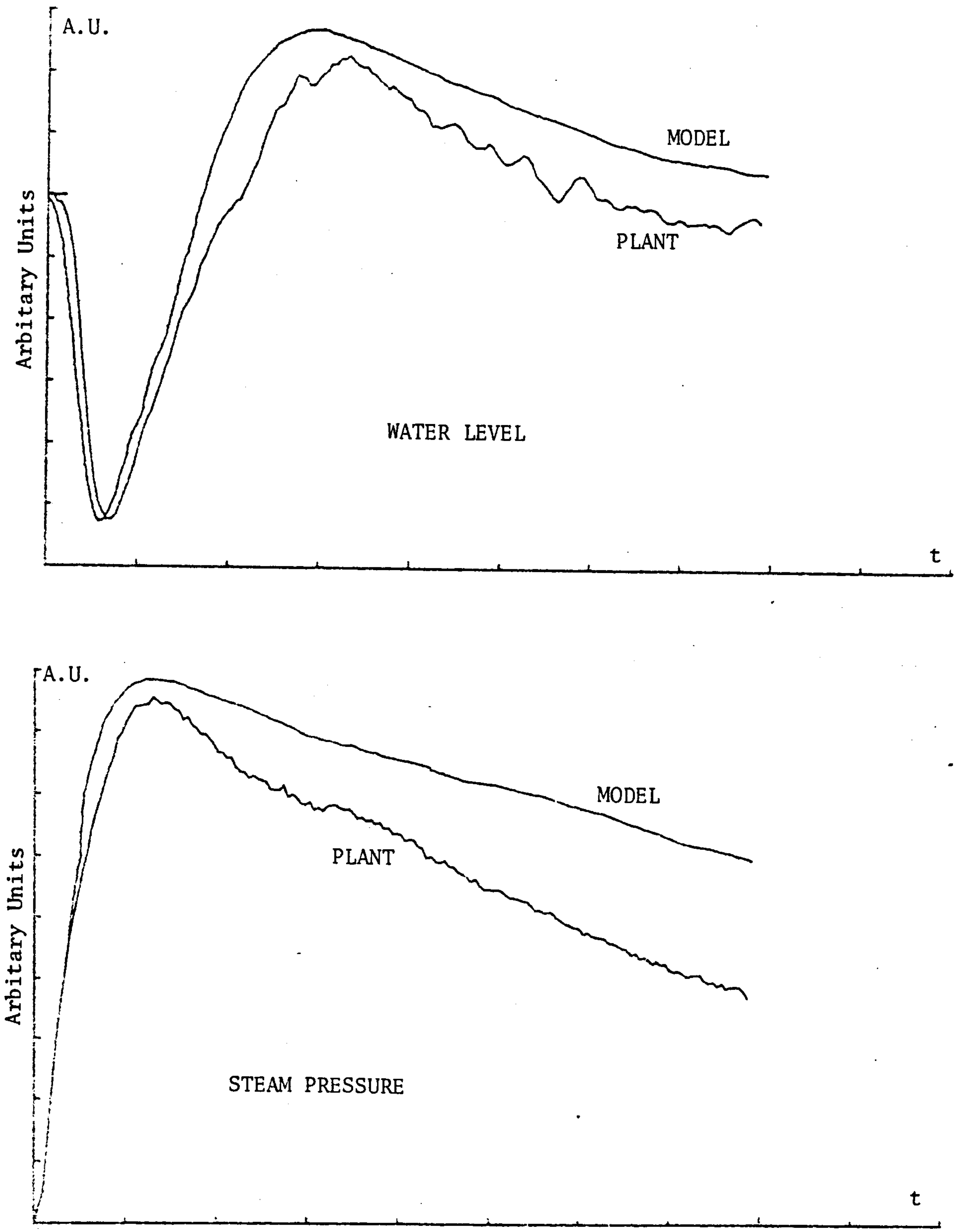

Figure 7.2 (Continued)

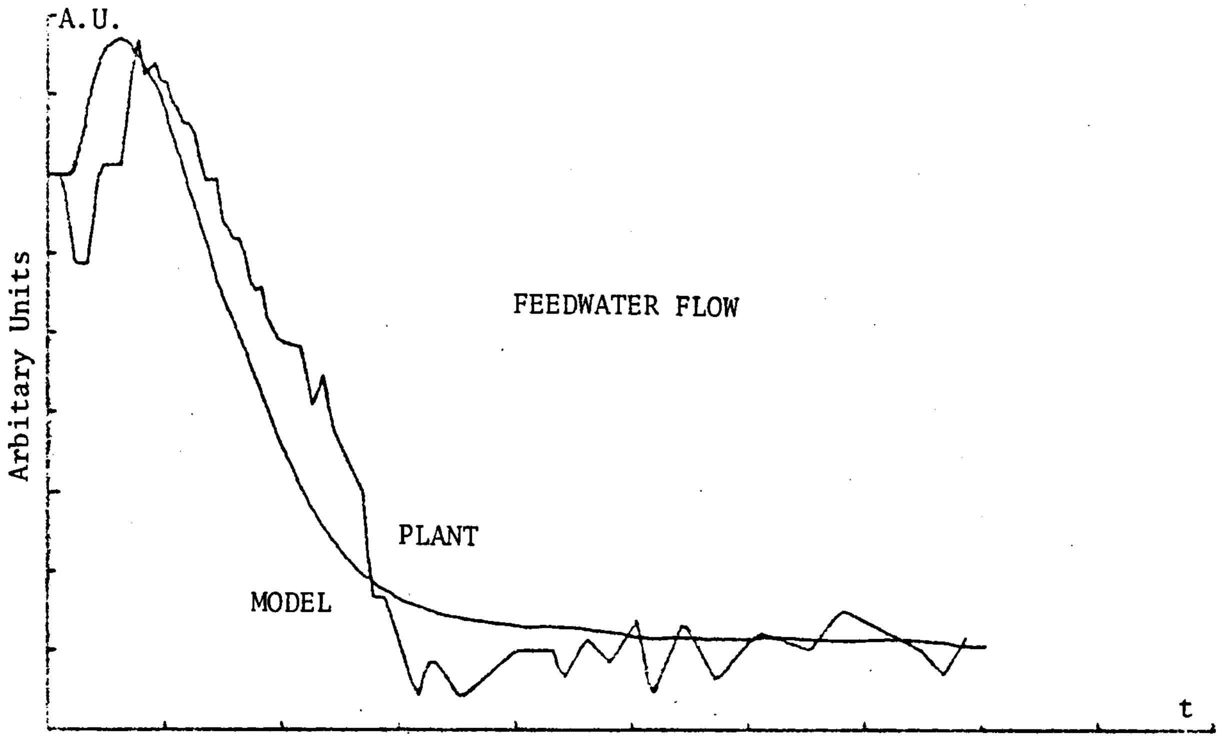

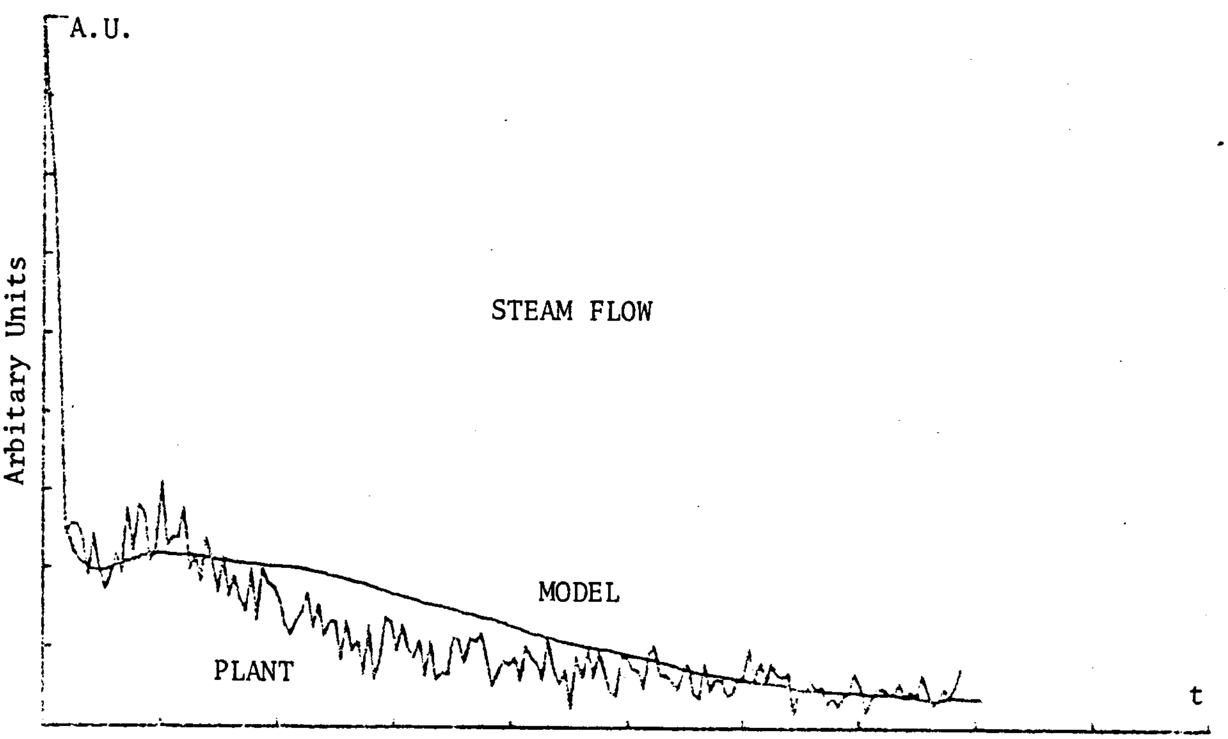

Figure 7.2 (Continued)

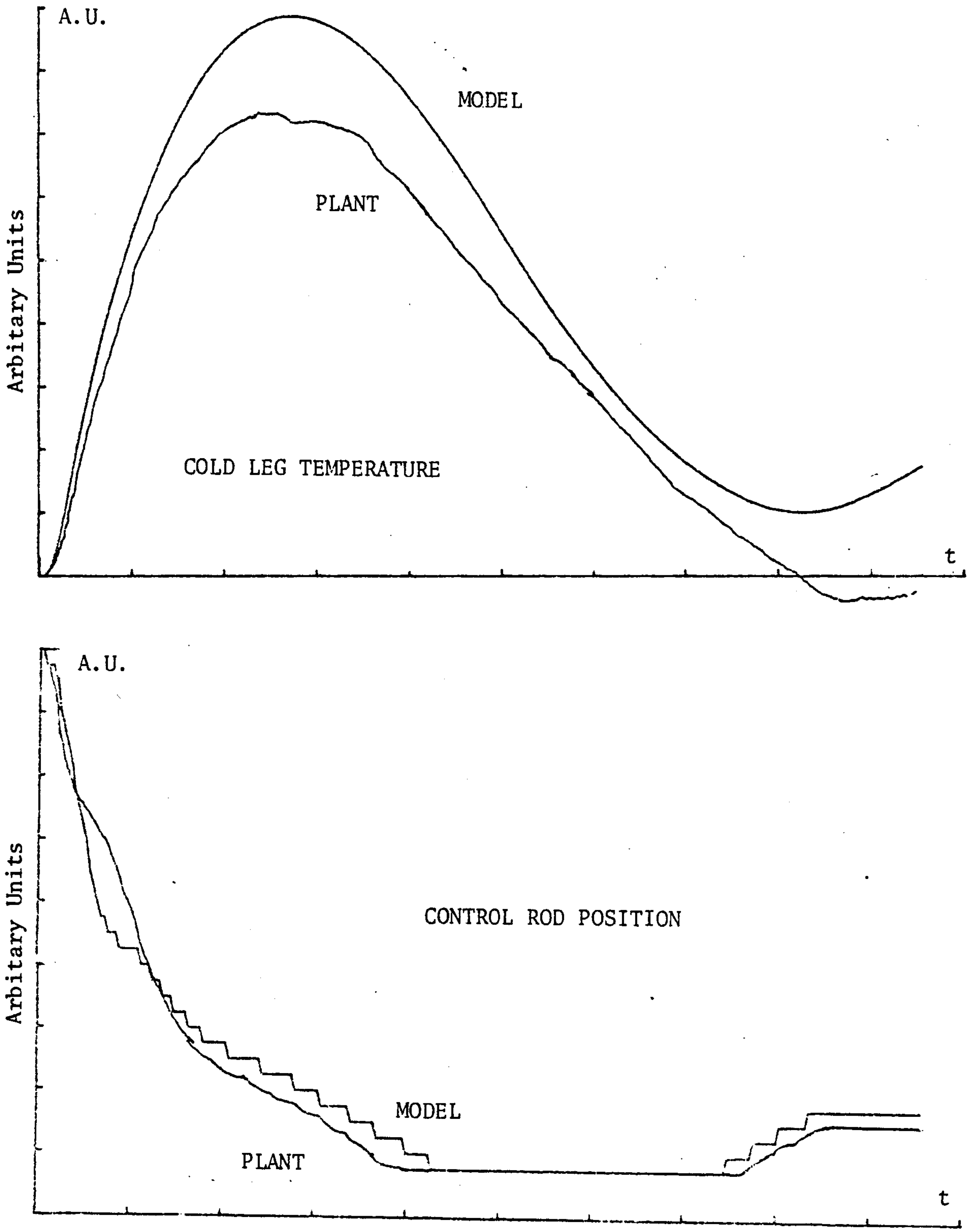

Figure 7.3 Performance of the Overall System Simulation for the 30-20% Power Demand Step Perturbation.

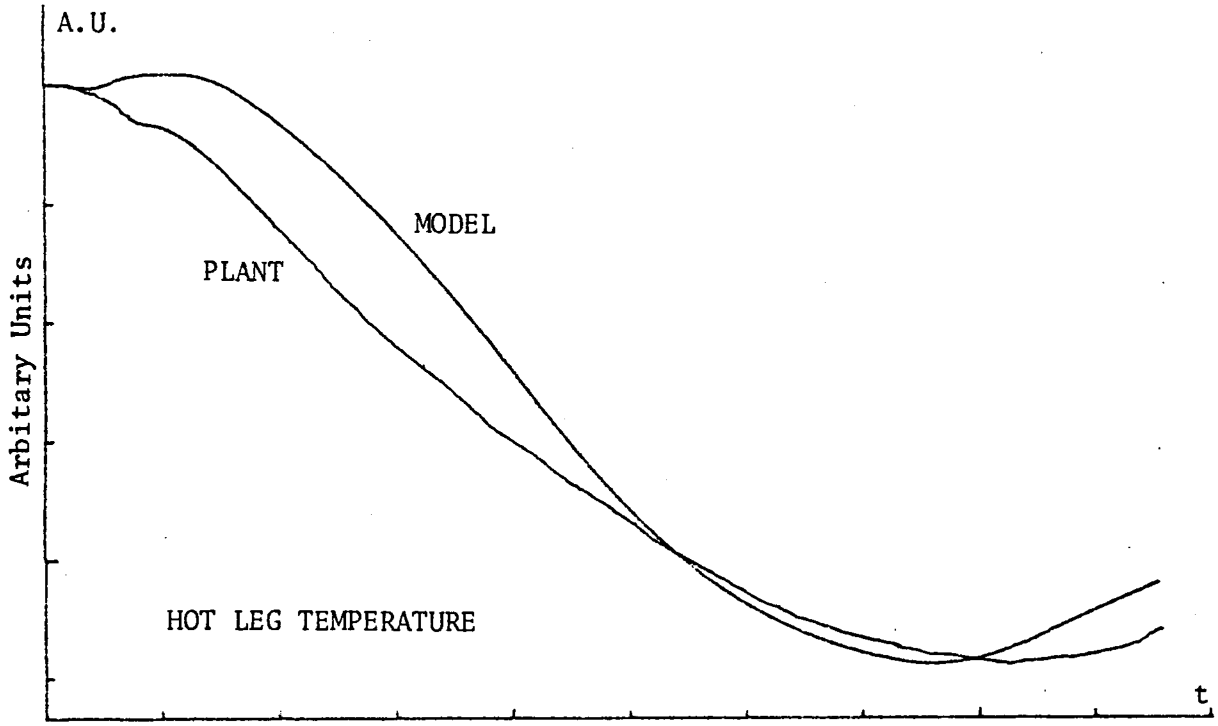

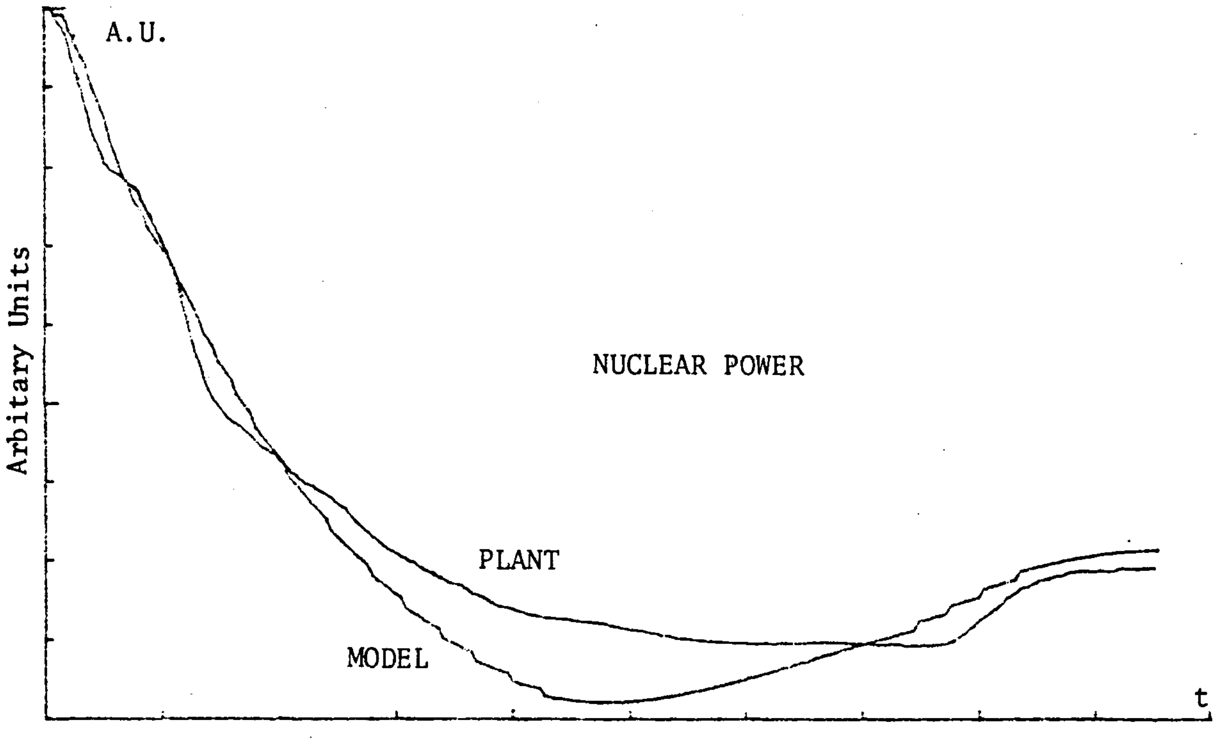

Figure 7.3 (Continued)

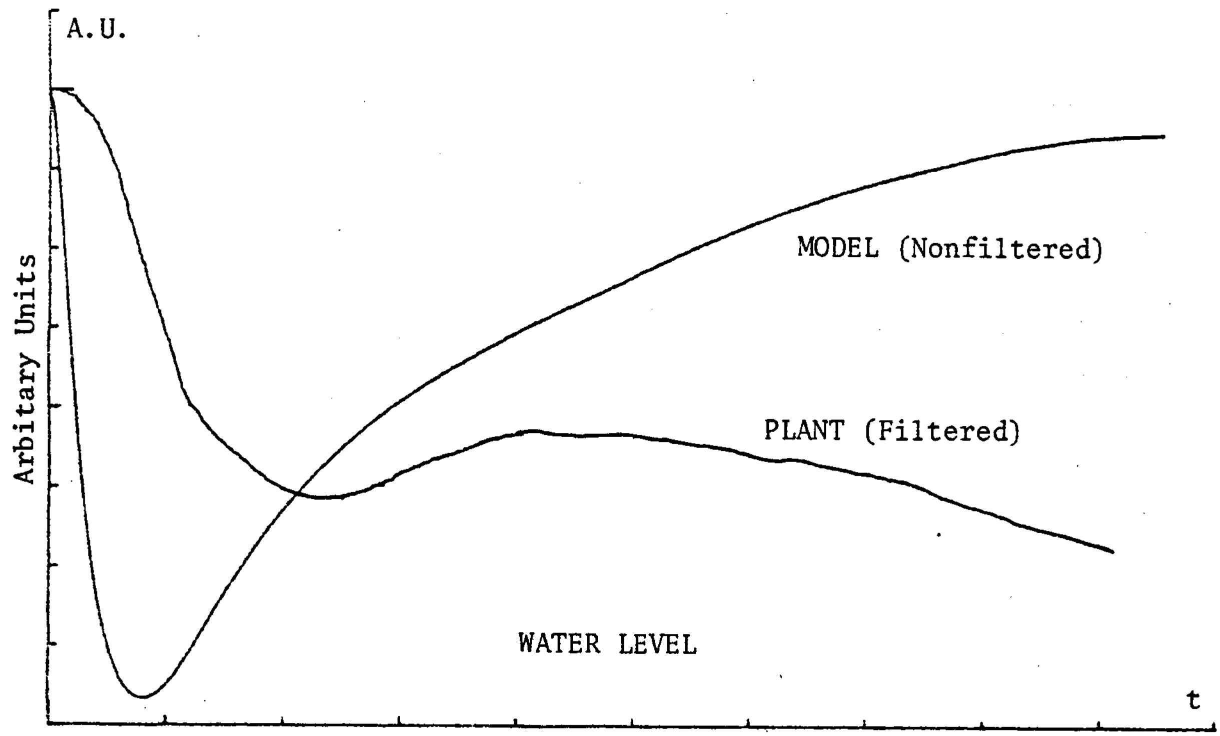

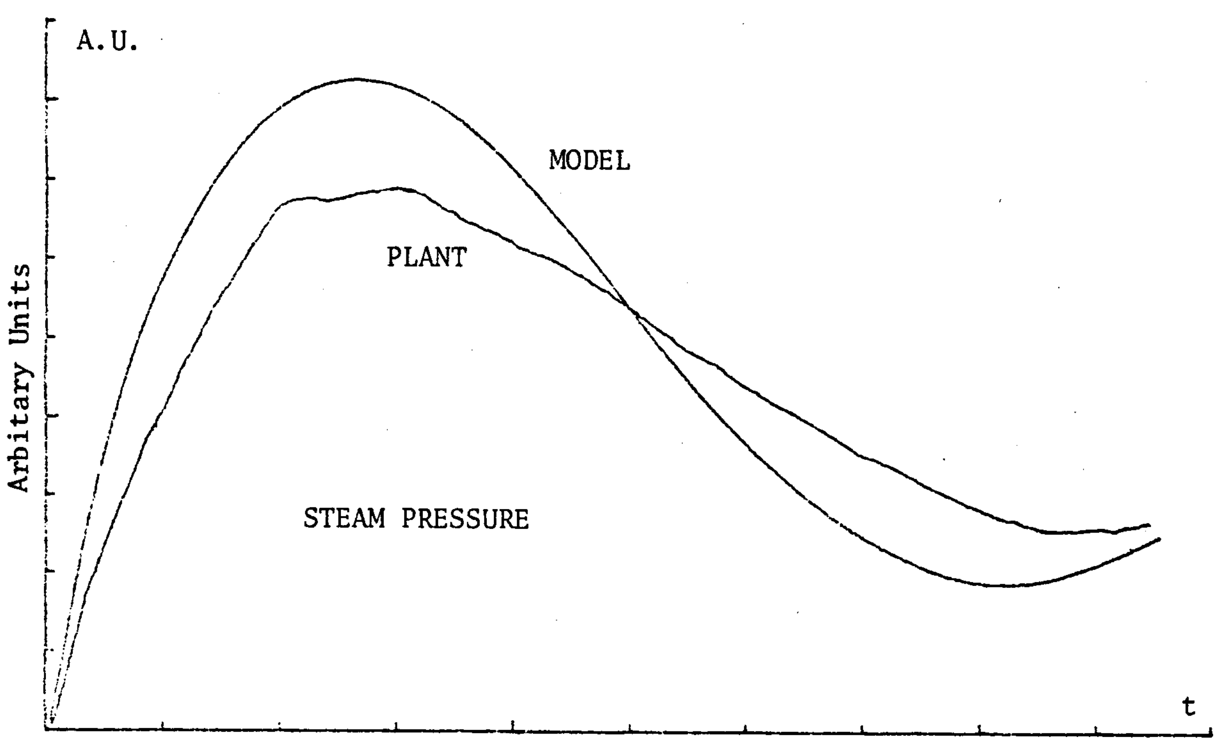

Figure 7.3 (Continued)

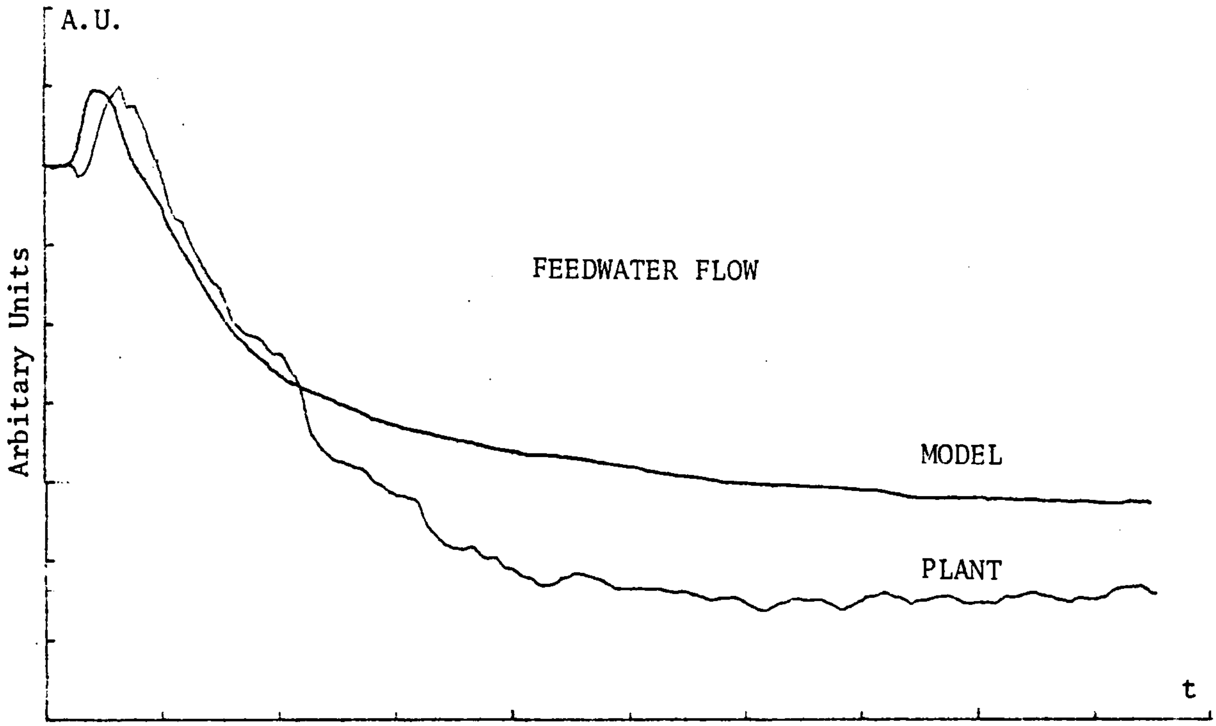

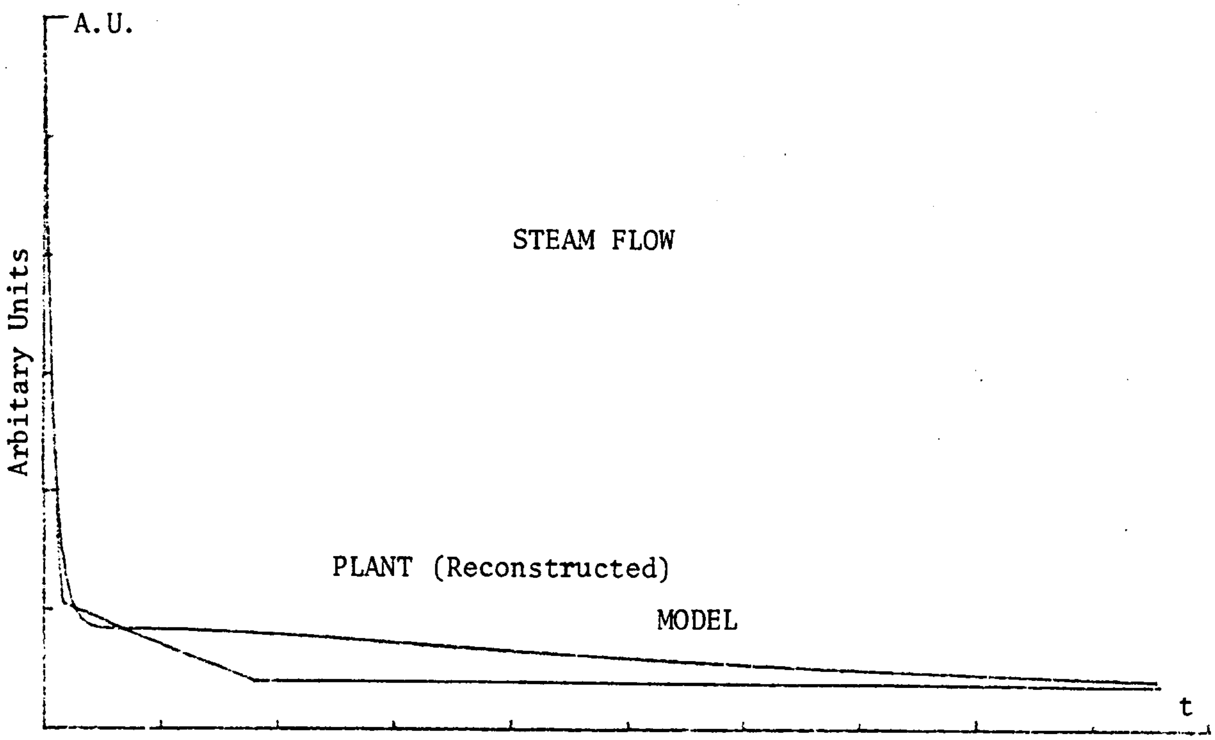

Figure 7.3 (Continued)

result in errors in the cold leg temperature prediction and in the primary coolant temperature in the core. This would result in differences in the nuclear power prediction from the plant transients in the opposite direction due to the moderator negative feedback effect. However, the simulated transients predicted in general the experiments with good accuracy. The nonlinear control rod motion was predicted also with good accuracy and this indicates that the responses of all three control chains of the reactor control (see Chapter 2) and the modeling of the control rod motion were satisfactory within the scope of this study.

At low power, similar remarks as above could be made on the performance of the simulation of the 30-20% power demand step perturbation. In this case though two points that were already discussed in previous chapters, should be stressed: (a) the experimental transients were filtered with a three-second filter and (b) the water level signal in particular was filtered with a 30-second filter. During the plant test the water level was not controlled as desired to its zero setpoint due to inadequate feedwater flow control. However, the simulated transient shows a steady drop of the water level to its zero setpoint due to a better action of the feedwater controller, as can be seen from the feedwater flow rate transient.

The parameters of the various transfer functions of the control system components, identified as optimal in obtaining a good water level and reactor control, are given in Table 7.2 for the full power and low power case. The notation corresponds to the one defined in Chapter 2 (see Figure 2.6, page 20).

Table 7.2

The Optimal Parameter Data of the Control Systems Simulated

At 100% Power	At 30% Power
$K^* = 9.9$ lbm/sec	$K^* = 9.9$ lbm/sec
$\tau_4 = 10.$ sec	$\tau_4 = 12.$ sec
$\tau_p = 2.0$ sec	$\tau_p = 2.0$ sec
CK = 0.7	CK = 1.0
CC = 1.0	CC = 1.0
CK1 = 0.5	CK1 = 0.3
CK2 = 1.0	CK2 = 1.5
$\tau_7 = 7.0$ sec	$\tau_7 = 5.0$ sec
$\tau_2 = 1.0$ sec	$\tau_2 = 10$ sec
$\tau_1 = 80.$ sec	$\tau_1 = 25.$ sec
$\tau_3 = 1.0$ sec	$\tau_3 = 5.0$ sec
ZKS = 0.30186 °F/%	ZKS = 0.30186 °F/%
$\tau_5 = 30.$ sec	$\tau_5 = 80.$ sec
$\tau_6 = 13.0$ sec	$\tau_6 = 15.0$ sec
$\tau_v = 35.$ sec	$\tau_v = 30.$ sec
$\tau_e = 2.5$ sec	$\tau_e = 2.5$ sec
$\tau_d' = 3.0$ sec	$\tau_d' = 3.0$ sec
$\tau_d = 5.0$ sec	$\tau_d = 15.0$ sec
$G_i = 17.6$ lbm/s/%	$G_i = 2.86$ lbm/s/%
$\tau_i = 8 \cdot 10^2$ sec	$\tau_i = 1.1 \cdot 10^3$ sec
D = 1.	D = 1.
B = 0.01	B = 0.01
A = 0.25	A = 0.1
C = 100.	C = 100.

Information on the nominal values of these parameters, available to the author after the completion of this dissertation, has shown that the parameter values found are within 30% of their nominal values.

CHAPTER 8

MODERN LINEAR CONTROL THEORY APPLICATION

8.1 Modern Approach to the Control of Industrial Process--The Linear-Quadratic-Gaussian (LQG) Theory

In the control of industrial processes, such as a large nuclear plant, a multitude of couplings between different variables occurs. This situation makes it attractive to consider control methods which allow for the treatment of the control problem in a multivariate state space, instead of assigning single loop controllers to single variables and individually handling the coupling phenomena between them.

The mathematical theory of linear optimal control has developed rapidly and it has become well established during the past 20 years. It is concerned with predicting a continuous control function of time, or a sequence of controls for the discrete-time case, which when applied to a plant during a specific future control time interval, will cause it to operate in some optimum manner. This optimum manner is specified by constructing a (quadratic in our case) function of the state and control variables, which is integrated over the central interval, and results in a scalar quantity that measures the quality of plant performance in response to the chosen control function.

However, the calculation of the control function requires the accurate knowledge of the state of the plant. Since only some of the state variables are measurable and also because of noise corrupted measurements, the complete state vector of the plant has to be estimated.

The results of the well established Linear Estimation theory are employed for this purpose, using white Gaussian noise.

The solution of the linear-quadratic deterministic control problem and the solution of the linear-quadratic-Gaussian estimation problem, lead, using the Separation Theorem (39), to the overall Linear-Quadratic-Gaussian (LQG) method. The detailed discussion of these problems, solution techniques and computational aspects may be found in reference (40). The formulation and the solution of the linear quadratic control problem and the linear Gaussian estimation problem are briefly described. The discrete-time case will be followed in this presentation since the implementation of the final algorithm will be done on a digital computer. The feasibility of this method for the control of our particular reactor core-steam generator system will be outlined.

8.2 The Linear Quadratic Control Problem

Although accurate descriptions of dynamic systems require nonlinear differential equations, it is usually possible to obtain a good approximation to the dynamic behavior of the system by linearizing the nonlinear equations around an equilibrium point. Thus, a time-invariant system can be described by the state-space equations (presented in Chapter 6 but repeated here for convenience);

$$\dot{\underline{x}}(t) = A\underline{x}(t) + B\underline{u}(t) \tag{8.1}$$

$$\underline{y}(t) = C\underline{x}(t) \tag{8.2}$$

with

$$\underline{x}(t_o) = \underline{x}_o \tag{8.3}$$

where

$\underline{x}$ is the nth order state vector

$\underline{u}$ is the mth order control vector

$\underline{y}$ is the rth order output vector, containing the observable states

$\underline{x_o}$ is the nth order initial state vector

A,B,C, are constant matrices, describing the dynamics of the system.

In the discrete-time case, equations (8.1) and (8.2) must be transformed into discrete-time difference equations. We assume that $\underline{u}(t)$ is constant between the sampling instants t_i and t_{i+1} and equal to $\underline{u}(i)$. Thus, integrating equation (8.1), we obtain

$$x(i + 1) = Dx(i) + Eu(i) \tag{8.4}$$

$$y(i) = Cx(i) \tag{8.5}$$

with the matrix relations

$$D = e^{A \cdot \Delta T} = I_n + A \cdot \Delta T + \frac{(A \cdot \Delta T)^2}{2!} + \ldots \tag{8.6}$$

$$E = (e^{A \cdot \Delta T} - I_n)A^{-1}B = \Delta T(I_n + \frac{A \cdot \Delta T}{2!} + \frac{(A \cdot \Delta T)^2}{3!} + \ldots)B \tag{8.7}$$

where

$\Delta T = t_{i+1} - t_i$ is the sampling time interval

I_n is the nxn unit matrix.

The cost function to be minimized is taken to be a weighted quadratic function of the control vector and the observable state vector:

$$J = \sum_{i=0}^{N-1} (u(i)^T Ru(i) + y^T(i)Qy(i)) \tag{8.8}$$

where

$Q \geq 0$ is a rxr weighting matrix

$R > 0$ is a mxm weighting matrix

N is the number of time samples in the control interval.

In order to obtain the optimal control we will use the Dynamic Programming method (39), which is based on the Optimality Principle that states: "Any control law which is optimal over the interval [i,N] is necessarily optimal over the interval $[i + 1, N]^n$."

We can consider the problem starting at any time instant i in the interval [0, N] and study the optimal $\hat{J}(x(i))$ defined by

$$J_i = \sum_{j=i}^{N-1} (u^T(j)Ru(j) + y^T(j)Qy(j)) .$$

If $\underline{u}(i)$ belongs to the series of optimal controls $[\hat{u}(i), \hat{u}(i+1), \ldots, \hat{u}(N-1)]$ that were taken during the time interval [i, N-1], the principle of optimality indicates that the series of optimal controls $[\hat{u}(i+1), \hat{u}(i+2), \ldots, \hat{u}(N-1)]$ allows one to obtain the minimum value of the quadratic criterion $\hat{J}[x(i+1)]$ defined in the interval [i+1, N-1] by

$$J_{i+1} = \sum_{j=i+1}^{N-1} (u^T(j)\ Ru(j) + y^T(j)\ Qy\ (j)) . \tag{8.9}$$

It is thus possible to define in a recursive way the minimal quadratic criterion by the relation

$$\hat{J}(x(i)) = \min_{u} \left(u^T(i)Ru(i) + y^T(i)Qy(i) + \hat{J}(x(i+1))\right) . \tag{8.10}$$

Now we can assume that $\hat{J}(x(i+1))$ is of the quadratic form:

$$\hat{J}(x(i+1)) = x^T(i+1)K(i+1)x(i+1) \tag{8.11}$$

where $K(i+1)$ is a square, symmetric, positive definite matrix. Using equations (8.4) and (8.11), equation (8.10) becomes

$$\hat{J}(x(i)) = \min_{u} \left(u^T Ru + y^T Qy + (Dx+Eu)^T K(i+1)(Dx+Eu)\right) . \tag{8.12}$$

The minimum $\hat{u}$ corresponds to the solution of $\partial\hat{J}/\partial\underline{u} = 0$, i.e.

$$R\hat{u} + E^T K(i+1)(Dx+Eu) = 0 \tag{8.13}$$

or

$$\hat{u} = -Lx \tag{8.14}$$

where

$$L = [R + E^T K(i+1)E]^{-1} E^T K(i+1)D . \tag{8.15}$$

Substituting equation (8.14) back into equation (8.2) yields:

$$\hat{J}(x(i)) = x^T L^T RLx + x^T C^T Qx + x^T((D^T - L^T E^T)K(i+1)(D-EL))x$$

or

$$J(x(i)) = x^T(i)K(i)x(i)$$

where

$$K(i) = L^T RL + C^T QC + (D-EL)^T K(i+1)(D-EL) \tag{8.16}$$

which by regrouping terms and using equation (8.15) becomes

$$K(i) = -D^T K(i+1)EL + C^T QC + D^T K(i+1)D \ . \tag{8.17}$$

The above recursive relationship for K is defined backwards in time. Thus, for any given application K(i) has to be calculated in advance for every time instant i of the time interval considered, and the results should be stored. Whenever any of the elements of the above matrices change, this calculation has to be repeated, and this is a serious constraint to most industrial applications.

We should thus consider that the time interval we have in mind to apply the control is practically infinite with respect to the time-scale of the physical phenomena considered. Thus, the criterion to be optimized takes the form

$$J = \sum_{i=0}^{\infty} (u^T(i)Ru(i) + y^T(i)Qy(i)) \ .$$

With the conditions we have imposed on matrices R and Q ($R > 0$, $Q \geq 0$), it can be shown (41) that equation (8.15) converges to a limiting unique solution when the system considered is controllable, i.e., when

$$\text{rank}[E,\ DE,\ D^2E,\ .\ .\ .\ ,\ D^{n-1}E] = n\ . \tag{8.16}$$

Thus, we can consider matrix K(i) as constant during the whole time interval and equal to a symmetric positive definite matrix K given by

$$K = -D^TKEL + C^TQC + D^TKD \tag{8.17}$$

where

$$L = [R + E^TKE]^{-1}E^TKD\ . \tag{8.18}$$

The solution of equation (8.17) will be discussed later.

Up to this point, we are able to calculate in a digital machine the feedback control, equation (8.14), of a linear deterministic system, that forces it to go from one steady-state to another in an optimal manner, as dictated by a quadratic criterion. However, in order to calculate this control, the complete state vector $\underline{x}$ of the physical process under study is assumed known, while only a few of its components are measurable.

In addition, the existence of noise associated with the actuators and the sensors, and the uncertainties in the system modeling, force us to consider a stochastic model, as representing more accurately the physical process. Then, results of the Linear Estimation Theory can be used to compute an estimate of the complete state vector, and the Separation Theorem allows us to use this estimate in calculating the optimal feedback control obtained so far.

8.3 The Linear Estimation Problem

In order to adapt a stochastic model to represent the physical process under study, there are three sources of uncertainties which must be taken into account (Figure 8.1):

1. Uncertainties associated with the system modeling: In addition to the control signals driving the system, there may be additional, stochastic, disturbances. Also, simplifications in the deterministic model can introduce errors, and despite the system identification study for certain key parameters, there may be inexact values for some parameters of the system.

2. Uncertainties associated with the actuators: The actual plant inputs are the translation of the commanded inputs u(t) by the actuators. There are always uncertainties introduced by the actuators since this translation of signals into actual inputs (reactivity, etc.) is not exact.

3. Uncertainties associated with the sensors: The physical quantities we measure (temperatures, pressures, etc.) are different from the true values since any sensor has a limited accuracy and also additional error may be introduced along the data transmission and acquisition chain.

The various uncertainties described above can be modeled in the stochastic case, by introducing white noise processes in the deterministic equations. The uncertainties associated with the modeling and the actuators are taken into account in the equation describing the state of the system, while the uncertainties associated with the sensors are taken into account in the observation equation.

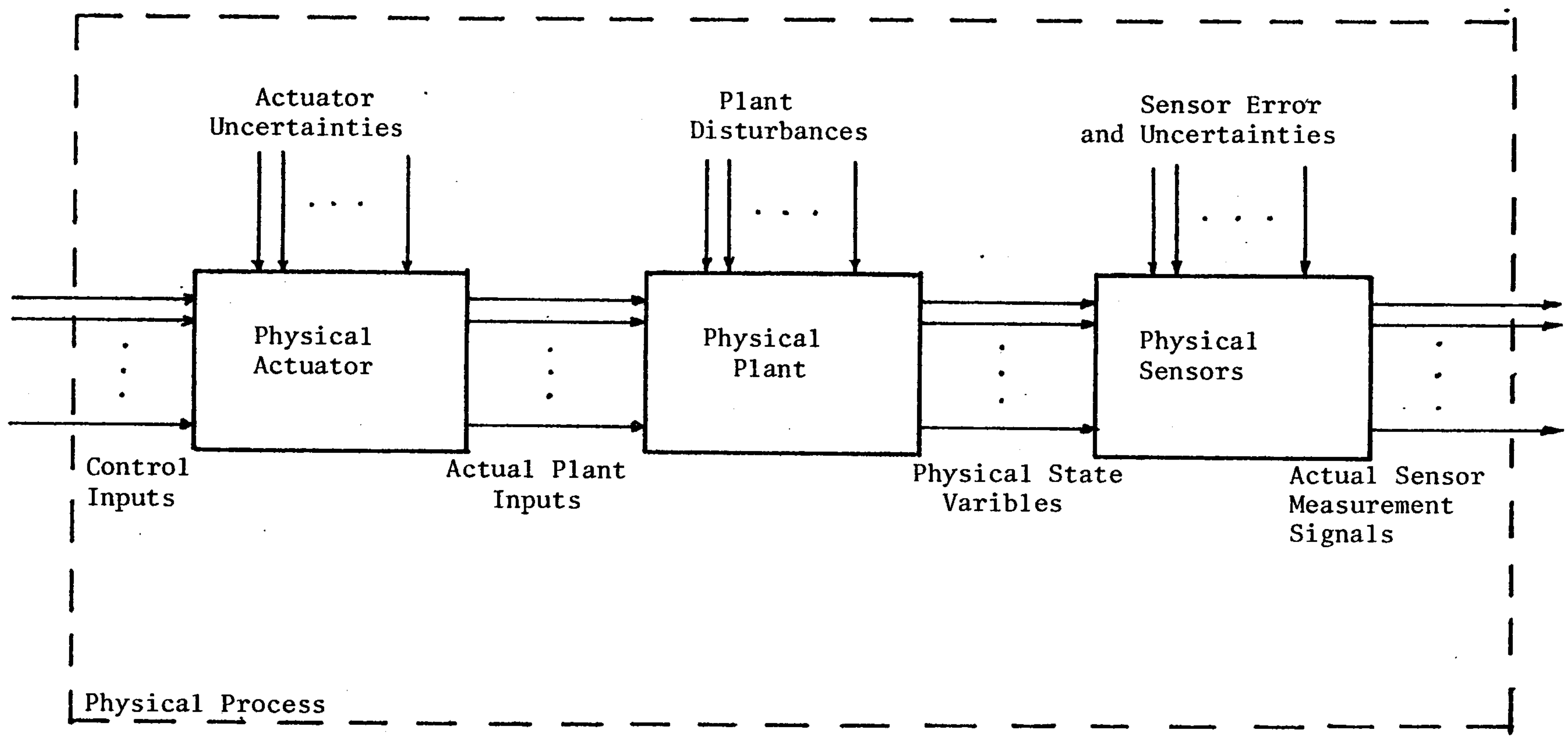

Figure 8.1 Schematic Diagram of the Overall Physical Process (42).

Thus, we have

$$x_{k+1} = Dx_k + Eu_k + w_k \tag{8.19}$$

$$y_k = Cx_k + v_k \tag{8.20}$$

where the two random vectors w_k and v_k are assumed white, discrete, Gaussian, uncorrelated, with zero mean, such that

$$E\{w_k\} = E\{v_k\} = 0$$

$$E\{x_o\} = \overline{x}_o$$

$$E\{w_k w_j^T\} = W \cdot \delta_{kj}$$

$$E\{v_k v_j^T\} = V \cdot \delta_{kj}$$

$$E\{ (x_o-\overline{x}_o)(x_o-\overline{x}_o)^T \} = W_o$$

$$E\{w_k x_o^T\} = 0$$

$$E\{v_k x_o^T\} = 0 \ .$$

We will further assume that the noise characteristics are invariant in time, i.e., the covariance matrices W and V are constant.

The estimation problem now is formulated as follows: Given the stochastic linear system of equations (8.19) and (8.20), find for each $k = 0, 1, 2, \ldots$, the best linear estimator $\hat{x}_{k+1/k}$ of the system state at time k+1, x_{k+1}, in terms of the output sequence up to and including time k, $Y_k = \{y_j\}^k_{j=0}$.

This estimation is optimal in the sense that the expected value of the square of the error magnitude, $\tilde{x}_{k|k-1} = \hat{x}_k - x_{k|k-1}$, is minimized, i.e.,

$$\mathrm{cov}\{\tilde{x}_{k|k-1};\ \tilde{x}_{k|k-1}\} .$$

is minimum and that $x_{k|k-1}$ is unbiased, i.e.,

$$E\{\tilde{x}_{k|k-1}\} = E\{x_k\} .$$

Various approaches to the solution of this problem can be found in the literature (43)-(45). Due to its length, the derivation of the solution will not be given here. However, the solution itself with the procedure to compute the estimator is outlined below (44).

The best linear estimator $\hat{x}_{k+1|k}$ of x_{k+1} in terms of the output sequence $Y_k = \{y_j\}^k_{j=0}$ may be expressed recursively using the estimation in the previous step, $\hat{x}_{k|k-1}$, and the newly available measurement y_k according to the recursive relation

$$\hat{x}_{k+1|k} = D\hat{x}_{k|k-1} + Eu_k + G(k)[y_k - C\hat{x}_{k|k-1}] \tag{8.21}$$

with initial conditions $\hat{x}_{o|-1} = \overline{x}_o$. The gain matrix G(k) is given for all k = 0, 1, 2, . . . by

$$G(k) = DP(k)C^T[CP(k)C^T+V]^{-1} \tag{8.22}$$

where the nxn positive definite symmetrix matrix P(k) is the covariance of the estimation error

$$\tilde{x}_{k|k-1} = x_k - \hat{x}_{k|k-1}$$

and may be precomputed using the iterative relation

$$P(k+1) = -D^T P(k) C G(k) + D^T P(k) D + W \qquad (8.23)$$

with initial condition

$$P_o = \text{cov}\,\{x_o;\, x_o\}\ .$$

If the initial time t_o at which observations have started is the distant past with respect to the phenomena studied, it can be shown (39) that the solution for P(k) converges to a constant, steady-state value P, if the system under study is observable, i.e.

$$\text{rank}[C,\ CD,\ CD^2,\ \ldots\ CD^{n-1}]^T = n\ . \qquad (8.24)$$

Then, equation (8.23) becomes

$$P = -D^T PCG + D^T PD + W \qquad (8.25)$$

with G given by

$$G = DPC^T[CPC^T + V]^{-1}\ . \qquad (8.26)$$

The computational structure of this estimator is described below:

Initial estimate is the $\hat{x}_{o|-1} = \overline{x}_o$.

At each time step $k = 0, 1, 2, \ldots$ the model of the system generates the best linear estimate

$$\hat{x}_{k+1|k-1} = D\hat{x}_{k|k-1} + Eu_k$$

while

$$\hat{y}_{k|k-1} = C\hat{x}_{k|k-1}$$

is also computed. Using the newly available measurement y_k, the error of the output estimation $\hat{y}_{k|k-1}$ is computed

$$\tilde{y}_{k|k-1} = y_k - \hat{y}_{k|k-1} = y_k - C\hat{x}_{k|k-1}$$

which can be shown (44) that is uncorrelated with past measurement sequence $Y_{k-1} = \{y_j\}_{j=0}^{k-1}$. The above $\tilde{y}_{k|k-1}$ is operated on by the gain G to generate the best linear estimate of the state x_{k+1} in terms of $\hat{y}_{k|k-1}$

$$G(y_k - C\hat{x}_{k|k-1}) .$$

The two parts of the best linear estimate of x_{k+1} are added together to give

$$\hat{x}_{k+1|k} = D\hat{x}_{k|k-1} + Eu_k + G(y_k - C\hat{x}_{k|k-1}) \tag{8.27}$$

which is the best estimate of x_{k+1}.

A flow diagram of the Linear Estimator is given in Figure 8.2 (44).

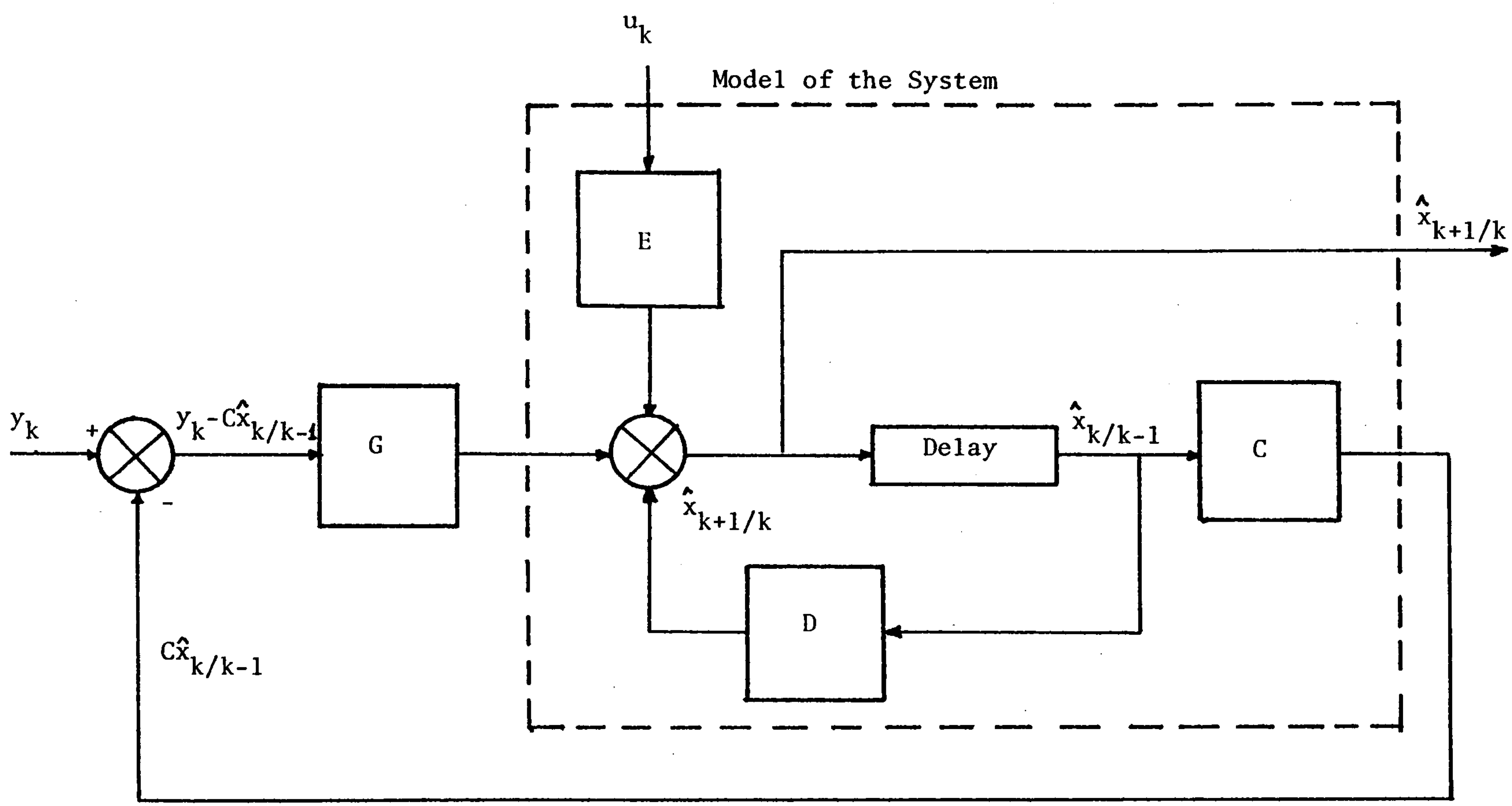

Figure 8.2 Flow Diagram of the Linear Estimator.

8.4 The LQG Algorithm--Feasibility Study for the Reactor Core Steam Generator System

The solution of the Linear Quadratic control problem provided us with the optimal feedback control given by equation (8.14) as a function of the states of the system, using the feedback gain L given by equation (8.18). Due to noise-currupted measurements and the fact that only some of the states are measurable, the estimation of the entire state vector was necessary and this estimate is given by equation (8.27) after solving the Linear Estimation problem by assuming white Gaussian noise. The calculation of a gain matrix (the Kalman gain matrix) was necessary in this step, and it is given by equation (8.26). Using then the separation theorem, this estimate can be used in the computation of the feedback control, so that equation (8.18) becomes

$$u = -L\hat{x} \ . \tag{8.29}$$

However, in order to compute the feedback gain matrix and the Kalman gain matrix, equations (8.17) and 8.25) must be solved. They are rewritten below:

$$K = -D^TKEL + D^TKD + C^TQC \tag{8.17}$$

with

$$L = [R + E^TKE]^{-1}E^TKD \tag{8.18}$$

and

$$P = -D^TPCG + D^TPD + W \tag{8.25}$$

with

$$G = DPC^T[CPC^T + V]^{-1} \quad . \tag{8.27}$$

Equations (8.17) and 8.25) are both of the same form. They are matrix equations of the Riccati type and since we are seeking the steady-state solutions, the controllability and observability condition should be satisfied (equations (8.16) and (8.24), respectively).

There are many methods proposed for the solution of the matrix Riccati equation, notably Vaughan (46), Hewer (47), Dorato and Lewis (48), and many authors have contributed to the development and understanding of the steady-state and transient solutions of the matrix Riccati equation (49)-(53).

In this study, an algorithm written by Barraud (54) for the solution of the discrete, steady-state matrix Riccati equation was used. It is based on an iterative solution not on matrix K, equation (8.17), but on a factorization S of K, such that $SS^T \equiv K$. The numerical stability of this method is reportedly superior to the other methods and the algorithm, consisting of about 1,000 Fortran statements, was furnished by its author for free use.

The main problem reported (55) in the solution of the matrix Riccati equation is the loss of the positive definiteness property of the matrix K, equation (8.17), after a number of iterations. However, if the solution converges to a positive definite matrix for both the control problem, equation (8.17), and the estimation problem, equation (8.25), the feedback gain L and the Kalmon gain G are readily computed, so that the simulation of a transient can start.

The flow diagram of the feedback control with estimator is shown in Figure 8.3 and it summarizes the LQG algorithm to be programmed. The reference control vector u^* is the amount of external control needed to bring the system to the new steady state, and the reference measurements y^* are the changes in the measurable states from the initial to the final steady-state, i.e.

$$y^* = Cx^*$$

where x^* is the state vector at the new steady-state computed by setting in equation (8.1) $\dot{x} = 0$, i.e.

$$Ax^* + Bu^* = 0 \ .$$

In our case the overall system of reactor core and steam generator together was considered as the system to be controlled, so that comparison could be made with the performance of the classical control system applied and simulated in Chapter 7. It is a set of 24 differential equations (nine equations representing the core, Appendix I, and 15 equations representing the steam generator, Appendix II). The four control variables are: steam exit flow, feedwater flow, feedwater temperature and control rod reactivity. The five measurable variables are: nuclear power, hot leg temperature, cold leg temperature, steam pressure, and steam generator water level.

The controllability and observability criteria, equations (8.16) and (8.24), were satisfied with the matrices of our system. However, the Riccati code failed to find a positive definite solution after the

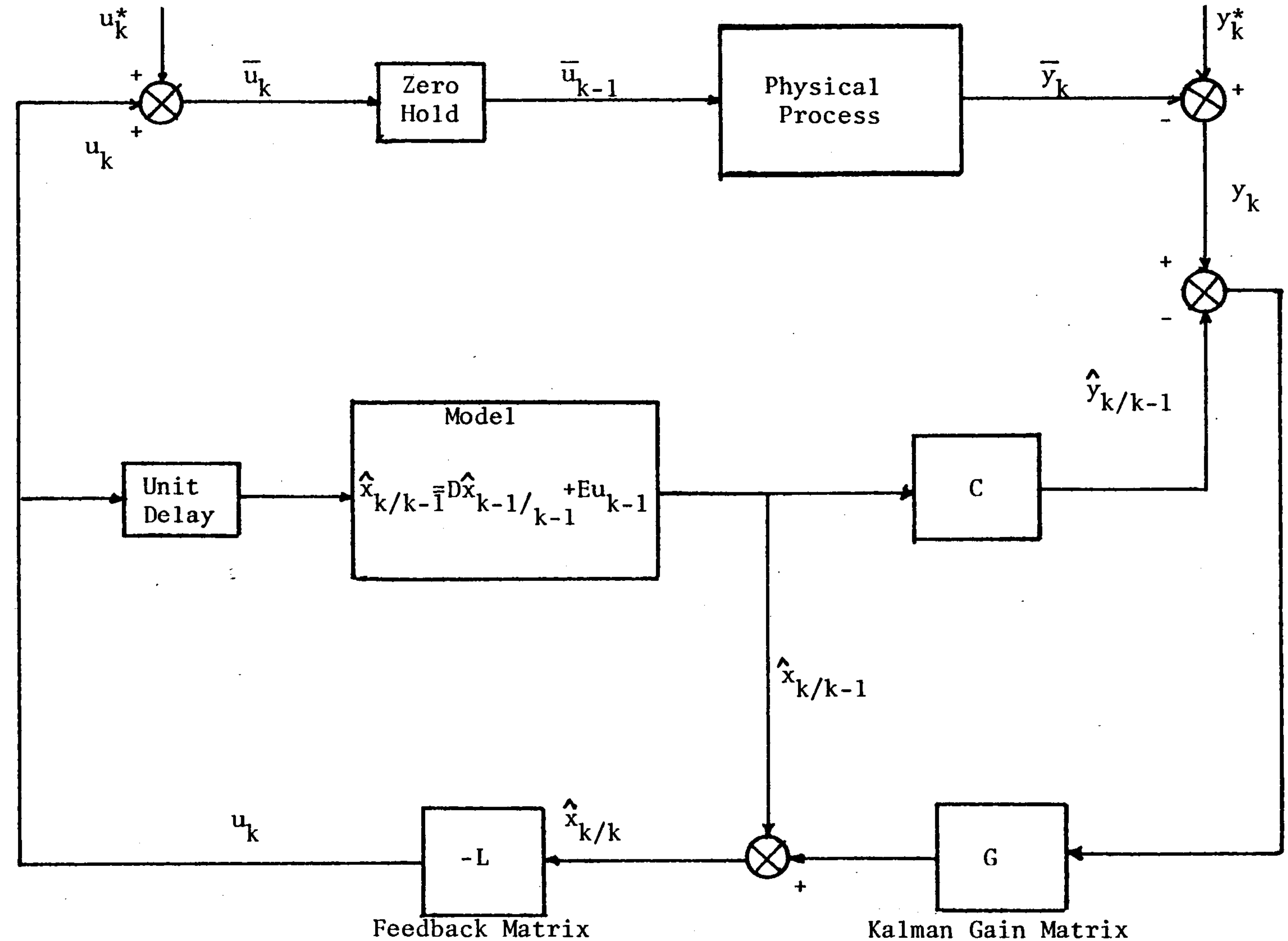

Figure 8.3 Flow Diagram of Feedback Control with Estimator. (18)

sixth iteration and thus no further action could be taken with the LQG algorithm for the system under study. Since this code was never tried for systems bigger than order 14, it is believed that the size of the system was too big to implement on this code, and this is actually one of the major problems cited in the literature with the matrix Riccati equation solution.

Since the reduction of the system size or a different strategy to attack the problem would require much additional time, not available because of the specific duration of the given project, further investigation of this solution technique was not attempted.

However, the major part of a future effort, i.e., the outline of the theory behind the method, the procedure to be followed in an application, the literature survey on the LQG method and on the matrix Riccati equation solution and finally the operational state of the Riccati code, is already accomplished. Since there are other authors (18), (19) who obtained good results with this method using low-order models for their systems, it is believed that a major effort to reduce considerably the size of the core-steam generator system could also lead to good results.

CHAPTER 9

CONCLUSIONS AND RECOMMENDATIONS

The need to study the control of the water level of a PWR U-tube steam generator, which is an important aspect of PWR control, led to an overall effort that covered many diverse areas of interest. The final system to be studied included the reactor core and the control system associated with it.

The model validation work, which is of capital importance in the study of the control of any physical process, was undertaken for the core and the steam generator low-order linear models, at full power and low power. The identification of the optimal values of certain key, nonmeasurable, parameters was done using experimental data after large step perturbations in power demand. Consequently, a time domain, multi-input, multi-output least squares parameter identification was carried out. The results have demonstrated that the simplified physical models represent the dynamic behavior of the main components of the pressurized water reactor satisfactorily. They realize a very good trade off between accuracy and complexity, and even though the linearity assumption is questionable for large relative perturbations (in the case of the 30-20% perturbation), they still predict well the experimental transients.

A program to perform the parameter identification routinely, using data from different experimental transients was written to be executed with minimum effort and cost on a minicomputer. Therefore, one can very easily undertake studies on the improvement of the model prediction by trying to identify additional parameters (for example the ratio of pressure drops in the boiling region and the recirculation loop (R_p) in the steam generator model), using more detailed models, especially for the reactor core, or employing different optimization schemes for the cost function minimization. In another direction, a systematic error analysis could be undertaken to furnish quantitative confidence margins for the optimal parameter values found by the identification.

In this work it was also pointed out that particular attention must be attached to the distortion of the experimental signals due to problems associated with the electronics of the transmition, acquisition, and recording of the data. Since experimental data of high quality are necessary in order to have meaningful results from the identification work, every effort must be taken to overcome problems of this nature. It was shown that problems of filtering encountered with the signals used as inputs and outputs for the models to be identified, can be solved systematically using standard procedures of noise analysis. The reconstruction of the approximate, nonfiltered, steam flow rate signal used as input to the steam generator model, is another example of important subtasks that might have to be undertaken to accomplish the identification work.

The study of a control system is usually the final objective in pursuing model validation work. In this study the currently used feedwater control system in a U-tube steam generator was examined and it was found (taking into account the constant feedwater temperature assumption and possible limitations of the optimal behavior of the models used) that it is sufficient in controlling the water level after large step perturbations in power demand, at full power and at ~ 30% power. The reactor control system predicted also satisfactorily the experimental transients. A real-time, simple and inexpensive way to simulate the entire multivariate industrial process was obtained. Thus, evaluation of possible changes in the control component setpoints can be made readily, and addition of control components or use of more detailed models can be handled easily (provided that expansion of the minicomputer capabilities is also undertaken). Simulating the feedwater temperature feedback mechanism and using a more detailed core model are some of the possible efforts in this direction.

The effort to use modern linear control theory, and in particular the Linear-Quadratic-Gaussian theory, for the eventual direct digital control of industrial processes, showed that there are numerical problems with the solution of the associated Riccati equation for high-order systems ((24×24) in this study) and thus with the implementation of the method. The use of the isolated steam generator (with a model of order 15) could result in better numerical behavior and would give the possibility to evaluate the performance of this approach in the control of the water level, as compared to the classical method used at present. The work done in this study and the steps taken for such a control approach could be used as the starting point for a new effort.

Finally, the implementation of all computations in this study on a medium size minicomputer should be emphasized. It was possible to simulate a large, complex industrial process in real-time to achieve safety and functional analyses with economy, flexibility, and accuracy. The integration package written in FORTRAN IV can be adopted in almost any digital computer, but its use on a minicomputer could also allow on-line studies.

LIST OF REFERENCES

LIST OF REFERENCES

1. Astrom, K. J. and Eykhoff, P. "System Identification--A Survey" Automatica, Vol. 7, pp. 123-162 (1971).

2. Cuenod, M. and Sage, A. P. "Comparison of Some Methods used for Process Identification" Automatica Vol. 4, pp. 235-269 (1968).

3. Gustavsson, I. "Survey of Application of Identification in Chemical and Physical Processes" Automatica, Vol. 11, pp. 3-24 (1975).

4. Nieman, R. E., Fisher, D. G., and Seborg, D. E. "A Review of Process Identification and Parameter Estimation Techniques" Int. J. Control, 1971, Vol. 13, No. 2, pp. 209-264.

5. Kerlin, T. W., Zwingelstein, G. C. and Upadhyaya, B. R. "Identification of Nuclear Systems" Invited Critical Review, Nuc. Tech. 36:7-38 (Nov. 1977).

6. Eykhoff, P. "System Identification" John Wiley and Sons, N.Y. (1974).

7. Nahavandi, A. N., Batenburg, A. "Steam Generator Water Level Control," J. Basic Eng., pp. 343-354 (June 1966).

8. Hennebicq, J. P. "Etudes de Fonctionnement d'un Processus Industriel" EDF Report, October 1976.

9. Hocepied, R. "Regulation Automatique du Niveau des Generateurs de Vapeur des Centrales Nucleaires PWR." ACEC-Revue N° 3-4 (1975).

10. Chungpeng Fan, "Automatic Control of Water Level for a PWR Plant with Natural Circulating Steam Generators during Low Power Operation" Power Plant Dynamics, Control and Testing Symposium, September 77, Knoxville, Tennessee.

11. Lipinski, W. C., "Optimal Digital Computer Control of Nuclear Reactor," Ph.D. Thesis, Illinois Institute of Technology (1969) also Argonne Nat. Lab. Report ANL-7530.

12. Cummins, J. D., Butterfield, M. H., "Application of Modern Control Theory in Nuclear Power," Proc. 1973 IAEA Conf: Nuclear Power Plant Control and Instrumentation.

13. Hagen, E. W. and Kerlin, T. W. "IAEA International Symposium on Nuclear Power Plant Control and Instrumentation," Nuclear Safety 15(1); 15-29 (Jan.-Feb. 1974).

14. Lunde, J. E. "Overview of Current Trends in Applications of Process Control Computers to Nuclear Power Plants," Proc. 1973 Conf. on Mathematical Models and Computational Techniques for Analysis of Nuclear Systems. Ann Arbor, Mich.

15. Bjorlo, T. J., Grumbach, R., Josefsson, R. "Digital Control of the Halden Boiling Water Reactor by a Concept based on Modern Control Theory" Nucl. Sci. and Engr. 39, 231-240 (1970).

16. Josefsson, R., Karlsson, R., Blomberg, P. E. "Improved Response of BWR Power Plants to Rapid Load Changes" Trans. Am. Nuc. Sec. 17, 435 (1973).

17. Atary, J., Shah, M. M. "Modeling and Analytical Control System Design of a Complete Nuclear Power Plant Prototype" Proc. I.E.E. (1971).

18. Frogner, B., "System Identification, Estimation and Optimal Feedback Control Theory Applied to the Control of a Nuclear BWR," Ph.D. Thesis, Univ. of California, Berkeley (1974).

19. De Keyser, R., Van Cauwemberghe, A. R., "Simulation and Self-Tuning Control in a Nuclear Power Plant," Proceedings of the Simulation of Control Systems, IMACS Symposium, Vienna (1978).

20. Zwingelstein, G. and Anastasiou, I. "Dynamic Model Validation for a Pressurized Water Reactor" IAEA Specialist's Meeting on Control System Commisioning and Dynamic Model Validation, Harrogate, U. K. June 1979.

21. Ali, M. A. A. "Lumped Parameter, State Variable Dynamic Models for U-Tube Recirculation Type Nuclear Steam Generators." Ph.D. dissertation, University of Tennessee, Knoxville, Tennessee (1976).

22. Petetrot, J. F. "GEVAP--Programme de Simulation Linéaire des Générateurs de Vapeur--Notice TP/PF/DC-325, Framatome, Paris (1976).

23. Bendat, J. S. and Piersol, A. G. "Random Data: Analysis and Measurement Procedures" Wiley-Interscience, N. Y. (1971).

24. Uhrig, R. E. "Random Noise Techniques in Nuclear Reactor Systems." The Ronald Press Company, N. Y. (1970).

25. Box, M. J., Davies, D., and Swann, W. H. "Nonlinear Optimization Techniques." Oliver and Boyd, Edinburgh (1968).

26. Wilde, D. J. "Optimum Seeking Methods," Prentice-Hall, Englewood Cliffs, N. J. (1964).

27. Bekey, G. A. and McGee, R. B. "Gradient Methods for the Optimization of Dynamic System Parameters by Hybrid Computation," in "Computing Methods in Optimization Problems" (Eds. A. B. Balakrishnan and L. W. Neustadt), Academic Press, N. Y. (1964).

28. Wilde, D. J. and Beightler, C. S. "Foundations of Optimization," Prentice-Hall, Englewood Cliffs, N. J. (1967).

29. Kowalik, J. and Osborne, M. R. "Methods for Unconstrained Optimization Problems, American Elsevier Publ., N. Y. (1968).

30. Powell, M. J. D. "A Survey of Numerical Methods for Unconstrained Optimization," SIAM Rev., 11, 79-97.

31. Dixon, L. C. W. "Nonlinear Optimization," English Universities Press, London (1972).

32. Nelder, J. A. and Mead, R. "A Simplex Method for Function Minimization" The Computer Journal, 7, pp. 308-313 (1963).

33. Westinghouse Nuclear Energy Systems, "Reference Safety Analysis Report, RESAR-3."

34. Goodwin, G. C., Payne, R. L., "Dynamic System Identification: Experiment Design and Data Analysis" Acad. Press (1977).

35. Kerlin, T. W. "Dynamic Analysis and Control of Pressurized Water Reactors" in Control and Dynamic Systems, Vol. 14, (Ed. C. T. Leondes) Academic Press (1978).

36. Zwingelstein, G. and Anastasiou, I. "Real Time Simulation of a U-Tube Steam Generator on a Minicomputer" Measurement and Control, MECO 79 Conference, Sorento, Italy, Sept. 1979.

37. Ball, S. J. and Adams, R. J. "MATEXP: A General Purpose Digital Computer Program for Solving Ordinary Differential Equations by the Matrix Exponential Method." USAEC Report ORNL-TM 1933 (1967).

38. Speedy C. B., Brown, R. F., and Goodwin, G. C. "Control Theory: Identification and Optimal Control" Oliver and Boyd, Edinburgh (1970).

39. Foulard, C., Gentil, S., and Sandaz, J. P. "Commande et Regulation par Calculateur Numérique" Editions Eyrolles, Paris (1977).

40. Special Issue on Linear-Quadratic-Gaussian Problem, IEEE Trans. Aut. Contr., Vol. AC-16-6 (Dec. 1971).

41. Athans, M. and Falb, P. L. "Optimal Control," McGraw-Hill (1966).

42. Athans, M. "The Role and Use of the Stochastic Linear-Quadratic-Gaussian Problem in Control System Design." IEEE Trans. Aut. Contr., Vol AC-16-6 (Dec. 1971).

43. Singh, M. G. and Titli, A. "Systems Decomposition, Optimization and Control" Pergamon International Library (1978).

44. Rhodes, I. B. "A Tutorial Introduction to Estimation and Filtering" IEEE Trans. Aut. Contr., Vol 16-6 (Dec. 1971).

45. Sorenson, H. W. and Stubberud, A. R. "Linear Estimation Theory" in "Theory and Application of Kalman Filtering" AGARD Monograph 139 (Ed. Leondes) (1970).

46. Vaughan, D. R. "A Nonrecursive Algebraic Solution for the Discrete Riccati Equation" IEEE Trans. Aut. Contr., Vol. AC-15-5 (Oct. 1970)

47. Hewer, G. A. "An Iterative Technique for the Computation of the Steady-State Gain for Discrete Optimal Regulator," IEEE Trans. Aut. Contr., Vol. AC-16-4 (Aug. 1971).

48. Dorato, P. and Levis, A. H. "Optimal Linear Regulators: The Discrete--Time Case" IEEE Trans. Aut. Contr. Vol 16-6 (Dec. 1971).

49. Caines, P. E. and Mayne, D. Q. "On the Discrete Time Matrix Riccati Equation of Optimal Control" Int. J. Control, 1970, Vol. 12, No. 5, 785-794.

50. Kleiman, D. L. "On an Iterative Technique for Riccati Equation Computations," IEEE Trans. Aut. Contr. Vol. AC-13-1 (Feb. 1968).

51. Porter, W. A. "On the Matrix Riccati Equation," IEEE Trans. Aut. Contr., Vol. AC-12-6 (Dec. 1967).

52. Man, F. T. "The Davidon Method of Solution of the Algebraic Matrix Riccati Equation" Int. J. Control, 1969, Vol. 10, No. 6, 713-719.

53. Potter, J. E. "Matrix Quadratic Solutions," J. SIAM, Appl. Math. Vol. 14, No. 3 (May 1966).

54. Barraud, A. "RICCAT--Un sous--Programme Fortran pour la Resolution des Equations de Riccati Discrétes," Annales E. N. S. M. 2e Semestre 1973, Nantes, France.

55. Barraud, A. "Sur la Resolution Numerique des Equations de Riccati--Cas Discret" Revue R. A. I. R. O. N° Oct. 1974-J-3, pp. 75-91.

56. Katz, E. M. "Planning, Performing and Interpreting Dynamic Measurements in Pressurized Water Reactors" Ph.D. dissertation, University of Tennessee, Knoxville (1975).

APPENDIXES

APPENDIX I

THE REACTOR CORE MODEL

I.1 Derivation of the Model Equations

Linearizing the point kinetics equations, using one delayed neutron group and assuming constant primary pressure, yields (56):

$$\frac{d\delta Q}{dt} = -\frac{\beta_T}{\Lambda}\,\delta Q + \bar{\lambda}\delta C + \frac{Q_o}{\Lambda}\,(\alpha_f \delta T_f + \alpha_c \delta T_1 + \delta\rho_{rod})$$

$$\frac{d\delta C}{dt} = \frac{\beta_T}{\Lambda}\,\delta Q - \bar{\lambda}\delta C$$

where δ represents variations from the initial equilibrium.

Q = nuclear power, Btu/sec

Q_o = equilibrium power, Btu/sec

β_T = total delayed neutron fraction

$\bar{\lambda}$ = average decay constant for one effective group of delayed neutrons, sec^{-1}

α_f = Doppler coefficient, $\Delta k/k/°F$

α_c = moderator temperature coefficient of reactivity, $\Delta k/k/°F$

T_f = fuel temperature, °F

T_1 = average temperature of coolant in core, °F

Λ = generation time, sec.

ρ_{rod} = control rod reactivity .

Since we simulate the reactor core at full power and at low power, we are interested in expressing the nuclear power state variable in percentage changes with respect to the nominal power $\overline{Q}$ (100%) (regardless the actual equilibrium power Q_o). Thus, we need $Q_N = \frac{\delta Q}{\overline{Q}} \cdot 100$ as a new state variable. We also use the product $\delta X = \overline{\lambda}\, \frac{\delta C}{\overline{Q}} \cdot 100$ as a new precursor state variable and the equations above become

$$\frac{d\delta Q_N}{dt} = -\frac{\beta_T}{\Lambda}\,\delta Q_N + \delta X + \frac{1}{\Lambda}\left(\frac{Q_o}{\overline{Q}} \cdot 100\right)(\alpha_f \delta T_f + \alpha \delta T_1 + \delta\rho_{rod}) \tag{I.1}$$

$$\frac{d\delta X}{dt} = \frac{\beta_T\,\overline{\lambda}}{\Lambda}\,\delta Q_N - \overline{\lambda}\delta X\ . \tag{8.2}$$

Using Mann's model, i.e., having two coolant nodes for each fuel node for the core heat transfer (see Figure 3.1, page 26), each coolant section is considered to be a well-stirred tank with its average temperature equal to its outlet temperature. The energy conservation equations then become

$$(MC_p)_f\,\frac{dT_f}{dt} = Q - h_{fc} \cdot A\,(T_f - T_1)$$

$$(MC_p)_c\,\frac{dT_1}{dt} = \frac{h_{fc} \cdot A}{2}\,(T_f - T_1) - (WC_p)\,(T_1 - T_{\ell p})$$

$$(MC_p)\,\frac{dT_2}{dt} = \frac{h_{fc} \cdot A}{2}\,(T_f - T_1) - (WC_p)(T_2 - T_1)$$

where

T_1, T_2 = reactor coolant temperatures at the two sections, °F

$T_{\ell p}$ = temperature of reactor coolant in lower plenum, °F

$(MC_p)_f$ = product of mass and specific heat of coolant, Btu/°F

$(MC_p)_c$ = product of mass and specific heat of coolant in one section, Btu/°F

W_p = reactor coolant mass flow rate, lbm/sec.

A = total core heat transfer area, ft^2

h_{fc} = average fuel to coolant effective heat transfer coefficient, Btu/hr sq. ft °F.

Linearizing the above three equations and taking into account that the new state variable for nuclear power is $\delta Q_N = \delta Q \cdot 100/\overline{Q}$, and that $2\ M_c/W_c = \tau_c$ is the coolant residence time in the core, the core heat transfer equations become

$$\frac{d\delta T_f}{dt} = \frac{(\overline{Q}/100)}{(MC_p)f}\ \delta Q_N - \frac{h_{fc}A}{(MC_p)_f}\ (\delta T_f - \delta T_1) \tag{I.3}$$

$$\frac{d\delta T_1}{dt} = \frac{h_{fc}\ A}{2(MC_p)_c} \cdot (\delta T_f - \delta T_1) - \frac{2}{\tau_c}\ (\delta T_1 - \delta T_{\ell p}) \tag{I.4}$$

$$\frac{d\delta T_2}{dt} = \frac{h_{fc}\ A}{2(MC_p)_c}\ (\delta T_f - \delta T_1) - \frac{2}{\tau_c}\ (\delta T_2 - \delta T_1)\ . \tag{I.5}$$

The equations for the lower and upper plenum and the hot leg and cold leg piping are obtained using the well-mixed tank model:

$$\frac{d\delta T_{up}}{dt} = \frac{1}{\tau_{up}}\ \delta T_2 - \frac{1}{\tau_{up}}\ \delta T_{up} \tag{I.6}$$

$$\frac{d\delta T_{H\ell}}{dt} = \frac{1}{\tau_{up}} \delta T_{up} - \frac{1}{\tau_{H\ell}} \delta T_{H\ell} \tag{I.7}$$

$$\frac{d\delta T_{\ell p}}{dt} = \frac{1}{\tau_{\ell p}} \delta T_{c\ell} - \frac{1}{\tau_{\ell p}} \delta T_{\ell p} \tag{I.8}$$

$$\frac{d\delta T_{c\ell}}{dt} = \frac{1}{\tau_{\ell}} \delta T_{PO} - \frac{1}{\tau_{\ell}} \delta T_{c\ell} \tag{I.9}$$

where

T_{up}, $T_{\ell p}$ = coolant temperatures at upper and lower plenum, °F

$T_{H\ell}$, $T_{c\ell}$ = coolant temperatures at the hot and cold leg, °F

T_{PO} = coolant temperature at the steam generator outer plenum, °F.

The parameters represented by τ's (sec) are the residence times in each node and they are calculated by $\tau = M/W_p$, where M is the coolant mass of the corresponding node.

I.2 Data Used

The design parameters for the core model are given here. The parameters having the same value at full and at low power are listed first, and the rest of the parameters follow, for each power level. The optimal values, as found by the identification work (Section 6.6, page 81) are used for the optimized parameters. The notation is explained in Section I.1.

$\overline{Q}$ = $2.5142 \cdot 10^6$ Btu/sec (nominal power at 100%)

W_p = $2.8 \cdot 10^4$ lbm/sec

$(MC_p)_f$ = $1.63 \cdot 10^4$ Btu/°F

A = $5.393 \cdot 10^4$ ft^2

τ_c = 0.88 sec

τ_{up} = 1.50 sec

$\tau_{\ell p}$ = 0.48 sec

$\tau_{h\ell}$ = 2.40 sec

$\tau_{c\ell}$ = 1.94 sec

$\overline{\lambda}$ = 0.082 sec^{-1}

Λ = $2.42 \cdot 10^{-5}$ sec .

<u>At Full Power</u>

Q_o = 100%

β_T = $6.4 \cdot 10^{-3}$

$(MC_p)_c$ = $1.665 \cdot 10^4$ Btu/°F node

h_{fc} = 236 Btu/hr. sq. ft. °F

α_f = -1.52 $\Delta k/k/°F$

α_c = -2.9 $\Delta k/k/°F$.

<u>At Low Power</u>

Q_o = 30%

β_T = $7.27 \cdot 10^{-3}$

$(MC_p)_c$ = $1.61 \cdot 10^4$ Btu/°F • node

h_{fc} = 215 Btu/hr. sq. ft. °F

α_f = -1.6 $\Delta k/k/°F$

α_c = -4.5 $\Delta k/k/°F$.

APPENDIX II

THE STEAM GENERATOR MODEL

II.1 Derivation of the Model Equations

A brief description of the steam generator model was given in Section 3.3, page 25, and a diagram of the nodes representing the model can be seen in Figure 3.2, page 28. For the purpose of completeness, the derivation of the model equations from the mass, energy and momentum conservation equations, presented in Ali's dissertation (21) will be given here, following the nodal description of Figure 3.2. Minor modifications made to the original Ali's version will be presented at the end together with the steady-state calculation iterative procedure.

A list of the notation used in this Appendix is given below. Since the model is linear, all state variables represent variations from equilibrium.

δ: Represents variation from equilibrium.

o: Index denoting value at equilibrium.

$T_{h\ell}$: Hot leg temperature.

$T_{PI}, T_{P1}, T_{P2}, T_{P3}, T_{P4}, T_{Po}$: Average coolant temperatures in the primary loop nodes.

$T_{M1}, T_{M2}, T_{M3}, T_{M4}$: Average tube metal temperatures in the metal nodes.

C_{P1}, C_m, C_{P2}: Specific heats of primary coolant, tube metal and secondary coolant, respectively.

W_{Pi}, W_{P1}, W_{P2}: Primary coolant mass flow rates at the P_{RI}, P_{R1}, and P_{R2} nodes, respectively.

W_{fi}: Feedwater flow rate.

W_1, W_2, W_3, W_4: Secondary coolant flow rates at the exits of the nodes D, S_1, S_2, and S_3, respectively.

$M_{Pi}, M_{P1}, M_{P2}, M_{P3}$: Primary coolant mass in the nodes PRI, PR1, PR2, and PR3, respectively.

M_d, T_d: Mass and temperature of the water in the downcomer.

$\rho_p, \rho_m, \rho_{s1}, \rho_r$: Densitites of the primary coolant, the U-tube metal, the saturated water and the water in the riser.

A_p, A_m, A_{fs}: Cross sectional areas of the primary coolant flow, the U-tube metal and the secondary coolant flow.

T_{fw}: Feedwater temperature.

W_s: Steam exit flow rate.

L_{s1}, L_{s2}: U-tube lengths corresponding to the subcooled and boiling regions, respectively.

L: Variation in the water level, in percentage of the minimum-maximum margin.

P: Secondary side pressure.

x_e: Steam exit quality.

T_{sat}: Secondary coolant saturation temperature.

U_{pm}: Heat transfer coefficient between the primary coolant and the tube metal (per unit tube length).

U_{ms1}: Heat transfer coefficient between the tube metal and the secondary coolant in the subcooled region (per unit tube length).

U_{ms2}: Heat transfer coefficient between the tube metal and the secondary coolant in the boiling region (per unit tube length).

V_s: Initial steam dome volume.

L_r: Height of the riser.

V_r: Volume of the riser.

R_p: Ratio of the pressure drops in the two-phase region to the sum of the pressure drops in the recirculation loop.

The Primary Side

One equation is used for each of the six nodes in the primary side (PRI,PR1,PR2,PR3,PR4,PRO). Each node is assumed to be a well-stirred tank (outlet temperature equal to the average temperature) and the primary flow rate, specific heat and density are assumed constant.

--Inlet plenum (PRI)

Energy conservation:

$$\frac{d}{dt}(M_{Pi}C_{P1}T_{PI}) = W_{Pi}C_{P1}(T_{h\ell} - T_{PI}) .$$

Linearizing the above yields:

$$\frac{d\delta T_{PI}}{dt} = \frac{W_{Pi}}{M_{Pi}}(T_{h\ell} - T_{PI}) . \tag{II.1}$$

--First Primary Node (PR1)

Mass conservation:

$$\frac{d(\rho_p A_p L_{s1})}{dt} = W_{Pi} - W_{P1} .$$

Since W_{Pi} is constant, linearizing the above yields:

$$\rho_p A_p \frac{d\delta L_{s1}}{dt} = -\delta W_{p1} \; . \tag{II.2}$$

Energy conservation:

$$C_{p1} \frac{d}{dt} (\rho_p A_p L_{s1} T_{p1}) = W_{pi} C_{p1} T_{PI} - W_{pi} C_{p1} T_{p1} - U_{pm} L_{s1} \left[\frac{T_{p1} + T_{PI}}{2} - T_{M1} \right] .$$

Linearizing the above and using (II.2) yields:

$$\frac{d\delta T_{p1}}{dt} = \left(\frac{1}{\tau_{p1}} - \frac{U_{pm}}{2C_{p1}\rho_d A_d} \right) \delta T_{PI} - \left(\frac{1}{\tau_{p1}} + \frac{U_{pm}}{2C_{p1}\rho_d A_d} \right) \delta T_{p1}$$

$$+ \frac{U_{pm}}{C_{p1}\rho_d A_d} \delta T_{M1} - \frac{U_{pm}}{C_{p1}\rho_d A_d L_{s1o}} \left(\frac{1}{2} (T_{PI} + T_{p1}) - T_{M1} \right)_o \delta L_{s1} \tag{II.3}$$

where $\tau_{P1} = M_{p1o}/W_{pi}$.

--Second Primary Node (PR2)

Mass conservation:

$$\frac{d}{dt} (\rho_p A_p L_{s2}) = W_{p1} - W_{p2} \; .$$

Since $L_{si} + L_{s2}$ = constant, linearizing the above yields:

$$\rho_p A_p \frac{d\delta L_{s1}}{dt} = \delta W_{p2} - \delta W_{p1} \; . \tag{II.4}$$

Comparing (II.2) and (II.4), we have $\delta W_{p2} = 0$.

Energy conservation:

$$C_{p1}\,\frac{d}{dt}\,(\rho_d A_d L_{s2} T_{p2}) = W_{p1} C_{p1} T_{p1} - W_{p2} C_{p1} T_{p2} - U_{pm} L_{s2}\left(\frac{T_{p1}+T_{p2}}{2} - T_{M2}\right) .$$

Linearizing the above and using the mass conservation and $M_{p2o} = \rho_p A_p L_{s2o}$ we obtain:

$$\frac{d\delta T_{p2}}{dt} + \frac{(T_{p1}-T_{p2})_o}{L_{s2o}}\;\frac{d\delta L_{s1}}{dt} = \left(\frac{1}{\tau_{p2}} - \frac{U_{pm}}{2C_{p1}\rho_p A_p}\right)\delta T_{p1} - \left(\frac{1}{\tau_{p2}} + \frac{U_{pm}}{2C_{p1}\rho_p A_p}\right)\delta T_{p2} + \frac{U_{pm}}{C_{p1}\rho_p A_p}\cdot \delta T_{M2} + \frac{U_{pm}}{C_{p1} M_{p2o}}\left(\frac{T_{p1}+T_{p2}}{2} - T_{M2}\right)_o \delta L_{s1} \quad \text{(II.5)}$$

3

where $\tau_{p2} = M_{p2o}/W_{pi}$.

--Third Primary Node (PR3)

The mass and energy balances for this node are analogous to the ones for the PR1 node. Thus; we have

$$\frac{d\delta T_{p3}}{dt} = \left(\frac{1}{\tau_{p3}} - \frac{U_{pm}}{2C_{p1}\rho_p A_p}\right)\delta T_{p2} - \left(\frac{1}{\tau_{p3}} + \frac{U_{pm}}{2C_{p1}\rho_p A_p}\right)\delta T_{p3} + \frac{U_{pm}}{C_{p1}\rho_p A_d}\,\delta T_{M3} + \frac{U_{pm}}{C_{p1} M_{p3o}}\left(\frac{1}{2}\,(T_{p2}+T_{p3}) - T_{M3}\right)_o \delta L_{s1} \quad \text{(II.6)}$$

(4)

where $\tau_{p3} = \tau_{p2}$ since $M_{p3o} = M_{p2o}$.

--Fourth Primary Node (PR4)

The mass and energy balances for this node are analogous to the ones for the PR2 node. Thus, we have

$$\frac{d\delta T_{p4}}{dt} - \frac{(T_{p3}-T_{p4})_o}{L_{s1o}} \frac{d\delta L_{s1}}{dt} = \left(\frac{1}{\tau_{p4}} - \frac{U_{pm}}{2C_{p1}\rho_p A_p}\right)\delta T_{p3} - \left(\frac{1}{\tau_{p4}} + \frac{U_{pm}}{2C_{p1}\rho_p A_p}\right)\delta T_{p4} + \frac{U_{pm}}{C_{p1}\rho_p A_p}\delta T_{M4} - \frac{U_{pm}}{C_{p1}M_{p4o}}\left(\frac{1}{2}(T_{p3}+T_{p4}) - T_{M4}\right)_o \delta L_{s1} \quad (5) \tag{II.7}$$

where $\tau_{p4} = \tau_{p1}$ since $M_{p4o} = M_{p1o}$.

--Outlet Plenum Node (PRO)

The equation for this node is analagous to the inlet plenum node equation:

$$\frac{d\delta T_{po}}{dt} = \frac{1}{\tau_{po}}(\delta T_{p4} - \delta T_{po}) \quad (6) \tag{II.8}$$

where $\tau_{po} = M_{po}/W_{pi}$.

The U-tube Metal Side

An energy balance is written for each of the four metal nodes (M1, M2, M3, M4). The movement of the boiling boundary L_{s1} is taken into account as follows: For a change δL_{s1}, an energy quantity of $\rho_m A_m C_{pm} \overline{T}_m \delta L_{s1}$ is transferred between the two nodes on each side of the boundary, where $\overline{T}_m$ is their average temperature.

--First Metal Node (M1)

$$C_m\rho_m A_m \frac{d}{dt}(L_{s1}T_{M1}) = U_{pm}L_{s1}\left(\frac{T_{PI} + T_{p1}}{2} - T_{m1}\right) - U_{ms1}L_{s1}\left(T_{M1} - \frac{T_d + T_{sat}}{2}\right) + \rho_m A_m C_m \left(\frac{T_{M1} + T_{M2}}{2}\right)\frac{d\delta L_{s1}}{dt} .$$

Linearizing the above yields:

$$\frac{d\delta T_{M1}}{dt} + \left(\frac{T_{M1} - T_{M2}}{2L_{s1}}\right)_o \frac{d\delta L_{s1}}{dt} = \frac{U_{pm}}{2\rho_m A_m C_m}\delta T_{PI} + \frac{U_{pm}}{2\rho_m A_m C_m}\delta T_{p1} - \frac{(U_{pm}+U_{ms1})}{\rho_m A_m C_m}\delta T_{M1} + \frac{U_{ms1}}{2\rho_m A_m C_m}\delta T_d + \frac{U_{ms1}}{2\rho_m A_m C_m}\left(\frac{\partial T_{sat}}{\partial P}\right)\delta P . \quad \text{(II.9)}$$

--The Second Metal Node (M2)

$$C_m\rho_m A_m \frac{d}{dt}(L_{s2}T_{M2}) = U_{pm}L_{s2}\left(\frac{T_{p1}+T_{p2}}{2} - T_{M2}\right) - U_{Ms2}Ls2\,(T_{M2} - T_{sat}) - \rho_m A_m C_m \left(\frac{T_{M1}+T_{M2}}{2}\right)\frac{dL_{s1}}{dt} .$$

Linearizing the above and taking $\frac{dL_{s2}}{dt} = -\frac{dL_{s1}}{dt}$, yields:

$$\frac{d\delta T_{M2}}{dt} + \left(\frac{T_{M1}-T_{M2}}{2L_{s2}}\right)_o \frac{d\delta L_{s1}}{dt} = \frac{U_{pm}}{2\rho_m A_m C_m}\delta T_{p1} + \frac{U_{pm}}{2\rho_m A_m C_m}\delta T_{p2} - \frac{(U_{pm}+U_{ms2})}{\rho_m A_m C_m}\delta T_{m2} + \frac{U_{ms2}}{\rho_m A_m C_m}\left(\frac{\partial T_{sat}}{\partial P}\right)\cdot \delta P .$$

(II.10)

--The Third Metal Node (M3)

The energy balance in this node is analagous to the one of the second node. Thus, we have:

$$\frac{d\delta T_{M3}}{dt} + \left(\frac{T_{M4}-T_{M3}}{2L_{s2}}\right)_o \frac{d\delta L_{s1}}{dt} = \frac{U_{pm}}{2\rho_m A_m C_m}\,\delta T_{p2} + \frac{U_{pm}}{2\rho_m A_m C_m}\,\delta T_{p3} - \frac{(U_{pm}+U_{ms2})}{\rho_m A_m C_m}\,\delta T_{M3} + \frac{U_{ms2}}{\rho_m A_m C_m}\left(\frac{\partial T_{sat}}{\partial P}\right)\delta P \; . \tag{II.11}$$

--The Fourth Metal Node (M4)

The energy balance in this node is analagous to the one of the first node. Thus, we have:

$$\frac{d\delta T_{M4}}{dt} + \left(\frac{T_{M4}-T_{M3}}{2L_{s1}}\right)_o \frac{d\delta L_{s1}}{dt} = \frac{U_{pm}}{2\rho_m A_m C_m}\,\delta T_{p3} + \frac{U_{pm}}{2\rho_m A_m C_m}\,\delta T_{p4} - \frac{(U_{pm}+U_{ms1})}{\rho_m A_m C_m}\,\delta T_{M4} + \frac{U_{ms1}}{2\rho_m A_m C_m}\,\delta T_d + \frac{U_{ms1}}{2\rho_m A_m C_m}\left(\frac{\partial T_{sat}}{\partial P}\right)\delta P \; . \tag{II.12}$$

The Secondary Side

The secondary coolant side consists of the nodes representing the downcomer (D), the subcooled region (S1), the boiling region (S2), the riser (S3) and the steam dome (S4). The mass and energy balances are written for each node and also a quasi-static balance of the pressure drops along the secondary loop, between the highest points of the downcomer and the riser.

--Downcomer Node (D)

We assume that the water density in the downcomer varies linearly with temperature. The range of the water level corresponds to (0%) and (100%) with respect to the metallic plate on top of the U-tube bundle (see Figure 2.5, page 17), and its variations are calculated in percentage using a conversion factor k (%/ft).

Mass conservation: $\frac{d}{dt}(\rho_d(V_d+KA_d\delta L)) = W_{fi} + (1-x_e)W_4 - W_1$ where $(1-X_e)W_4 = W_r$ is the recirculation flow rate. Linearizing the above yields:

$$k\,\frac{d\delta L}{dt} + \frac{V_d}{\rho_d A_d}\left(\frac{\partial \rho_d}{\partial T}\right)\frac{d\delta T_d}{dt} = \frac{1}{\rho_d A_d}\left(\delta W_{fi} + (1-x_e)_o\,\delta W_4 - W_{4o}\delta x_e - \delta W_1\right) . \tag{II.13}$$

Energy conservation:

$$C_{p2}\frac{d}{dt}(\rho_d(V_d + kA_d L)) = C_{p2}\left((1-x_e)W_4 T_{sat} + W_{fi}T_{fi} - W_1 T_d\right) .$$

Linearizing the above equation, we obtain

$$\frac{V_d}{A_d}\left(1 + \frac{T_d}{\rho_d}\left(\frac{\partial \rho_d}{\partial T}\right)\right)_o \frac{d\delta T_d}{dt} + kT_{do}\frac{d\delta L}{dt} = \frac{1}{\rho_d A_d}\Big[-W_{4o}T_{sat_o}\delta x_e + \\ + (1-x_{eo})T_{sato}\delta W_4 + \\ + (1-x_{eo})W_{4o}\left[\frac{\partial T_{sat}}{\partial P}\right]\delta P - T_{do}\delta W_1 \\ - W_{1o}\delta T_d + T_{fio}\delta W_{fi} + W_{fio}\delta T_{fi}\Big] . \tag{II.14}$$

--Subcooled Node (S1)

In this node the water temperature increases from T_d to T_{sat}. Its density is taken as the average of the density in the downcomer (ρ_d) and the density of saturated water (ρ_{s1}). The variations of ρ_{s1} in time are negligable compared to the variations of ρ_d.

Mass conservation: $\frac{d}{dt}\left(\frac{\rho_d+\rho_{s1}}{2} \cdot L_{s1}A_{fs}\right) = W_1 - W_2$.

Linearizing the above equation yields:

$$\frac{d\delta L_{s1}}{dt} + \left(\frac{L_{s1}}{\rho_{s1}+\rho_d}\right)_o \left[\frac{\partial\rho_d}{\partial T}\right]\frac{d\delta T_d}{dt} = \frac{2}{A_{fs}(\rho_{s1}+\rho_d)_o} (\delta W_1 - \delta W_2) \quad . \qquad \text{(II.15)}$$

Energy conservation:

$$C_{p2}A_{fs}\frac{d}{dt}\left(L_{s1}\frac{\rho_{s1}+\rho_d}{2} \cdot \frac{T_d+T_{sat}}{2}\right) = U_{ms1}L_{s1}\left[T_{m1} - \frac{T_d+T_{sat}}{2}\right]$$
$$+ U_{ms1}L_{s1}\left[T_{m4} - \frac{T_d+T_{sat}}{2}\right]$$
$$+ C_{p2}(W_1T_d - W_2T_{sat}) \quad .$$

Linearizing the above equation yields:

$$\frac{A_{fs}C_{p2}L_{s1o}}{4}\left[\left((T_d+T_{sat})_o\left[\frac{\partial\rho_d}{\partial T}\right] + (\rho_{s1}+\rho_d)_o\right)\frac{d\delta T_d}{dt}\right.$$
$$\left. + (\rho_{s1}+\rho_d)_o\left[\frac{\partial T_{sat}}{\partial P}\right]\frac{d\delta P}{dt}\right] + \frac{A_{fs}C_{p2}}{4}(\rho_{s1}+\rho_d)_o(T_d+T_{sat})_o\frac{d\delta L_{s1}}{dt}$$
$$= (U_{ms1}L_{s1o}(\delta T_{M1} + \delta T_{M4}) + U_{ms1}(T_{M1}+T_{M4}-T_d-T_{sat})_o\,\delta L_{s1} + (C_{p2}W_{1o}$$

$$- U_{ms1}L_{s1o})\delta T_d - (C_{p2}W_{2o} + U_{ms1}L_{s1o})\left[\frac{\partial T_{sat}}{\partial P}\right]\delta P + C_{p2}(T_{do}\delta W_1$$

$$- T_{sato}\delta W_2) \quad . \tag{II.16}$$

--Boiling Node (S2)

The steam quality in this node increases from zero to the exit quality x_e (Mean value $\overline{x} = x_e/2$). We assume a homogeneous water-steam mixture and we define a mean density and a mean enthalpy as follows:

$$\rho_b = 1/(v_f + \overline{x}v_{fg}) \tag{II.17}$$

$$h_b = h_f + \overline{x}h_{fg}$$

with $v_{fg} = v_g - v_f$ and $h_{fg} = h_g - h_f$.

Mass conservation: $\frac{d}{dt}(\rho_b A_{fs} L_{s2}) = W_2 - W_3$.

Linearizing the above equation, we obtain

$$A_{fs}\left\{-\rho_{b_\circ}\frac{d\delta L_{s1}}{dt} + L_{s2_\circ}\frac{d\delta\rho_b}{dt}\right\} = \delta W_2 - \delta W_3 \quad . \tag{II.18}$$

The calculation of $\frac{d\delta\rho_b}{dt}$ is performed by taking the time derivative of equation (II.17) and then linearizing it, to obtain finally

$$\frac{d\delta\rho_b}{dt} = D_1\frac{d\delta P}{dt} - D_2\frac{d\delta x_e}{dt} \tag{II.19}$$

where

$$D_1 = -\rho_{b_o}{}^2\left[\frac{\partial v_f}{\partial P} + \frac{x_e}{2}\frac{\partial v_{fg}}{\partial_p}\right]_o \;,\; D_2 = \rho_{b_o}{}^2\left(\frac{v_{fg}}{2}\right)_o \;. \qquad (II.20)$$

Thus, equation (II.18) becomes

$$A_{fc}\rho_{bo}\frac{d\delta L_{s1}}{dt} - A_{fs}L_{s2o}D_1\frac{d\delta P}{dt} + A_{fc}L_{s2o}D_2\frac{d\delta x_e}{dt} = -\delta W_2 + \delta W_3 \qquad (II.21)$$

Energy conservation:

$$\frac{d}{dt}(\rho_b A_{fc}L_{s2}h_b) = U_{ms2}L_{s2}(T_{M2}-T_{sat}) + U_{ms2}L_{s2}(T_{M3}-T_{sat}) + W_2h_f - W_3(h_f+x_eh_{fg}) \;.$$

Linearizing the above equation yields

$$\begin{aligned}
A_{fc}\Bigg\{&\left[L_{s2}h_bD_1 + \rho_bL_{s2}\left(\frac{\partial hf}{\partial P} + \frac{x_e}{2}\frac{\partial h_{fg}}{\partial P}\right)\right]_o\frac{d\delta P}{dt} + \left(\frac{\rho_bL_{s2}h_{fg}}{2}\right.\\
&\left.-L_{s2}h_bD_2\right)_o\frac{d\delta x_e}{dt} - \rho_{bo}h_{bo}\frac{d\delta L_{s1}}{dt}\Bigg\} = -U_{ms2}(T_{M2}+T_{M3}-2T_{sat})_o\,\delta L_{s1}\\
&+ U_{ms2}L_{s2o}(\delta T_{M2}+\delta T_{M3})\\
&- \left[2U_{ms2}L_{s2o}\left[\frac{\partial T_{sat}}{\partial P}\right] + W_{3o}x_{eo}\frac{\partial h_{fg}}{\partial P}\right]\delta P\\
&+ h_{fo}\delta W_2 - (h_f+x_eh_{fg})_o\,\delta W_3\\
&- W_{3o}h_{fg}\delta x_e \;. \qquad (II.22)
\end{aligned}$$

--Steam Dome Node (S3)

The steam volume in this node consists of the volume of the upper part of the steam generator, between the free water surface and the separators

Mass conservation:

$$\frac{d}{dt}\left(\rho_g(V_s - kA_d\delta L)\right) = x_e W_4 - W_{so}$$

where W_{so} is the steam exit flow and $\rho_g = 1/v_g$.

Linearizing the above equation, we obtain

$$V_s \frac{\partial \rho_g}{\partial P} \cdot \frac{d\delta P}{dt} - k\rho_g A_d \frac{d\delta L}{dt} = x_{eo}\delta W_4 + W_{4o}\delta x_e - \delta W_{so} \cdot \qquad \text{(II.23)}$$

--Pressure Drops in the Recirculation Loop

At any time the difference in static pressure (Δp) between the downcomer on one side and the heating channel with the riser on the other side, is equal to the sum of pressure drops (Δp_s, Δp_d) in the loop. The recirculation ratio at a given steady-state is assumed to be known.

Momemtum conservation: $\Delta p = \Delta p_s + \Delta p_d$

where $\Delta p_s = C_s\overline{W}^2$ (single-phase flow) ,

$\Delta p_d = C_d\overline{W}^2$ (two-phase flow)

where the mean flow rate $\overline{W}$ is defined as a weighted average of W_1 and W_3: $\overline{W} = \varepsilon W_1 + (1-\varepsilon)W_3$.

Thus, $\Delta p = (C_s + C_d)\overline{W}^2$ and $\overline{W} = \dfrac{\sqrt{\Delta p}}{\sqrt{C_s+C_d}}$. (II.24)

Linearizing equation (II.24) yields

$$\delta\overline{W} = \frac{1}{\sqrt{C_s+C_d}}\ \delta\sqrt{\Delta p} - \frac{\sqrt{\Delta p_\circ}}{2(C_{so}+C_{do})^{\frac{3}{2}}}\ \delta C_d = \frac{W_\circ}{\sqrt{\Delta p_\circ}}\ \delta\sqrt{\Delta p} - \frac{\sqrt{\Delta p_\circ}}{2(C_{so}+C_{do})^{\frac{3}{2}}}\ \delta C_d\ . \tag{II.25}$$

We also have

$$\Delta p = \rho_d L_d - \left\{\frac{\rho_d+\rho_{s1}}{2}\, L_{s1} + \rho_b L_{s1} + \rho_r L_r\right\} \tag{II.26}$$

where the steam density in the riser (ρ_r) is given by

$$\rho_r = 1/(v_f + x_e v_{fg})\ . \tag{II.27}$$

The above relationship, similar to equation (II.17), gives

$$\delta\rho_r = D_{1r}\delta p - D_{2r}\delta x_e \tag{II.28}$$

where

$$D_{1r} = -\rho_{ro}{}^2\left[\frac{\partial v_f}{\partial p} + x_e\,\frac{\partial v_{f\delta}}{\partial p}\right]_o\ ,\quad D_{2r} = \rho_{ro}{}^2 v_{fo}\ . \tag{II.29}$$

Thus, evaluating $\delta\sqrt{\Delta p}$ from equation (II.26) and using (II.28) yields

$$\delta\sqrt{\Delta p} = \frac{1}{2\sqrt{\Delta p_\circ}}\left\{\rho_{do}k\delta L + \left(\rho_b - \frac{\rho_d+\rho_{s1}}{2}\right)_o \delta L_{s1} - (L_{s2o}D_1+L_{ro}D_{1r})\delta P \right.$$

$$\left. + (L_{s2o}D_2+L_{ro}D_{2r})\delta x_e + \left(L_d - \frac{L_{s1}}{2}\right)_o \frac{\partial\rho_d}{\partial T}\ \delta T_d\right\}\ . \tag{II.30}$$

In order to evaluate δC_d for equation (II.25), we assume that C_d is proportional to the mean specific volume of the steam water mixture (22):

$$C_d = \frac{1}{v_f}\left[v_f\left(1 - \frac{x_e}{2}\right) + v_g \frac{x_e}{2}\right] \cdot C_{ds} = \left[1 + \frac{v_{fg}}{v_f} \frac{x_e}{2}\right] C_{ds} \ . \qquad \text{(II.31)}$$

Assuming that variations in v_f and v_g are neglibable compared to variations in x_e, we have

$$\delta C_d = C_{dso} \frac{v_{fg}}{v_f} \frac{\delta x_e}{2} = \frac{C_{do}}{\left(1 + \frac{v_{fg}}{v_f} \frac{x_{eo}}{2}\right)} \frac{v_{fg}}{v_f} \frac{\delta x_e}{2} \ . \qquad \text{(II.32)}$$

But using $\Delta p_d = C_d \overline{W}^2$ we have $C_{do} = \dfrac{\Delta P_{do}}{\overline{W}_o^{\,2}}$ and using $\Delta p = (C_s + C_d)\overline{W}^2$ we obtain $(C_s + C_d)_o^{\frac{3}{2}} = \dfrac{(\Delta p_o)^{\frac{3}{2}}}{\overline{W}_o^{\,3}}$ so that the last term of equation (II.25) becomes

$$\frac{\sqrt{\Delta p_o}}{2(C_d + C_d)_o^{\frac{3}{2}}} \cdot \delta C_d = \frac{1}{4}\left\{\frac{\Delta p_d}{\Delta p_o} \cdot \frac{W_o}{\left(1 + \frac{v_{fg}}{v_f} \frac{x_e}{2}\right)} \frac{v_{fg}}{vf}\right\} \delta x_e \ . \qquad \text{(II.33)}$$

Substituting (II.30) and (II.33) in equation (II.25), and knowing that $\delta \overline{W} = \varepsilon \delta W_1 + (1-\varepsilon)\, \delta W_3$, we obtain

$$\varepsilon\delta W_1 + (1-\varepsilon)\delta W_3 = \frac{W_o}{2\Delta p_o}\left[\rho_{do}k\delta L + \left(\rho_d - \frac{\rho_d+\rho_{s1}}{2}\right)_o \delta L_{s1} - (L_{s2}D_1 + L_rD_{1r})_o\ \delta P + (L_{s2}D_2+L_rD_{2r})_o\delta x_e + \left(L_d - \frac{L_{s1}}{2}\right)_o\cdot\frac{\partial \rho_d}{\partial T}\ \delta T_d\right] - \frac{R_p}{4}\left[\frac{W_o}{\left(1 + \frac{v_{fg}}{v_f}\ \frac{x_{eo}}{2}\right)}\cdot\frac{v_{fg}}{v_f}\right]_o \delta x_e\ . \tag{II.34}$$

--Riser Node (S4)

Mass conservation: $\frac{d}{dt}(\rho_rV_r) = W_3 - W_4$.

Linearizing the above and using equation (II.28) we obtain

$$V_r\left(D_{1r}\frac{d\delta P}{dt} - D_{2r}\frac{d\delta x_e}{dt}\right) = \delta W_3 - \delta W_4\ . \tag{II.35}$$

Steady-State Calculations (22)

Before the calculation of any transient, it is necessary to have coherent data for the steady-state to be used as the starting point. This is done in the beginning of the steam generator code, the unknowns being the primary side temperatures, while the secondary side variabes are imposed (Actually the reverse could be done equally well.).

The parameters assumed known for this calculation are: W_p, T_{sat}, T_{fw}, W_s with $W_s = W_{fi}$. The global heat transfer coefficients for the subcooled and boiling zones are:

$$\frac{1}{h_1} = \frac{1}{U_{pm}} + \frac{1}{U_{ms1}}\ ,\ \frac{1}{h_2} = \frac{1}{U_{pm}} + \frac{1}{U_{ms2}}\ . \tag{II.36}$$

The unknowns are the heat quantities Q_1, Q_2, Q_3, Q_4 transferred (see Figure II.1), the boiling boundary L_{s1} and the primary temperatures.

The energy balance for each node is written:

$$Q_1 = W_p C_{p1}(T_{PI} - T_{p1}) \tag{II.37}$$

$$Q_1 = \frac{h_1 L_{s1}}{2} (T_{PI} + T_{p1} - T_d - T_{sat}) \tag{II.38}$$

$$Q_4 = W_p C_{p1}(T_{p3} - T_{p4}) \tag{II.39}$$

$$Q_4 = \frac{h_1 L_{s1}}{2} (T_{p3} + T_{p4} - T_d - T_{sat}) \tag{II.40}$$

$$Q_2 = W_p C_{p1}(T_{p1} - T_{p2}) \tag{II.41}$$

$$Q_2 = \frac{h_2 L_{s2}}{2} (T_{p1} + T_{p2} - 2T_{sat}) \tag{II.42}$$

$$Q_3 = W_p C_{p1}(T_{p2} - T_{p3}) \tag{II.43}$$

$$Q_3 = \frac{h_2 L_{s2}}{2} (T_{p2} + T_{p3} - 2T_{sat}) \tag{II.44}$$

$$Q_2 + Q_3 = Q_B \tag{II.45}$$

$$Q_1 + Q_4 = Q_{NB} \; .$$

The nine equations above (II.37-II.45) are then solved in an iterative way for L_{s1}.

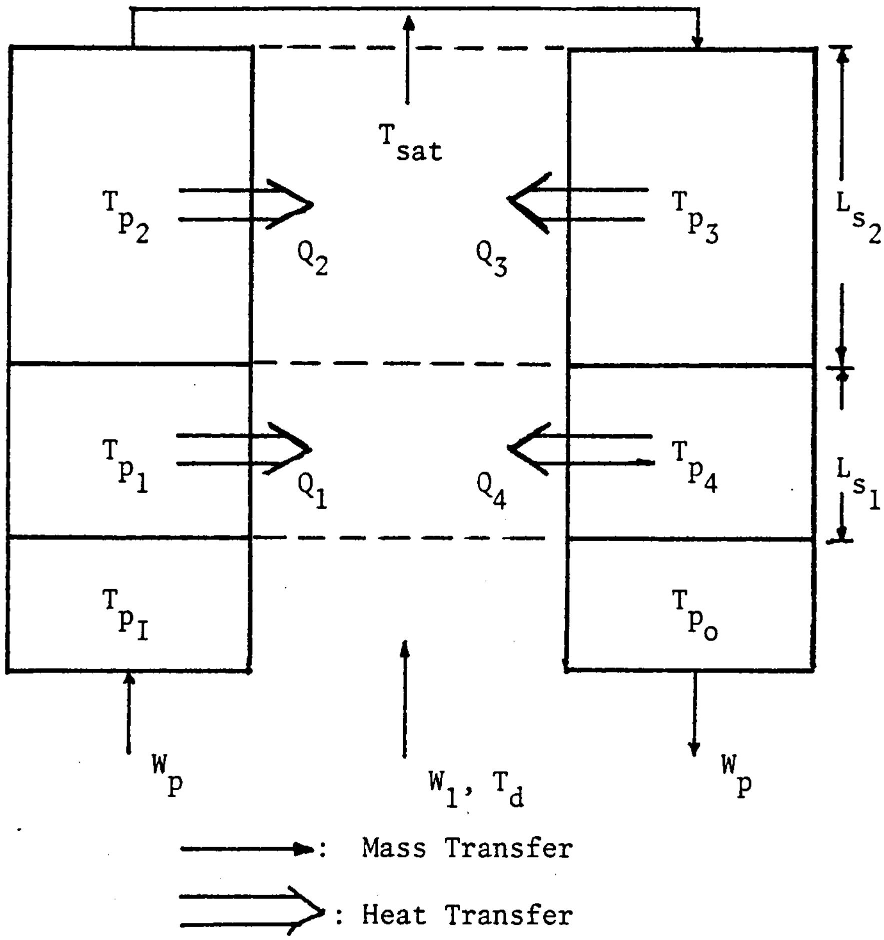

Figure II.1 Schematic Diagram of the Heat Balances in the Steam Generator Used for Steady-State Calculations.

Defining $\alpha = W_p C_{p1}$, $\beta = h_1 L_{s1}/2$, $\gamma = h_2 L_{s2}/2$, the system of equations above can be written as

$$P \cdot XI = UI \tag{II.46}$$

where $XI = [Q_1, Q_2, Q_3, Q_4, T_{PI}, T_{p1}, T_{p2}, T_{p3}, T_{p4}]^T$

and $UI = [0, -\beta(T_d+T_{sat}), 0, -\beta(T_d+T_{sat}), 0, -2\gamma T_{sat}, 0,$

$- 2\gamma T_{sat}, Q_B]^T$.

The square (9 × 9) matrix P is a function of α, β, and γ.

Equation (II.46) is solved by matrix inversion to give

$$XI = P^{-1} \cdot UI .$$

Then the quantity Q_{NB} is calculated and the criterion $Q_1 + Q_4 - Q_{NB} \leq 10^{-3} Q_{NB}$ has to be satisfied. If not, the value of L_{s1} is modified as a function of the error and the system is to be solved again. Our experience shows that convergence is achieved in about four to five iterations.

Modifications to the Original Version

Several modifications were made to Ali's original model and they are included in the presentation given in this Appendix. They were made in order to improve the agreement between this linear model and a nonlinear detailed code (22), and they are listed below:

(a) The heat transferred between the primary side and the tube metal is calculated on average primary temperature, for example $Q_{pm1} = U_{pm}L_{s1}\left[\frac{1}{2}(T_{p1} + T_{pI}) - T_{M1}\right]$ instead of

$Q_{pm1} = U_{pm}L_{s1}(T_{p1} - T_{M1})$.

(b) In the calculation of the recirculation flow, the average secondary flow was taken as $\overline{W} = \varepsilon W_1 + (1-\varepsilon)W_3$, with an optimal value for the weighting factor ε equal to 0.5, found by comparing the results with the response of the EVA code (22). In the original version $\overline{W} = W_1$ (i.e., ε=1).

(c) The real cross section of the downcomer was modeled while initially the downcomer was assumed cylindrical. In this way we can define separately the downcomer volume V_d and the downcomer cross sectional flow area A_d near the free water surface.

(d) In the initial version, the pressure drop in the boiling region was assumed independent of the steam quality (R_p=0 in equation (II.34)), and the subcooled water density was assumed constant $\left(\frac{\partial p_d}{\partial T} = 0\right)$.

II.2 Data Used

The design parameters for the steam generator model are given here. The parameters having the same value at full and at low power are listed first, and the rest of the parameters follow, for each power level. The optimal values, as found by the identification work (Section 6.7, page 91) are used for the optimized parameters. The notation is explained in Sections II.1 and in Chapter 6.

NT (total number of U-tubes) = 3388

D_o (outside tube diameter) = $7.297 \cdot 10^{-2}$ ft

T (tube thickness) = $4.3965 \cdot 10^{-3}$ ft

$W_p = 9.3377 \cdot 10^3$ lbm/sec

$\rho_m = 530$ lbm/ft^3

$C_{pm} = 0.1055$ Btu/lbm $\cdot$ °F

V_p (volume of primary coolant) = $1.077 \cdot 10^3$ ft^3

$V_s = 3.884 \cdot 10^3$ ft^3

A_o (heat transfer area) = $5.1538 \cdot 10^4$ ft^2

P_{pr} (primary pressure) = 2280 psi

$\rho_b = 45$ lbm/ft^3

V_d (initial downcomer volume) = $1.12 \cdot 10^3$ ft^3

A_d (downcomer cross sectional area) = $1.036 \cdot 10^2$ ft^2

D_ℓ (initial water height) = 42.19 ft

$A_{fs} = 54.88$ ft^2

$V_r = 7.119 \cdot 10^2$ ft^3

$L_r = 11.81$ ft .

At Full Power

$W_s = 1.102 \cdot 10^3$ lbm/sec

P_s (Secondary pressure) = 854 psi

$T_{sat} = 524.3$ °F

$T_{fw} = 463.7$ °F

$\rho_{s1} = 49.07$ lbm/ft^3

$C_{p2} = 1.169$ Btu/lbm °F

$R_p = (\Delta p_d/\Delta p_o) = 0.6$

$\partial\rho_d/\partial T = -1.6$

$L_{slo} = 4.92$ ft

$x_{eo} = 0.19$

$C_{pl} = 1.34$ Btu/lbm °F

HP = 5950 Btu/hr. ft^2 °F

K_t (Tube metal (Inconel) heat capacity) = 10.07 Btu/hr. ft °F

UM = K_t/T = 2290 Btu/hr. ft^2 ° F

HS1 = 5590 Btu/hr. ft^2 °F

HS2 = 11000 Btu/hr. ft^2 °F .

<u>At Low Power (30%)</u>

$W_s = 3.307 \cdot 10^2$ lbm/sec

$P_s = 970$ psi

$T_{sat} = 542.$ °F

$T_{fw} = 343.4$ °F

$\rho_{s1} = 46.88$ lbm/ft^3

$C_{p2} = 1.236$ Btu/lbm °F

$R_p = 0.45$

$\partial\rho_d/\partial T = -1.8$

$L_{slo} = 6.56$ ft

$x_{eo} = 0.06$

$C_{pl} = 1.31$ Btu/lbm °F

HP = 6120 Btu/hr. ft^2 °F

$K_t = 10.354$ Btu/hr. ft °F

UP = K_t/T = 2350 Btu/hr. ft^2 °F

$HS1 = 5750$ Btu/hr. ft^2 °F

$HS2 = 11300$ Btu/hr ft^2 °F .

APPENDIX III

THE SIMPLEX OPTIMIZATION ALGORITHM

The Simplex method minimizes a function of n variables $f(x_1, \ldots, x_n) = f(\underline{x})$ by comparing the values of the function at n + 1 points P_i in the n-dimensional space. The set of these n + 1 points is called a simplex. For two variables it is a triangle, for three variables it is a tetrahedron, etc. Then, the point with the highest value is replaced by another point. The simplex adapts itself to the local shape of the error function surface in the n-dimensional shape, and contracts on to the final minimum (32).

Let us define as

P_h the point corresponding to $f_h = \max(f_i)$, $i = 1, 2, \ldots, n+1$

P_s the point corresponding to $f_s = \max(f_i)$, $i = 1, 2, \ldots, n+1$, $i \neq h$

P_l the point corresponding to $f_l = \min(f_i)$, $i = 1, 2, \ldots, n+1$

P_o the point corresponding to $f_o = f(x_o)$, where x_o is the center of gravity defined as $\underline{x}_o = \frac{1}{n} \sum_{\substack{i=1 \\ i \neq h}}^{n+1} \underline{x}_i$.

At each stage in the process P_h is replaced by a new point; three operations are used: reflection, expansion, and contraction. These are defined as follows: the reflection of P_h is denoted by P_r and its coordinates are defined by the relation (Figure III.1(a)).

$$P_r = (1 + \alpha)P_o - \alpha P_h$$

where α is a positive constant, the reflection coefficient.

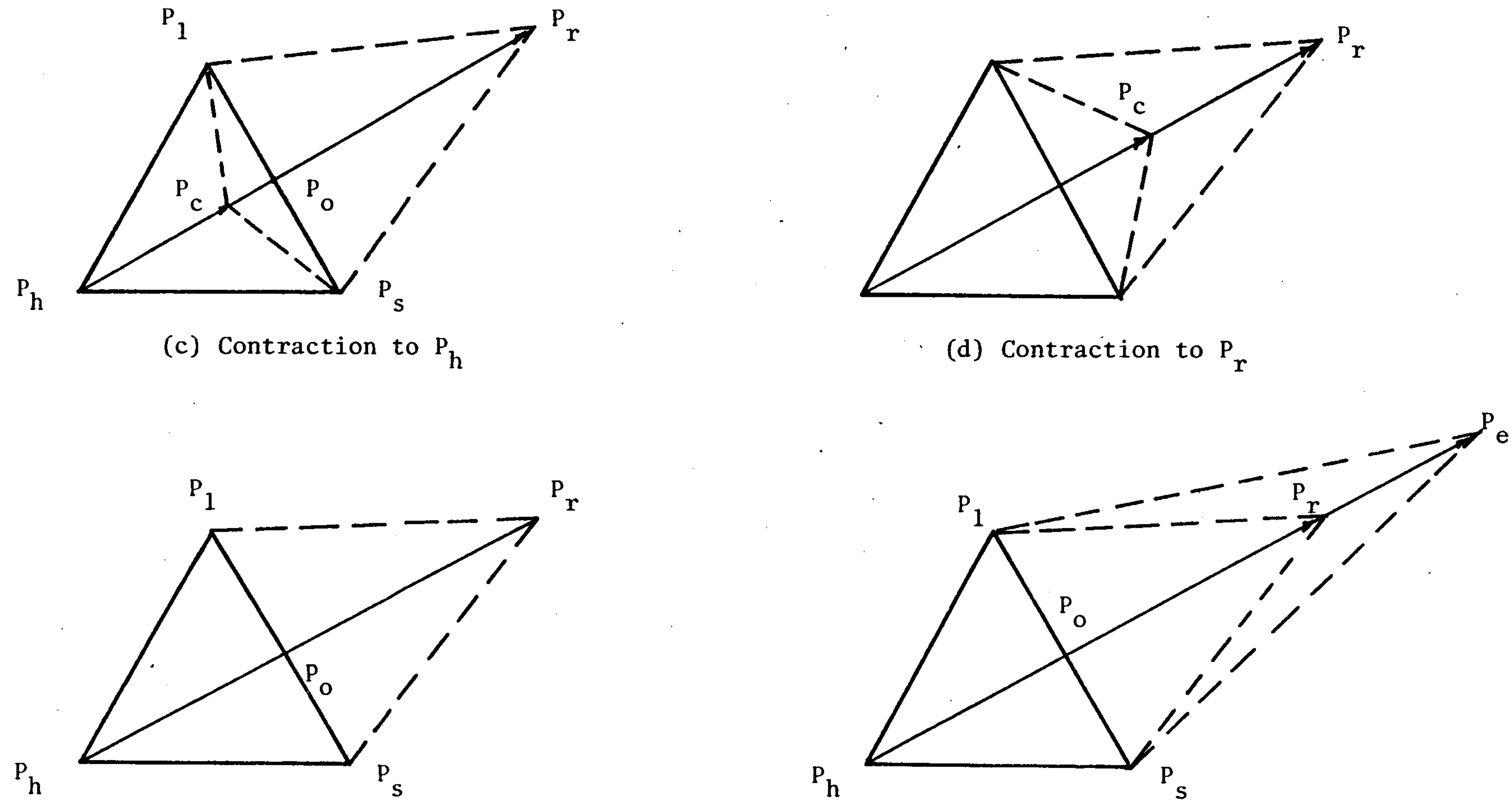

(c) Contraction to P_h

(d) Contraction to P_r

(a) Reflection

(b) Expansion

Figure III.1 Schematic of the Simplex Operations.

If $f_s > f_r > f_e$, we replace P_h by P_r and we restart the procedure with the new simplex.

If $f_r < f_1$, we can expect that following the direction defined by the reflection, we can have a further decrease in the cost function and thus we expand the simplex to that direction. The expansion consists of replacing P_r by P_e by the relation, Figure III.1(b)

$$P_e = \gamma P_r + (1 - \gamma)P_o$$

where γ is a constant greater than unity, the expansion coefficient.

If $y_e < y_1$, the expansion has succeeded, and we replace P_h by P_e to restart the process.

If $y_e > y_1$, the expansion has failed and we replace P_h by P_r to restart the process.

If after the reflection we had $f_h > f_r > f_s$, we define a new P_h, by either the old P_h or P_r, whichever has the lower f value, and we contract the simplex (Figure III.1(c) and (d)) defining a new point P_c according to

$$P_c = \beta P_h + (1 - \beta)P_o$$

where the contraction coefficient β lies between 0 and 1.

If $f_c < f_h$, the contraction has succeeded and we replace P_h by P_c.

If $f_c > f_h$, we reconstruct the simplex around P_1 and the vectors $\underline{x}_i$ of the new simplex are calculated by

$$\underline{x}_i = \frac{1}{2}(\underline{x}_i + \underline{x}_1)$$

and we restart the process.

The coefficients α, β, γ give the factor by which the volume of the simplex is changed by the operations of reflection, contraction or expansion respectively and it was found (32) that convenient values are: $\alpha = 1$, $\beta = 0.5$, $\gamma = 2$.

The criterion adopted by Nelder and Mead to halt the procedure is concerned with the variation in the f value over the simplex rather than changes in the $\underline{x}$'s. The form chosen is to compare the error of the y's with a preset value ε according to

$$\left(\frac{1}{n}\sum_{i=1}^{n}(f(\underline{x}_i) - f(\underline{x}_o))^2\right)^{\frac{1}{2}} < \varepsilon$$

and to stop when it falls below this value.

VITA

Yiannis Anastasiou was born in Greece on August 20, 1950, the son of Tassos and Tassoula Anastasiou.

He obtained his B.S. degree from the Physics Department of the University of Thessaloniki in 1973.

He continued his studies working for his Master of Engineering degree at the Engineering Physics Department of McMaster University in Canada. In 1974 he joined the Nuclear Engineering Department of the University of Tennessee to work for his doctoral degree. For the last year and a half, he worked at the Centre d'Etudes Nucleaires in Saclay, France to complete the research work for the Ph.D. requirements.